

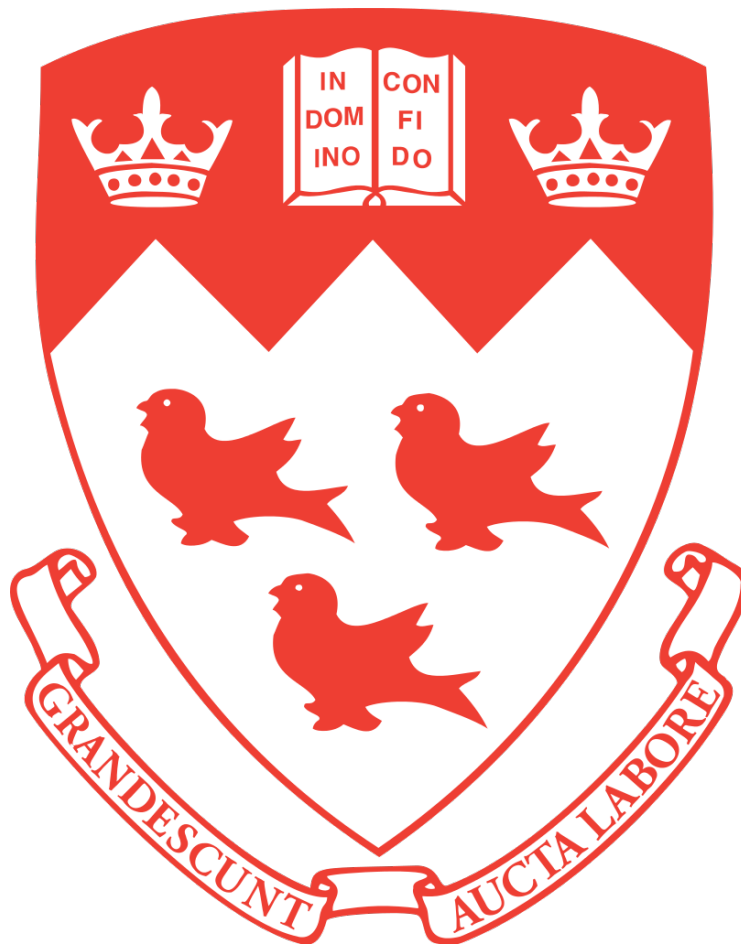
Purple Bacteria for Wastewater Treatment and Resource Recovery

Mamdouh Jaber

Department of Civil Engineering and Applied Mechanics

McGill University, Montreal

April 2020



A thesis submitted to McGill University in partial fulfillment of the requirements of the degree
of Master of Engineering

© Mamdouh Jaber, 2020

ABSTRACT

Wastewater treatment plants are transitioning into resource-recovery centers that reduce pollution from the wastewater by transforming it into valuable resources. Purple phototrophic bacteria (PPB) have been shown to exhibit accumulative properties under anaerobic conditions while utilizing infrared light as their primary energy source, which reduces energy input into the biochemical process. Manipulating their accumulative properties will allow carbon, phosphorus and energy recovery from wastewater in the form of poly-hydroxyalkanoates (PHAs), poly-phosphates (poly-P) and hydrogen gas, respectively. This work first aimed to investigate the viability of treating wastewater using PPB. A 4-L anaerobic photobioreactor was constructed and illuminated with 850 nm infrared light. Steady-state analysis showed satisfactory chemical oxygen demand (COD) removal with soluble COD dropping to less than 30 mg/L. The enriched biomass under this reactor accumulated about 5 mg-P/L of ortho-phosphates corresponding to 6% of the total dry weight of solids. Fluorescence microscopy analysis with the dye 4',6-diamidino-2-phenylindole (DAPI) suggested that a portion of the accumulated P was in the form of poly-P. An enrichment experiment was conducted to investigate the effect of isolating the carbon sources of the synthetic wastewater (normally comprises eight carbon sources) on the microbial community composition. rRNA gene amplicon sequencing revealed the presence of fermenters when fermentable substrates (starch, milk or glycerol) were fed to the reactors, while only a small amount fermenting bacteria were present when reactors were fed acetate. The latter fermenters were likely fermenting microbial metabolites and macromolecules. The PPB accounted for 50% of the sequence reads when the reactors were illuminated with 850 nm, while they were only 30% of the reads with the 940 nm light. Microbial composition of the reactors fed complete wastewater appeared to be more similar to the fermentable substrates than the acetate reactors. A second experiment was done to examine

the effect of intermittent illumination on poly-P accumulation. The corresponding results were inconclusive as some of the reactors receiving intermittent lighting outperformed the continuously illuminated control while others did not. The pH in all reactors other than the dark control increased significantly. Interaction between pH and poly-P accumulation appears to be significant, but the exact nature of these interactions remains unknown.

RÉSUMÉ DE RECHERCHE

L'industrie des eaux usées se redéveloppe pour tenir en compte la récupération des ressources qui pourra réduire la pollution des eaux usées en la transformant en des ressources bénéfiques. Les bactéries pourpres phototrophes (BPP) ont démontré leur capacité à accumuler des ressources intracellulaires en conditions anaérobies tout en utilisant la lumière infrarouge comme source d'énergie principale, ce qui permet d'avoir une énergie d'entrée réduite dans le processus biochimique. En manipulant les propriétés accumulatives des BPP, le carbone, le phosphore et l'énergie peuvent être récupérés des eaux usées sous la forme de poly-hydroxyalkanoates (PHAs), poly-phosphates (poly-P) et de gas hydrogène, respectivement. Ce projet vise premièrement à examiner la viabilité de traiter les eaux usées en utilisant les BPP. Un photo-bioréacteur anaérobie de 4 L fut construit et illuminé avec de la lumière infrarouge à 850 nm. L'analyse en régime permanent a montré une élimination satisfaisante de la Demande Chimique en Oxygène (DCO) avec une réduction de la DCO soluble jusqu'à moins de 30 mg/L. La biomasse enrichie sous cette configuration du réacteur a accumulé environ 5 mg-P/L correspondant à 6% du poids sec de solides. La microscopie en fluorescence utilisant le colorant 4',6-diamidino-2-phenylindole (DAPI) a suggéré que le phosphore accumulé était sous forme de poly-P. Une expérience d'enrichissement a été réalisée pour étudier l'effet de la séparation des sources carboniques de l'eau usée synthétique (qui contient huit sources de carbones) sur la composition des communautés microbiennes. Le séquençage d'amplicons de gène d'ARNr 16S, a révélé une différence majeure entre les réacteurs alimentés par l'acétate et ceux alimentés par les substrats fermentescibles (amidon, lait en poudre et glycérol). La composition microbienne des réacteurs alimentés avec l'eau usée synthétique complète était plus proche de celle des réacteurs alimentés avec substrats fermentescibles que des réacteurs à acétate. De plus, les BPP comprenaient 50% des séquences

lorsque les réacteurs étaient illuminés à 850 nm, alors qu'ils ne comprenaient que 30% des séquences dans les réacteurs à 940 nm. Une seconde expérience a été réalisée pour examiner l'effet de l'illumination intermittente sur l'accumulation des poly-P. Les résultats correspondants étaient peu concluants puisque quelques réacteurs recevant l'illumination intermittente ont eu une meilleure performance que le réacteur contrôle à illumination continue, alors que d'autres ne montraient pas ce même résultat. Le pH dans tous les réacteurs à part celui de contrôle a augmenté considérablement. Les interactions entre le pH et l'accumulation des poly-P s'est révélée importante, mais la nature exacte de ces interactions demeure inconnue.

ACKNOWLEDGEMENTS

First and foremost, I want to express my sincere thanks to Professor Dominic Frigon for his supervision, guidance and mostly his patience. It didn't matter what time of day or night, Professor Frigon was always available to offer his knowledge and reassurance; and for that, I will always be grateful.

I also want to extend my appreciation to all the members (Alex, Arshath, Claire, Julie, Sampriti, Sarayu and Vini) of the environmental engineering lab for illuminating this beautiful environment with their companionship.

I would also like to acknowledge the people who have lent me their hands and facilitated the completion of this project. Namely, our lab technician, John Bartczak who helped with the reactor construction, my summer student, Thomas Callum who helped with various experiments and my friends, Sarah El Outayek and Marilena Anghelopoulou who've helped with the review of the document.

This work was made possible through the financial aid provided by McGill University, Natural Sciences and Engineering Research Council of Canada (NSERC) and Trojan Technologies.

I wish to acknowledge the contribution of Pierre Lepage of Génome Québec Innovation Centre, Montréal, Canada for expediting amplification and sequencing work.

Last but not least, my parent and my sisters whom were always a fountain of love and support even though I was very distant during the completion of this dissertation.

PREFACE

This thesis is presented in monograph format conforming to the thesis guidelines set by the Graduate and Postdoctoral Studies (GPS). The thesis comprises 7 chapters. Chapter 1 is an introduction. Chapter 2 is the literature review and research gaps. Chapter 3 presents the materials and methods. Chapter 4 presents the operation of 4-L biomass reactor. Chapter 5 presents an enrichment experiment done with the biomass extracted from the 4-L reactor. Chapter 6 presents a poly-phosphate accumulation experiment done with the biomass from the 4-L reactor. Chapter 7 reiterates the major conclusions from Chapters 4,5 and 6 and presents potential future work.

Contribution of the Authors

Mamdouh Jaber: Experimental design (Chapters 4,5 and 6), execution of experiments (Chapters 4,5 and 6), analysis of data (Chapters 4,5 and 6) and preparation of the initial draft.

Thomas Callum: Assisted in experimental design (Chapter 6), execution of experiments (Chapter 6) and analysis of data (Chapter 6).

Dominic Frigon: Supervision of research, overseeing of experimental design (Chapter 4,5 and 6), guidance of data analysis (Chapter 4,5 and 6) and revision of the document.

TABLE OF CONTENTS

Abstract	i
Résumé de recherche	iii
Acknowledgements	v
Preface	vi
List of Tables	ix
List of Figures	x
List of Abbreviations	xiv
1 Introduction	1
1.1 Wastewater Treatment: A Historical Perspective and Future of the Art	1
1.2 Objectives of this work	4
1.3 Thesis Organization	4
2 Literature Review	6
2.1 Phototrophy in Natural Systems: The Driving Force for Colour Niches	6
2.2 Phylogeny of Phototrophic Purple Bacteria	7
2.3 The Photosynthetic Apparatus: Generating Biochemical Energy from Light	10
2.4 Metabolism of the Purple Bacteria	13
2.4.1 Nitrogen Fixation	14
2.4.2 PHA Accumulation	16
2.4.3 Poly-Phosphate Metabolism by Purple Bacteria	17
2.5 Purple Bacteria in Wastewater Treatment	21
2.5.1 COD, Nitrogen and Phosphorus Removal in Photobioreactors by PPB	21
2.5.2 Selective Pressure for Poly-P Accumulators	22
2.6 Research Gaps	23
3 Materials and Methods	24
3.1.1 Synthetic Wastewater	24
3.1.2 Light Source	25
3.1.3 Analytical Methods	26
3.1.4 Bioinformatics Analysis	32
3.1.5 Statistical Methods	34
4 Main Large 4-L Biomass Reactor	35
4.1 Introduction	35
4.1.1 Objectives:	35
4.2 Experimental Setup	36
4.2.1 Reactor Geometry and Design	36

4.3	Results and Discussion	37
4.3.1	Start-up of Reactor	37
4.3.2	Steady-state Analysis	38
4.3.3	DAPI Staining	41
4.3.4	Microbial Community Structure	42
4.4	Conclusions	44
5	Enrichment Experiment in Small 60-ml Reactors	46
5.1	Introduction	46
5.2	Experimental Setup	47
5.3	Results	47
5.3.1	Temporal Dynamics of the Biomass	47
5.3.2	Biomass at the End of the Experiment	52
5.3.3	Structures of the Communities Enriched under Different Reactor Conditions	54
5.4	Discussion	68
5.4.1	Biomass Yield and Bacteriochlorophyll Content	68
5.4.2	Diversity	69
5.4.3	PPB Population	70
5.4.4	Fermenter Population	71
5.5	Conclusions	72
6	Intermittent IR illumination as a selective pressure for Poly-P accumulators	74
6.1	Introduction	74
6.2	Experimental Design	75
6.2.1	Experimental Setup	75
6.3	Results and Discussion	76
6.4	Conclusions	81
7	Conclusions and Future Work	82
7.1	Conclusions	82
7.2	Future Work	83
	APPENDIX A: Lamp Characterization	92
	APPENDIX B: Enrichment Reactor Images	93
	APPENDIX C: QIIME 2 Commands	96
	APPENDIX D: Phylogenetic Classification of Purple Bacteria	98

LIST OF TABLES

Table 3-1: Prepared Syntho composition.....	24
Table D-1: Phylogenetic classification of the purple bacteria within the <i>Proteobacteria</i> phylum.	98

LIST OF FIGURES

- Figure 2-1: Colour niche of phototrophic organisms. (A): Irradiance profile in water. The steep drops are due to interception either by oxygen or water. (B): The different niches of microorganisms; the segregations match the irradiance drops. Reproduced with permission from International Society for Microbial Ecology (Stomp et al., 2007). 7
- Figure 2-2: Maximum likelihood phylogenetic tree summarizing the evolution of the *pufM* and *pufL* genes using amino acid sequences. Bootstrap values of 95% were used. Reproduced with permission from Frontiers in Microbiology (Imhoff et al., 2017). 8
- Figure 2-3: Energy transfer between various components in the photosystem. Arrows indicate direction of energy transfer. The energy transferred from the reaction center to carotenoids corresponds to triplet energy; the opposite arrow indicated singlet transfer. 11
- Figure 2-4: Overview of various PPB metabolic modes. Under oxic conditions, PNSB respire using oxygen to produce energy. Under these conditions they grow either heterotrophically or autotrophically. Anaerobically, PNSB leverage their bacteriochlorophyll (a or b) to harvest energy from the incident light. PPB also behave heterotrophically or autotrophically under these conditions. Reproduced with permission from Nature Biotechnology (Larimer et al., 2004). 14
- Figure 2-5: General structure of PHBV polymer. (B) Corresponds to HB monomers. (V) Corresponds to HV monomers..... 16
- Figure 2-6: Different structures of poly-P. These structures are built from polymerization of the terminal phosphate from ATP forming an identical phosphoanhydride bond in the polymer. Polymer formation can result in a linear chain form (a) or a branched form (b) and (c). 19
- Figure 4-1: (A) Side view of the reactor setup. The lamp (850 nm IR source) is shown on the left with the reactor on the right. The distance between the lamp and the reactor is 30 cm. Three stirring plates can be seen underneath the reactor. During operation, a cardboard box is placed over the setup to block any external light from reaching the reactor. (B) Reactor schematic showing front, side and top views. Grey corresponds to the stainless steel and blue is the borosilicate glass. 37
- Figure 4-2: Reactor performance during steady-state operation. (A): COD profiles (soluble: sCOD and total: tCOD). (B): Total solids profiles (total: TS, volatile: VS and fixed: FS). (C): Suspended solids profiles (total: TSS, volatile: VSS and fixed: FSS). (D): Total phosphorus profiles. Day 0 corresponds to the measurement taken on May 5th (three months after the start of the reactor). Dashed lines in the plots represent the average measurement over time. Standard error did not exceed 10% and was not shown for clarity..... 39
- Figure 4-3: Presumed biomass phosphorus content. Calculation is done using phosphorus closure with respect to the VSS level. 41

Figure 4-4: DAPI staining of the enriched biomass. Picture was taken using biomass from day 32. Blue regions correspond to fluorescence from DAPI-DNA interactions. Yellow regions are likely due to DAPI-poly-P fluorescence. Image was taken using a 100x objective. 42

Figure 4-5: Family-level abundance. The major phyla represented were *Proteobacteria* (36%), *Bacteroidetes* (15%), and *Firmicutes* (43%). DNA from three samples taken at the same time was used to generate the plot. 44

Figure 5-1: OD660 time series for (A): 850 nm reactors and (B): 940 nm reactors during the SBR operation. Horizontal axis expressed in dimensionless time (t/HRT) with $HRT = 8$ days. OD660 is used as an estimator for biomass concentration. Time 0 corresponds to the end of batch operation (8 days) and start of SBR operation. Measurements were taken in triplicates. Standard error was less than 10% in all cases and was not shown to improve clarity..... 48

Figure 5-2: Absorption spectra over the range 350 - 1000 nm. (A) Spectra for reactors receiving 850 nm IR. (B) Spectra for reactors receiving 940 nm IR. Within the IR range (700 - 1000 nm), two distinct peaks develop corresponding to BChl-a. Plot was generated using data from Day 0. 49

Figure 5-3: OD810 and OD870 temporal profiles for the reactors illuminated at 850 nm. (A): OD810 corresponding to the pigment content of the light-harvesting complexes. (B) OD870 corresponding to the pigment content of the reaction center. (C) OD810/OD660 ratio. (D): OD870/OD660 ratio. Plots C and D were magnified by starting the vertical axis at 0.6. Horizontal axis expressed in dimensionless time (t/HRT) with $HRT = 8$ days. Time 0 corresponds to the end of the batch operation (8 days) and start of SBR operation. Measurements were taken in triplicates. Standard error was less than 10% in all cases and was not shown to improve clarity. 50

Figure 5-4: OD810 and OD870 temporal profiles for the reactors illuminated at 940 nm IR. (A): OD810 corresponding to the pigment content of the light-harvesting complexes. (B) OD870 corresponding to the pigment content of the reaction center. (C) OD810/OD660 ratio. (D): OD870/OD660 ratio. Plots C and D were magnified by starting the vertical axis at 0.6. Horizontal axis expressed in dimensionless time (t/HRT) with $HRT = 8$ days. Time 0 corresponds to the end of the batch operation (8 days) and start of SBR operation. Measurements were taken in triplicates. Standard error was less than 10% in all cases and was not shown to improve clarity. 51

Figure 5-5: Suspended solids measurements. Height of the combined bars corresponds to total solids. Measurement represents average of the triplicates; error bars represent standard error ($n = 3$). (A): Data for 850 nm reactors. (B): Data for 940 nm reactors. Two-way ANOVA was done to test the significance of the substrate main effect (p -value = 0.002), wavelength main effect (p -value = 0.20) and substrate-wavelength interactions (p -value = 0.39). Glycerol was the only group that is different from the rest identified by the least square difference. 52

Figure 5-6: Bacteriochlorophyll a content measured at the of the SBR operation. Measurements corresponds to the average of the three replicates normalized per unit VSS. Error bars represent standard error ($n=3$). Two-way ANOVA was done to test the significance of the substrate main effect (p -value = 0.023), wavelength main effect (p -value = $8E-4$) and substrate-wavelength

interactions (p-value = 0.69). Letters indicate substrate conditions with non-significant differences identified by the least square difference. 53

Figure 5-7: Species richness plot. Measurements correspond to the average number of observed OTUs. Error bars represent standard error (n = 3). Two-way ANOVA was done to test the significance of the substrate main effect (p-value = 3E-6), wavelength main effect (p-value = 0.55) and substrate-wavelength interactions (p-value = 0.045). Letters indicate substrate conditions with non-significant differences identified by the least square difference. 55

Figure 5-8: Average Hill's number from the Shannon index. Measurements correspond to the average Hill's number. Error bars represent standard error (n = 3). Two-way ANOVA was done to test the significance of the substrate main effect (p-value = 7E-6), wavelength main effect (p-value = 0.12) and substrate-wavelength interactions (p-value = 0.49). Letters indicate substrate conditions with non-significant differences identified by the least square difference..... 56

Figure 5-9: Evenness plot. Evenness was calculated by taking the exponential of the Shannon index and dividing that by the richness. Measurements correspond to the average. Error bars represent standard error (n = 3). Two-way ANOVA was done to test the significance of the substrate main effect (p-value = 7E-6), wavelength main effect (p-value = 0.12) and substrate-wavelength interactions (p-value = 0.49). Letters indicate substrate conditions with non-significant differences identified by the least square difference. 57

Figure 5-10: PCoA plot using Jaccard dissimilarity to visualize the differences in OTU community structures grown on different carbon sources and illuminated at (A) 850 nm and (B) 940 nm. Panel A and B depict the same plane of data, but the points were separated in two plots for clarity. Percentages on the axes represent the proportion of variation represented by the PCoA axis. Start (circles) means at the start of the SBR incubation (end of batch incubation) and End (squares) means the end of the SBR incubation. Seed is the community structure of the inoculum from the 4-L biomass reactor..... 59

Figure 5-11: PCoA plot using Bray-Curtis distance matrix to visualize the differences in OTU community structures grown on different carbon sources and illuminated at (A) 850 nm and (B) 940 nm. Panel A and B depict the same plane of data, but the points were separated in two plots for clarity. Percentages on the axes represent the proportion of variation represented by the PCoA axis. Start (circles) means at the start of the SBR incubation (end of batch incubation) and End (squares) means the end of the SBR incubation. Seed is the community structure of the inoculum from the 4-L biomass reactor..... 61

Figure 5-12: Phylum-level abundance of the classified OTUs at the beginning and end of the SBR operation. 850 nm reactors at the start (A) and at the end (B). 940 nm reactors at the start (C) and at the end (D). 63

Figure 5-13: Abundance of different families within the *Proteobacteria*. Blue bars represent *Gammaproteobacteria*. Green bars represent *Alphaproteobacteria*. Red bars represent *Betaproteobacteria*. 850 nm reactors at (A) Start and (B) end. 940 nm reactors at (C) start and (D) end..... 65

Figure 5-14: Abundance of PPB for the 850 nm reactors at (A): start and (B): end and for the 940 nm reactors at (C): start and (D): end. Enumeration was done on family level. Data from the three replicates were averaged. 67

Figure 6-1: COD profiles over time. (A) Total COD for 850 nm reactors. (B) Total COD for 940 nm reactors. (C) Soluble COD for 850 nm reactors. (D) Soluble COD for 940 nm reactors..... 77

Figure 6-2: Phosphate profile over time. Measurements correspond to the average of four replicates; error bars represent one standard deviation. (A): Soluble phosphate profile for 850 nm reactors. (B): Soluble phosphate profile for the 940 nm reactors. (C): Difference between total phosphate and soluble phosphate measurement for 850 nm reactors. (D): Difference between total phosphate and soluble phosphate for 940 nm reactors. Two-way ANOVA was done to assess significance of the substrate main effect, wavelength main effect and substrate-wavelength interactions. Results indicate that none of parameters were significant. 79

Figure 6-3: pH profile over time for the batch reactors. Horizontal axis represents dimensionless time in multiples of HRT. Vertical axis is magnified (starting at 6) to highlight differences between reactors. One-way ANOVA was done to assess the significance of the differences using data after 2.5 HRTs. Letters indicate reactors with non-significant differences identified by the least square difference. 80

Figure A-1: 850 nm irradiance profile at variable distances. Measurements were taken from the center of the lamp at distances of 29 cm, 45.5 cm and 62 cm. 92

Figure A-2: 940 nm irradiance profile at variable distances. Measurements were taken from the center of the lamp at distances of 12.5 cm, 29 cm and 45.5 cm. 92

Figure B-1: Images of the reactors after the initial batch incubation. (A): Controls from left to right, Syntho, Acetate, Starch, Milk and Glycerol. (B): 850 nm Syntho reactors. (C): 850 nm Acetate reactors. (D): 850 nm Starch reactors. (E): 850 nm Milk reactors. (F): 850 nm Glycerol reactors. 93

Figure B-2: Images of the reactors after the initial batch incubation. (A): 940 nm Syntho reactors. (B): 940 nm Acetate reactors. (C): 940 nm Starch reactors. (D): 940 nm Milk reactors. (E): 940 nm Glycerol reactors. 94

Figure B-3: Images of the reactors after the sequencing batch operation. (A): Controls from left to right, Syntho, Acetate, Starch, Milk and Glycerol. (B): Syntho reactors. (C): Acetate reactors. (D): Starch reactors. (E): Milk reactors. (F): Glycerol reactors. 95

LIST OF ABBREVIATIONS

A

AS: Activated sludge

ADP: Adenosine diphosphate

ATP: Adenosine triphosphate

B

BChl-a: Bacteriochlorophyll a

BPh: Bacteriopheophytin

C

CO₂: Carbon dioxide

COD: Chemical Oxygen Demand

D

DAPI: 4',6-diamidino-2-phenylindole

ddH₂O: double distilled water

DNA: deoxyribonucleic acid

E

EBPR: Enhanced biological phosphorus removal

F

FITC:

G

GDP: guanosine diphosphate

GTP: guanosine triphosphate

H

HRT: Hydraulic retention time

H₂: Hydrogen gas

I

IR: Infra-red

M

MMC: Mixed microbial community

O

O₂: Oxygen gas

OD: Optical Density

OTU(s): Operational taxonomic unit(s)

P

PAO(s): Phosphorus accumulating organism(s)

PCoA: Principal coordinate analysis

PHA(s): Poly-hydroxyalkanoate(s)

PHB: Poly-hydroxybutyrate

PHBV: Poly-hydroxybutyrate-co-hydroxyvalerate

PHV: Poly-hydroxy valerate

poly-P: Poly-phosphate

PBR: Photo bioreactor

PNSB: Purple non-sulfur bacteria

PPB: Purple Phototrophic Bacteria

PPK: poly-P Kinase

PSB: Purple sulfur bacteria

PTS: phosphotransferase system

R

rRNA: Ribosomal ribonucleic acid

S

SBR: Sequencing Batch Reactor

sCOD: Soluble chemical oxygen demand

SRT: Solids retention time

SS: Suspended solids

T

tCOD: total chemical oxygen demand

TN: Total nitrogen

TP: Total phosphorus

TS: Total solids

TSS: Total suspended solids

V

VFA: Volatile fatty acid

VS: Volatile solids

VSS: Volatile suspended solids

W

WWTP: Wastewater treatment plant

1 INTRODUCTION

1.1 Wastewater Treatment: A Historical Perspective and Future of the Art

Since the industrial revolution, anthropogenic wastes have been constantly increasing, which became problematic as the environment's natural capacity to treat wastes has remained constant. Treatment plants were designed to reduce the strength of wastes discharged such that the environment could complete the treatment without any adverse effects on local human, animal and plant populations. However, treating wastes is not the only concern associated with the increased industrial activity, and the accompanied rise in consumption puts significant pressures on natural resources. As demand for resources kept increasing and with increasing ambitions of treating wastewater as a net-energy source (McCarty et al., 2011), the concept of a waste became more obsolete and the wastewater treatment industry started redeveloping into resource-recovery centers - plants that remove pollution from the water by converting it into nutrients, resources and energy.

Current discharge regulations only aim to preserve environmental conditions, which explains why treatment plants have only been concerned with removing pollution. The vast increase in research on resource-recovery processes have demonstrated the advantage of a resource-recovery process with respect to sustainable development. The ensuing social forces have driven resource-recovery innovation to be led by technology providers, which culminated in the shift towards resource-recovery for treatment plants. Fundamentally, resource-recovery is a broad term that describes any process that aims to convert wastes into valuable products. In the context of wastewater treatments plants, biological resource-recovery takes place either through (a) direct biomass uptake to increase the biomass's market value (e.g. higher nutrient fertilizer), or (b) microbial production of valuable by-products. Enhanced biological phosphorus removal (EBPR) is an example of a

biomass uptake recovery process. EBPR enriches for a biomass capable of accumulating significantly larger quantities of phosphorus than typical activated sludge biomass does through assimilation. The EBPR-specialized biomass concentrates phosphorus from the wastewater in intracellular reserve polymers of poly-phosphates (poly-P). Anaerobic digestion is an example of a microbial production process. The process takes in wastewater or waste activated sludge to anaerobically convert it to methane gas. This process reduces the amount of solid wastes to be disposed of by the plant while recovering energy.

The economic feasibility of a resource-recovery process relies on high conversion yields coupled with a low process energy and chemical inputs. The classical activated sludge process heavily relies on aeration to provide the biochemical metabolic energy for biomass growth. Aeration accounts for over 50% of the process energy demands of a typical wastewater treatment plant (Metcalf and Eddy, 2003). Considering the mechanical energy required to aerate, aeration is an inefficient method for delivering metabolic energy to the microorganisms for high yield biochemical transformations. Also, biomass respiration converts some of the carbon and nitrogen in the wastewater into CO₂ and nitrates, respectively. This reduces the capacity for resource-recovery of the process. It is clear that to promote the implementation of a resource-recovery process, the treatment has to reduce its dependence on aeration (i.e. anaerobic process) and respiration.

Anaerobic processes require lower process energy input than aerobic ones. However, these processes are associated with poor biomass yields as the environment lacks in energetic electron acceptors (i.e. oxygen and nitrates). The anaerobic biomass derives its energy through low-energy electron acceptors (e.g. sulfates) or from fermentation. In either case, a greater portion of the substrate is consumed to produce metabolic energy than in an aerobic environment. In addition,

due to the lower metabolic energy available, anaerobic biomass tend to grow more slowly and to provide limited nutrient removal (McCarty et al., 2011).

Limitations associated with anaerobic systems can be addressed by supplementing them with light energy. Light promotes the growth of specialized photoheterotrophs that decouple their energy and carbon needs, which are both met by the organic substrate for chemoheterotrophs typically grown in wastewater treatment systems. Photoheterotrophs meet their energy needs with light and their carbon needs with organic substrates. Assuming the energy production efficiency to be the same, delivering biochemical energy for high yield conversions by illumination is theoretically more efficient than by aeration because of the reduced number of factors leading to inefficient transfers. Incidentally, the advancements in light-emitting diodes has made it possible to provide light energy with virtually no heat dissipation compared to conventional light sources. Anaerobic photo bioreactors (PBRs) promise to combine the energy efficiency of an anaerobic process with the high growth rates of an aerobic one while also achieving higher conversion yields due to the reduced demand on substrate for energy.

The current thesis aims to contribute to the transition from conventional wastewater treatment to a resource recovery process through utilization of an alternative to the conventional activated sludge wastewater treatment process. The proposed alternative under study incorporates an external infrared (low energy) light source to supplement an anaerobic process that is operated in such a fashion that the biomass exhibits accumulative behavior leading to high nutrient removal and high carbon conversion yields.

1.2 Objectives of this work

From the published literature, a number of knowledge gaps were noted that can have implications on the engineering and operation of PBRs cultivating PPB. The main knowledge gaps identified are the effect of the wavelength of the incident light on the growth of PPB and the microbial structure of the enriched microbial communities. Following the recognition of these knowledge gaps, the objectives of this thesis are:

1. Construction of a first (in our lab) 4-L scale infrared (IR) photobioreactor and the description of its basic operation, enriched microbial community and poly-phosphates accumulation. (Chapter 4)
2. Description of the microbial populations that grow on each of the carbonaceous components of synthetic wastewater (Syntho) as sole carbon sources. (Chapter 5)
3. Determination of the capacity to predict the synthetic wastewater community based on the independent results of individual carbon sources. (Chapter 5)
4. Comparison of the level of poly-phosphate accumulation between reactors subjected to intermittent and continuous illumination. (Chapter 6)
5. Investigation of the effect of changing IR wavelength (850 nm and 940 nm) on poly-P accumulation and the microbial community. (Chapters 5 and 6)

1.3 Thesis Organization

This thesis consists of seven chapters and four appendices. Following Chapter 1, the chapters are organized as follows:

Chapter 2, Literature Review: Review of the relevant literature required to properly discuss the operation of a photobioreactor and the behavior of the enriched biomass. The chapter begins with

a review on phototrophy, the different color niches of phototrophic organisms then restricts discussion to purple bacteria. The photosystem of a prototypical purple organism is reviewed including the pigments, light-harvesting centers and the reaction center. The chapter then follows with some of the metabolic properties of purple bacteria. Poly-phosphates as a potential resource to be recovered by purple bacteria is also reviewed; a hypothesis is introduced involving the selection of phosphorus accumulators in a photobioreactor. The chapter concludes with some of the identified research gaps with applicable potential for wastewater treatment.

Chapter 3, Materials and Methods: This chapter describes the various chemical and physical tests conducted to quantify wastewater properties (chemical oxygen demand (COD), solids, phosphates). The preparation of the feed (synthetic wastewater) used for all the experiments is described.

Chapter 4, Main Large (4-L) Reactor: Report on the construction of a PBR enriching for PPB. The report covers the steady-state performance described through COD, solids and phosphate data. The enriched microbial populations using 16S rRNA gene amplicon sequencing analysis are also described. This chapter addresses objective 1.

Chapter 5, Enrichment Experiment in Small (60-mL) Reactors: Experiment that enriches PPB in serum vials fed with single carbon sources of the main feed. The experiment also compares the effects of changing light wavelength on the microbial community. The communities are described through abundance analysis at the phylum-level with the major phyla being discussed more deeply. Similarity analysis between reactors is visualized through principal coordinate analysis. This chapter addresses objectives 2 and 3.

Chapter 6: Effect of Intermittent Illumination on Poly-P Accumulation by PPB: The hypothesis discussed earlier in the literature review is tested in this experiment. The effect of light wavelength on poly-P accumulation is compared. This chapter addresses objective 4.

Chapter 7: Conclusions: The major conclusions of chapters 4,5 and 6 are reiterated with a general discussion on their implications. Potential for future work is mentioned.

2 LITERATURE REVIEW

2.1 Phototrophy in Natural Systems: The Driving Force for Colour Niches

Phototrophy is the ability to derive metabolic energy from light. Diverse bacterial species are phototrophs, and each of them are equipped with light harvesting systems that can absorb light at specific wavelengths. As the light's wavelength relates to the energy it carries (short wavelength corresponds to high energy), the metabolic capacity and the electron donor of choice of each phototrophic species depends on the wavelength they absorb. At the short wavelength of the spectrum, oxygenic cyanobacteria can use low-energy electrons in water while producing oxygen. Conversely, at the long wavelength of the spectrum, anoxygenic purple bacteria rely on high-energy electron donors such as organic compounds or hydrogen gas. This series of specialized metabolisms generates a complex ecological system in nature.

As light is transmitted through water, critical wavelengths are responsible for resonance of either dissolved oxygen or water directly; these regions within the spectra are inaccessible to microorganisms. It is hypothesized that "colour niches" have developed around these absorption regions with each different niche exhibiting a unique pigment specialized at harvesting light at its respective wavelength (Stomp et al., 2007). The organisms utilizing IR fall under the purple bacteria classification. These produce bacteriochlorophylls a or b, which produce absorption peaks

at around 800, 870 and 1000 nm for purple nonsulfur bacteria and around 850 nm for purple sulfur bacteria. The discussion hereafter is focused on purple bacteria.

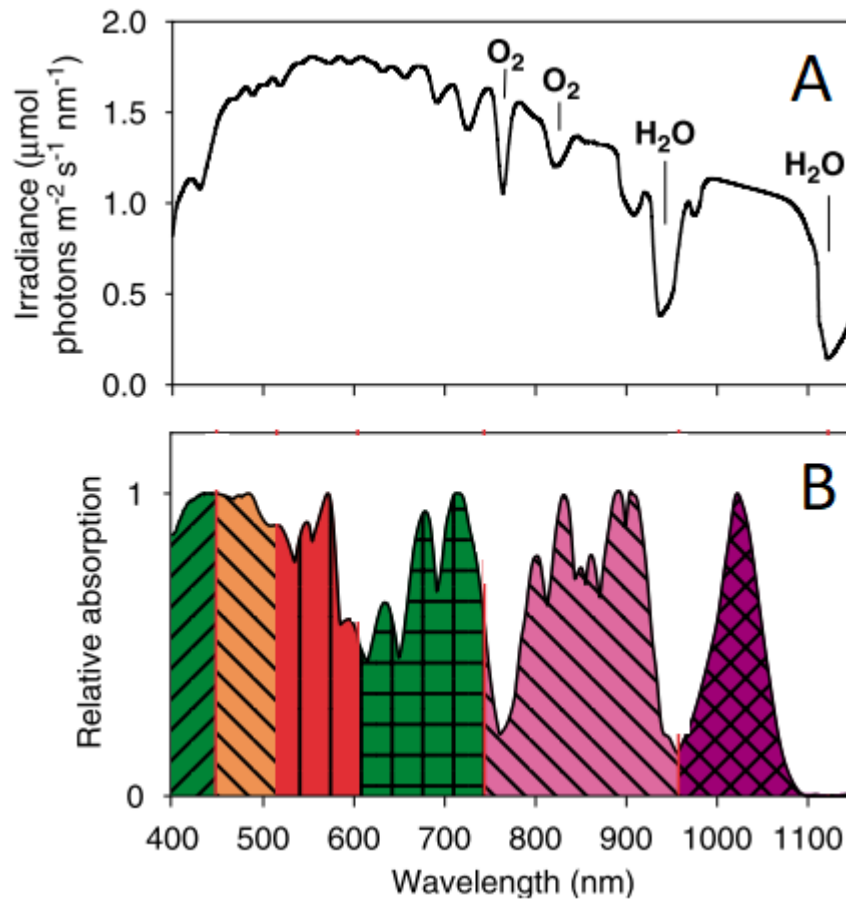


Figure 2-1: Colour niche of phototrophic organisms. (A): Irradiance profile in water. The steep drops are due to interception either by oxygen or water. (B): The different niches of microorganisms; the segregations match the irradiance drops. Reproduced with permission from International Society for Microbial Ecology (Stomp et al., 2007).

2.2 Phylogeny of Phototrophic Purple Bacteria

The phototrophic purple bacteria (PPB) fall under the phyla *Alphaproteobacteria* and *Betaproteobacteria* for the purple non-sulfur bacteria (PNSB) and *Gammaproteobacteria* for the purple sulfur bacteria (PSB). Since the classification PPB is mainly phenotypic (i.e., production of

In recent years, the molecular study of microorganisms in their natural habitat and of isolates using both *pufML* and 16S rRNA gene sequences increased tremendously our knowledge and understanding of the diversity of PPB. For example, it is clearer today based on the phylogeny of known *pufML* genes that the evolution of the photosynthetic apparatus likely started within the members of the order *Chloroflexales*. Then, evolutionary forces gave rise to the other PPB through speciation and possible lateral gene transfer. As a result, the phylogeny of the *pufML* genes appears to be consistent with the phylogeny of the 16S rRNA for some orders (e.g. *Chloroflexales*, *Chromatiales*, *Rhodobacterales* and *Burkholderiales*) harbouring PPB genera. However, this is not the case for the genera of other orders (e.g. *Rhizobiales*) that are more sparsely distributed through the *pufML* tree (Figure 2-2) (Imhoff et al., 2017).

The expansion of the knowledge of the diversity of PPB was in the most part due to the discovery of several aerobic anoxygenic phototrophic purple bacteria genera (Yurkov and Hughes, 2017). This discovery deviates from the initial hypothesis that PPB are strictly anaerobes due to detrimental effect of oxygen on the main light-harvesting pigments, thus, making both metabolisms mutually exclusive. The phylogenetic distribution of aerobic and anaerobic taxa does not seem to follow a strict evolutionary pattern. Anaerobic PPB genera are assembled in a few mainly monophyletic lineages among the aerobic PPB (Imhoff et al., 2017). At the same time, both aerobic and anaerobic PPB genera are closely related with respect to the *pufML* and 16S rRNA gene data. From this pattern, it seems that the evolutionary process can be understood as the expansion of the initial anaerobic lineages to occupy new aerobic habitats.

2.3 The Photosynthetic Apparatus: Generating Biochemical Energy from Light

Cells transfer biochemical energy between reactions through a molecule known as adenosine triphosphate (ATP), which is primarily produced by the enzyme ATPase (or ATP synthase). ATP synthase's operation is mediated by a cationic gradient across the cell's membrane, most commonly a proton gradient known as the proton motive force (PMF). Phototrophic organisms generate this gradient through their photosynthetic apparatus that uses specialized pigments to harvest light energy at specific wavelengths. The collection of light energy culminating with the production of biochemical energy in the form of ATP is known as photophosphorylation. This process relies upon a network of interconnected molecules imbedded within the membrane of the cell.

Bacteriochlorophyll a (BChl-a) is a light harvesting pigment located in the membrane and capable of withdrawing photons in the infrared range (Madigan et al., 2015). The pigment is present in light harvesting complexes (a dense structure of pigments) in the membrane as well as the reaction center, which initiates cyclic electron transport. The absorption of the pigment is maximized in the 800 – 950 nm range and is dependent on the supporting polypeptides (chromophores) attached to it (Hu et al., 2002). As an example, BChl-a present in the light-harvesting complexes harvest photons at a wavelength of 800 or 850 nm while BChl-a in the reaction center is capable of harvesting photons at 875 nm (Hu et al., 2002). Considering the narrow absorption bandwidth for BChl-a, this distinction in absorption wavelengths allows the organism to cover more of the infrared range while also allowing for spontaneous excitation transport from higher to lower energy between the light harvesting complexes (LHCs) and the reaction center (Figure 2-3).

PPB also produce carotenoids, a class of unsaturated hydrocarbons, which are the compounds responsible for giving these organisms their red-orange colors (Kuo et al., 2012). These molecules are either embedded within the LHCs of the cell or suspended within the environment (Cogdell and Frank, 1987). Within LHCs, carotenoids are capable of harvesting photons in the blue range of the visible spectrum (around 500 nm), thus supplementing the phototrophic capabilities of the cell (Kuo et al., 2012). In addition, carotenoids serve a critical role in photoprotection in mildly aerobic environments. The reaction center occasionally catalyzes a reaction that produces singlet oxygen (i.e. excited form of oxygen) by transferring electrons to it. This reactive oxygen species directly oxidizes BChl. As such, the reaction center is catalyzing a self-destructive process (Cogdell and Frank, 1987). Carotenoids protect BChls by extracting the electrons from the reaction center before they can form singlet oxygen. This is feasible as carotenoids have a low-lying energy state below BChl's ground state (Hu et al., 2002). To a lesser extent, carotenoids suspended in the medium can directly react with singlet oxygen before it can damage BChl. As such, energy transfer between carotenoids and BChls occurs in both directions (Hu et al., 2002) (Figure 2-3).

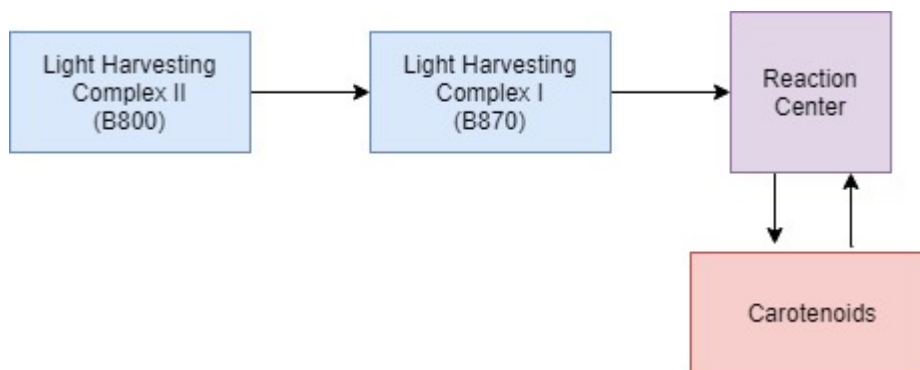


Figure 2-3: Energy transfer between various components in the photosystem. Arrows indicate direction of energy transfer. The energy transferred from the reaction center to carotenoids corresponds to triplet energy; the opposite arrow indicated singlet transfer.

The photosystem of purple bacteria is explained using *Rhodobacter sphaeroides* as a prototypical organism (Hu et al., 2002). Once the light harvesting pigments (bacteriochlorophyll or carotenoids) are excited, excitation is transferred to the BChl on L unit in the reaction center. In the reaction center, three protein subunits L, M and H provide the scaffolding necessary to support two BChl-a monomers (the special pair), two bacteriopheophytin monomers and one beta-carotene (Cogdell et al., 1997). The excitation in the reaction center is used to promote an electron in BChl-a to a higher energy state. The excited BChl-a and its associated bacteriopheophytin undergo charge separation forming BChl⁺ and BPh⁻. Charge separation is crucial for maintaining cyclic electron transport between various electron carriers as BChl⁺ is more receptive to low-energy electrons. Cyclic electron flow starts with BPh⁻ reducing quinone into hydroquinone. The electron transport subsequently proceeds through cytochrome bc₁ and cytochrome c₂ and culminating with the electron returning back to the original BChl. The reduction of quinone into hydroquinone sequesters two protons from the cytoplasm and the oxidation back to quinone releases the two protons into the periplasm. This establishes the proton gradient across the cell membrane that is the driving force for ATP synthesis.

For growth of microorganisms, the production of only ATP is not sufficient. Organisms also require reducing power, which is conserved in the reduced form of nicotinamide adenine dinucleotide (NADH). In the case of PNSB, the harvested light is not energetic enough to raise the electron energy to the level of NADH. NADH is produced through oxidation of organic substrate (organotrophy) (Madigan et al., 2015). Photosynthetic organisms can also leverage their photosystem to promote electrons from low energy donors into NADH. Contrary to other phototrophs, electrons transported from BPh to Q do not pass through an intermediate cofactor. The electrons in QH₂ are at a lower energy level than NADH, which requires that they first get

energized. This process is called reverse electron flow, which is an ATP-consuming process. Reverse electron flow results in a net consumption of electrons, to maintain cyclic flow of electrons for photophosphorylation, an inorganic electron donor can supplement this by donating electrons to an FeS cofactor (Madigan and Jung, 2009).

2.4 Metabolism of the Purple Bacteria

Purple bacteria are a class of anoxygenic photosynthetic organisms with a highly distinct metabolism to the other phototrophs. Metabolically, PSB are less sensitive to reduced sulfur compounds (i.e. elemental sulfur and sulfide) and are more capable of using them as electron donors when growing photoautotrophically. Physiologically, PSB are highly dependent on sulfide for electrons and are virtually absent when environmental concentrations are low. Heterotrophic capabilities of PSB are limited as they grow mainly on organic acids (Madigan and Jung, 2009). In contrast, PNSB are typically referred to as “metabolically versatile” organisms as they exhibit a variety of metabolic modes and can utilize many organic carbon sources. They are able to survive in both aerobic and anaerobic environments. This is contrary to most other anaerobic phototrophs that are fatally sensitive to oxygen. This metabolism allows them to grow in many environments. As such, purple bacteria have been discovered in a lot of systems in nature as well as engineered systems (e.g. WWTPs) (Madigan and Jung, 2009). Consequently, their metabolism has garnered a lot of attention from the scientific community

Under aerobic environments, PNSB derive their energy and reducing power (i.e. electrons carried by NADH) needs from the oxidation of organic and inorganic compounds (i.e. organotrophy and lithotrophy, respectively). As for their carbon needs, it is either provided directly from consumption of organic compounds or through the carbon fixation of CO₂ (i.e. chemotrophy and autotrophy, respectively) (Figure 2-4). Anaerobically, these organisms would derive their energy

from light (i.e. phototrophy). Alternatively, energy can be derived through fermentation. However, it appears that they have limited fermentative capabilities (Madigan and Jung, 2009).

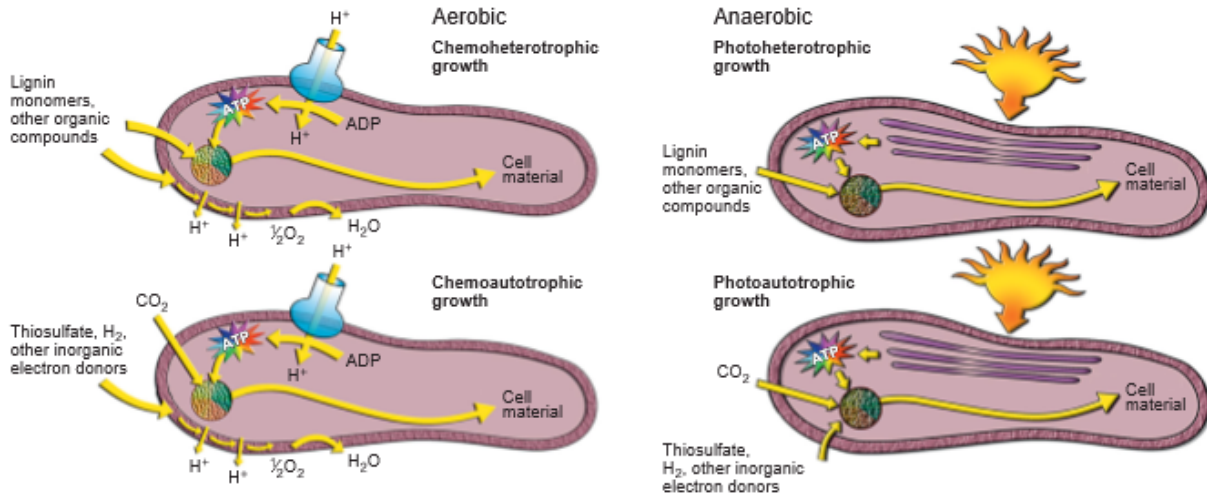


Figure 2-4: Overview of various PPB metabolic modes. Under oxic conditions, PNSB respire using oxygen to produce energy. Under these conditions they grow either heterotrophically or autotrophically. Anaerobically, PNSB leverage their bacteriochlorophyll (a or b) to harvest energy from the incident light. PPB also behave heterotrophically or autotrophically under these conditions. Reproduced with permission from Nature Biotechnology (Larimer et al., 2004).

2.4.1 Nitrogen Fixation

In addition to their versatility in carbon, energy, and reductant sources, purple bacteria can also assimilate nitrogen from various fixed sources, including ammonia and nitrate. Furthermore, virtually all purple bacteria are capable of fixing nitrogen into ammonia by reducing nitrogen gas (Madigan et al., 2015). The process is catalyzed by the enzyme nitrogenase. Different metal cofactors (iron [Fe], vanadium [V] or molybdenum [Mo]) in the nitrogenase enzyme result in different stoichiometries for nitrogen fixation (Equations 1,2 and 3) (Basak et al., 2014).





Considering that Mo-nitrogenase requires the least amount of energy and electrons to fix the same amount of nitrogen, it is clearly the most efficient enzyme. It is therefore understandable that most purple bacteria appear to have Mo-nitrogenase. Some purple bacteria can express multiple variations of nitrogenase. For example, sequencing of the complete genome of *Rhodospseudomonas palustris* revealed the presence of the genes encoding all three nitrogenases (Larimer et al., 2004). This gives the organism the ability to adapt to metal deficiencies in environment. Additionally, V-nitrogenase and Fe-nitrogenase are more efficient at dissipating excess reducing power giving the organism a more flexible metabolism. Because nitrogen fixation is metabolically very costly, ammonia strongly represses nitrogenase expression, making it the main controlling factor of nitrogenase expression. Finally, the strong electron acceptation capacity of oxygen gas irreversibly inhibits nitrogenase (Trchounian, 2015)

In the absence of nitrogen, Mo-nitrogenase seems to also catalyze a reaction (Equation 4) similar to that of hydrogenase except that is it dependent on ATP instead of reductant carrier (Ghosh et al., 2017):



This property attracted a lot of attention from the renewable energy community for the industrial production of hydrogen. Because of this, the metabolism of purple bacteria is very well characterized and several metabolic models have been constructed (Basak et al., 2014; Carlozzi et al., 2010)

2.4.2 PHA Accumulation

Under excess carbon, reductant and energy conditions, PPB can store a lipid polymer known as poly-hydroxyalkanoate (PHA). PHAs are intracellular polymers synthesized as carbon and energy reserves for microorganisms and they form stored as cytoplasmic granules (Guerra-Blanco et al., 2018) of molecular weights ranging between 10,000 and 3,000,000 g/mol (Reis et al., 2011).

In PPB, short-chain fatty acids are converted into either hydroxy-butyrate (HB) or hydroxy-valerate (HV) (Albuquerque et al., 2011; Ghimire et al., 2016). These two monomers are subsequently used to synthesize a polymer of HB and HV known as PHBV (Figure 2-5). HB monomers are produced from the utilization of shorter VFAs such as acetate and butyrate while propionate and valerate were associated with HV production (Wang et al., 2017). The ATP cost of HV synthesis is lower than that of HB (Wang et al., 2017), as such, HV synthesis is a more favored pathway. This observation is consistent with change in volatile fatty acid (VFA) of mixed VFA systems, HV precursors are consumed before HB precursors (Albi and Serrano, 2016). By manipulating VFA composition in the feed, it is possible to alter the HB and HV content of the PHA produced.

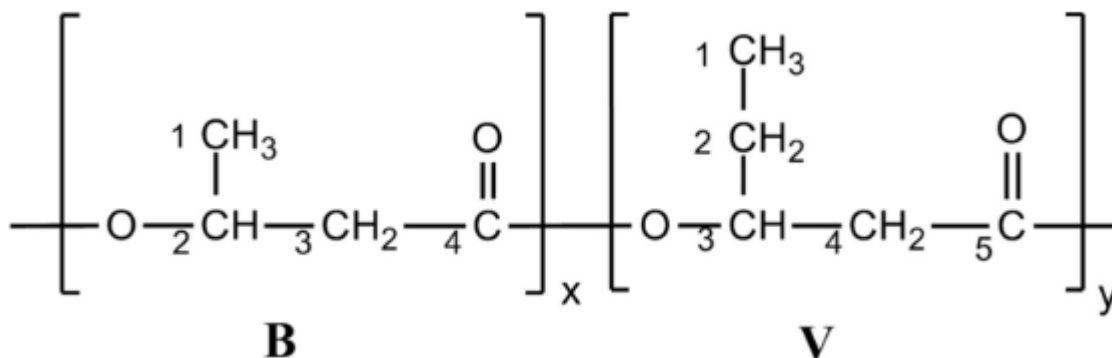


Figure 2-5: General structure of PHBV polymer. (B) Corresponds to HB monomers. (V) Corresponds to HV monomers.

The capability of PPB to accumulate PHA have also attracted a lot of interest from the biotechnology community. This is because these compounds have similar characteristics to conventional petroleum-based plastics. Consequently, PHAs can be used as renewable and biodegradable plastics. Studies have established that the physical properties of the PHA polymer (e.g. melting temperature, glass transition temperature and crystallinity) are dependent on the length of the monomer side chain, with longer side chains (i.e. HV) being less crystalline (Ghosh et al., 2017; Reis et al., 2011)

2.4.3 Poly-Phosphate Metabolism by Purple Bacteria

Phosphorus and nitrogen are key nutrients responsible for the aging of waterbodies (algal blooms and eutrophication). Unlike nitrogen, phosphorus lacks a gaseous form, limiting its removal mechanisms to either biomass assimilation or accumulation of storage polymers decoupled from growth. Assimilative-removal corresponds to the phosphate taken out of the aqueous phase by incorporation into the biomass. Considering that the average biomass elemental composition in activated sludge systems is $C_5H_7O_2NP_{0.1}$, the mass of proportion of phosphorus of the biomass' dry weight corresponds to 2-3%. This highlights the limited capacity of assimilative nutrient removal, which can be remedied by dosing extra COD into the reactor. Accumulative removal of ortho-phosphates relies on the ability of some microorganisms to store phosphates into polymers of poly-phosphates (poly-P). These organisms have phosphorus contents in biomass as high as 10%. Therefore, the accumulative removal is much more efficient at utilizing the available COD to accomplish the treatment objectives.

Regulation of the polymer is done through the enzymes poly-P kinase 1 (PPK1), poly-P kinase 2 (PPK2), exopolyphosphatase (PPX) and phototransferase (Madigan et al., 2015). PPK1 is

responsible for regulating an equilibrium between ATP and poly-P; the enzyme is capable of catalyzing the reaction in either direction. PPK2 catalyzes the breakdown of poly-P by transferring the terminal phosphate in poly-P to guanosine diphosphate (GDP) forming guanosine triphosphate (GTP). Similarly, PPX catalyzes the hydrolysis of poly-P resulting in a discharge of phosphate. Phosphotransferase system (PTS) transfers a terminal phosphate to AMP forming ADP. Intricate control of these reactions allows the microorganisms to regulate the pools. Organisms lacking PPK1 were also observed to accumulate poly-P, indicating that there are more enzymes that are capable of creating the polymer.

It seems that one of the primary functions of poly-P is to store energy (Albi and Serrano, 2016). Phosphate-accumulators are capable of storing excess energy by polymerizing the extra ortho-phosphates (from ATP) into a chain of poly-P. The bonds formed in the polymer are identical to the high energy bonds in ATP. This allows these organisms to accumulate energy reserve in the form of poly-P to act as an energy reserve. Depending on the specific mechanism for polymerization of ortho-phosphates, different forms of the polymer have been observed (Figure 2-6).

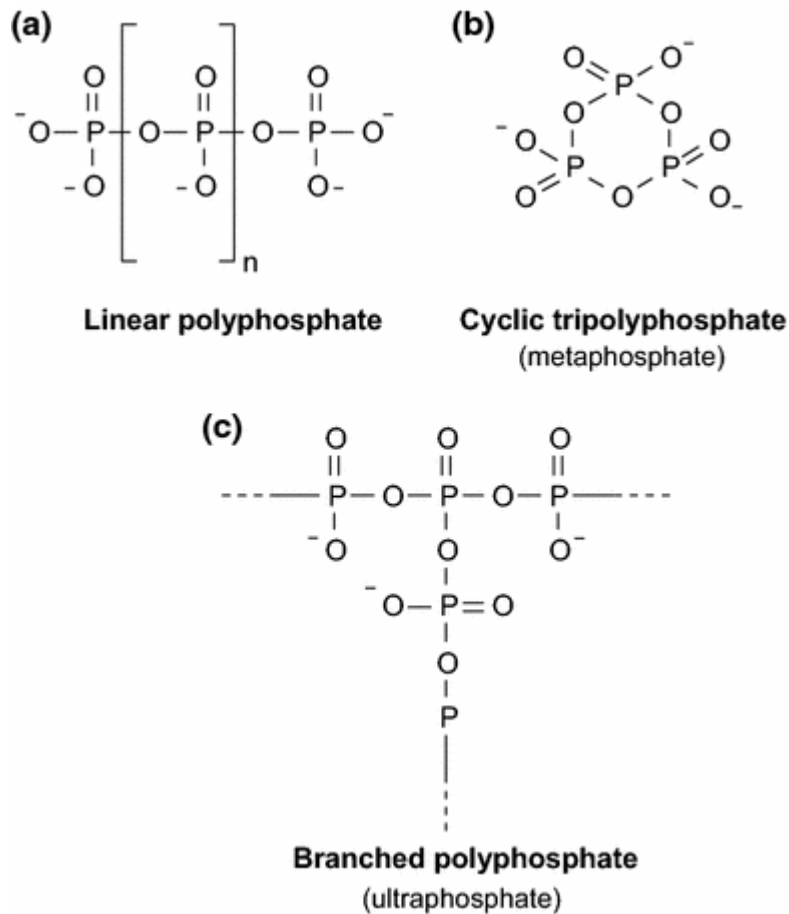


Figure 2-6: Different structures of poly-P. These structures are built from polymerization of the terminal phosphate from ATP forming an identical phosphoanhydride bond in the polymer. Polymer formation can result in a linear chain form (a) or a branched form (b) and (c).

In bacteria, poly-P serves purposes beyond energy and phosphorus storage. The polymer can serve structural purposes by combining with other complexes, can mediate ion transport through the membrane, and can act as a stress-protective polymer for proteins either to dissipate heat to avoid enzymatic denaturization or as pH control buffer (Albi and Serrano, 2016).

In an experiment growing pure cultures of *Rhodobacter sphaeroides* using malate as a carbon source, an increase in the P/C ratio was shown to linearly increase poly-P content in the organism, leading to 6.2% [mg-P/mg-biomass] poly-P content under a P/C ratio of 10 (Hiraishi et al., 1991).

In another study, aqueous nitrogen limitations were investigated on the same organism under similar light conditions. The study found that when the medium was deficient in nitrogen, nitrogenase activity increased, which limited the organism's ability to accumulate poly-P since nitrogenase activity was responsible for dissipating ATP (Hiraishi and Kitamura, 1985). This further highlights the importance of inhibiting nitrogenase when attempting to accumulate polymers as its activity seems to conflict with PHA production and poly-P accumulation.

In a study using eight different isolates (CC1, CC2, CC7, CC8, G11, GN5, GX4 and GE1) of *Rhodospseudomonas palustris* from an activated sludge reactor, the capacity for phosphorus accumulation was assessed under phosphate-rich nitrogen-sufficient media (Liang et al., 2010). Using light-dark cycling as an environmental stress for poly-P accumulation, the study found that all the isolates were capable of accumulating phosphorus with an average content of 6% [mgP/mgVSS]. G11 exhibited the highest yield with a maximum content of 15%. The study also demonstrated the effects of oxygen on poly-P accumulation. Under aerobic environments, light or dark, the phosphorus content of the organisms dropped over time. This could be due to the inhibitory effects of oxygen on BChl, which in turn reduced the organism's access to the external energy source forcing it to utilize the internal poly-P reserves. The effect of pH was also investigated by comparing behavior under buffered and non-buffered setups. Under pH-buffered conditions, the organisms accumulated slightly more polymer. In non-buffered conditions, the pH was observed to increase, which suggests that either the accumulation process is sensitive to an increase in pH or that the poly-P reserves could be used for mild pH control.

2.5 Purple Bacteria in Wastewater Treatment

2.5.1 COD, Nitrogen and Phosphorus Removal in Photobioreactors by PPB

Research involving PPBs in non-sterile settings is currently very limited. Yet, it is critical to wastewater treatment because wastewater cannot be feasibly sterilized. In order to fully realize their usefulness in wastewater treatment and resource-recovery, we must be able to select for their growth. Infrared light has been shown to be a very consistent selective pressure (Hulsen et al., 2018).

Hulsen et al. (2014) provided one of the first proof of concepts of a mixed-microbial reactor of PPB cultivated in a batch mode using real wastewater from Australia. These photobioreactors removed over 60% of the COD and assimilated almost all the nitrogen and phosphorus. These initial results were later scaled up to a continuous membrane bioreactor operated at an SRT of 3 days that removed nearly 100% of the COD and all the phosphate available (7 mg-P/L). 16S rRNA gene amplicon sequencing of the reactor community showed clear PPB dominance (abundance greater than 70% of the reads).

The same research group also demonstrated the removal efficiency of PPB with highly saline wastewater (NaCl concentration of about 30 g/L). Highly saline wastewaters are indicative of industrial wastewaters. Also, with a solids retention time (SRT) of three days and membrane solids separation, the removal efficiencies achieved by the anaerobic photobioreactor reached 90% of the COD, 70% of the total nitrogen, and fluctuated between 30 and 60% for the total phosphorus. The microbial community was analyzed using 16S rRNA amplicon sequencing. Between 40 and 50% of the reads were associated with phototrophic bacteria (mainly belonging to the genus *Rhodovulum*). The abundance of phototrophic organisms decreased to zero rapidly when the reactor operation was made aerobic. This was due to toxic effect of oxygen on the light-harvesting

pigments. Similar performance was achieved with red sea salt instead of NaCl. However, the microbial community comprised of only 20% (by reads) phototrophic organisms (Hulsen et al., 2019). These results highlight the potential of using photobioreactors receiving IR in wastewater treatment.

2.5.2 Selective Pressure for Poly-P Accumulators

In open microbial communities, there is a presence of a diverse set of organisms that contribute specialized metabolic functions to the overall community. Some functions are more beneficial than others, thus, one aim is enhancing the desired metabolism by setting up appropriate ecological conditions that favors the growth of organisms contributing the ideal metabolic function. In order to promote the accumulation of poly-P by purple bacteria, the operation of the reactor must be adjusted such as to give them a competitive advantage.

In an EBPR process, biomass is cycled between oxic or anoxic (high metabolic energy environment with active electron acceptor transport chain for ATP production) and anaerobic (low metabolic energy environment with limited ATP production) environments. ATP is required to transport acetate across the membrane, and it is limited in the anaerobic environment. Phosphate accumulating organisms (PAOs) are capable of using their poly-P to synthesize ATP in the absence of O_2 or NO_3^- . Biomass cannot be produced immediately and the excess carbon and reducing power are stored in PHA. PHA is later utilized when the biomass is returned to the oxic or anoxic environment to produce new biomass and replenish the poly-P pool. Since other chemo-organo-heterotrophs do not have access to this energy source, these organisms will have a limited capacity to uptake acetate while in the anaerobic environment. As such, this cycling gives PAOs a competitive edge over the non-accumulating heterotrophs. Following our hypothesis that poly-P is mainly an energy reserve for the PPB, we further hypothesize that cycling between light and

dark environments will impose a positive selective pressure on poly-P accumulators because they would survive better in the dark periods. As a result, the biomass will have higher phosphate uptake and poly-P accumulation metabolism.

2.6 Research Gaps

Following the hypothesis that different organisms express different color niches allowing them to acquire energy from different light sources. These color niches create characteristic absorptions profiles based on the organism(s) enriched. What remains unexplored is how different IR wavelengths can have an impact on the organisms enriched and the behavior they exhibit.

While adequate wastewater treatment performance appears to be viable using PBRs and PPB appear to be able to accumulate resources (PHA and poly-P), the potential for resource recovery from wastewater in mixed-microbial settings remains an unexplored territory. The objectives formulated in Chapter 1 were designed to address some of these research gaps (resource recovery from wastewater, enrichment variance due to IR wavelength).

3 MATERIALS AND METHODS

This chapter lists the general analytical methods used in the following chapters. Experimental set up of each experiment is discussed in its respective chapter.

3.1.1 Synthetic Wastewater

Synthetic wastewater (Syntho) was prepared according to Nopens et al. (2001) with adjustments to the phosphorus composition.

Table 3-1: Prepared Syntho composition.

Constituents	Supplier (CAT #)	Concentration (mg/L)
Carbon sources		
Sodium acetate	Fisher Scientific, 136118	120
Dry meat extract ¹	BD, 211520-500G	15
Glycerol	Fisher Scientific, BP229-1	40
Starch		50
Milk Powder ¹	Nestle, 43402073	120
LAS	Aldrich Chemistry, 289957-500G	10
Genapol X-080	Sigma Aldrich, BCBN8857V	10
Nitrogen sources		
Peptone		15
Urea	Anachemia, 96238-380	75
Uric Acid	Sigma Aldrich, U2625-25G	9
Ammonium Chloride	Fisher Scientific, 135887	11
Phosphorus sources		
Tripotassium Phosphate	Acros Organics, 387685000	20
Magnesium Hydrogen Phosphate	Chem Cruz, SC-250282	25
Other		
Diatomaceous earth	Fisher Scientific, S75114	10

1: Also, a nitrogen source

For the carbonaceous constituents (except milk powder), 200x stock solutions of each constituent was prepared. Milk powder was not added due to the difficulty of preserving the consistency of

the solution over time. For nitrogenous constituents (except uric acid) and diatomaceous earth, a complete 200x stock solution was prepared. Uric acid was not added to this stock due its limited solubility.

Starch is inherently insoluble under ambient conditions. 200x starch stock solution was prepared by adding 10 g of starch powder to about 700 mL of double-distilled water (ddH₂O). The solution was then placed on a hot plate at 300 °C until the powder completely dissolved. While heating, the solution was occasionally stirred. Solution was then transferred to a volumetric flask and topped to a volume of 1 L. Stock was then transferred to a clean bottle and sterilized in the autoclave.

The 50x phosphorus stock was prepared using tripotassium phosphate and magnesium hydrogen phosphate. Magnesium hydrogen phosphate (1250 mg) was added to about 700 mL of ddH₂O. Monitored using a pH-meter, the solution was acidified using 1 M HCl, pH was maintained around 5. Once powder has completely dissolved (typically takes overnight), 1 g of tripotassium phosphate was added and the pH was adjusted to 7 using 5 N NaOH. Solution was then transferred to a volumetric flask, its volume adjusted to 1 L using ddH₂O, transferred to a clean bottle and sterilized in the autoclave.

Synthetic wastewater was prepared by diluting the stock solutions down to 1x with ddH₂O. Uric acid powder and milk powder were added directly to the complete solution. The complete feed had a measured COD content of 430 mg/L, TP content of 20 mg-P/L, 40 mg-N/L and a pH of 7.05.

3.1.2 Light Source

IR was delivered to the reactors through a camera IR emitter. These lamps operate when placed in the dark. A piece of tape was placed in the center of the lamp to block the light sensor

ensuring the lamp is continuously operating. Lamp characterization is available in APPENDIX A: Lamp Characterization.

3.1.3 Analytical Methods

3.1.3.1 *Chemical Oxygen Demand (COD)*

Chemical oxygen demand was assessed photometrically using potassium dichromate as an oxidizing reagent (APHA, 2012). COD reagent was prepared using 5.108 g of potassium dichromate and 33.3 g of mercury sulfate to 300 mL of ddH₂O in a 500-mL volumetric flask. Sulfuric acid (167 mL) was slowly poured into the flask and the volume was adjusted to 500 mL with ddH₂O. A stir bar was then added and stirred magnetically overnight. Sulfuric acid reagent was prepared by adding 4.8575 g of silver sulfate directly to a 500-mL bottle of sulfuric acid. Contents were magnetically stirred overnight. Bottle-top dispensers were added to the reagent bottles. A 2-mL sample was transferred to a clean test tube. Oxidizing reagent (1.2 mL) was added using the bottle-top dispenser. Sulfuric acid reagent (2.8 mL) was slowly dispensed to the inner wall of the test tube such that it settled to the bottom and formed two distinct layers; this slows down the exothermic reaction involving H₂SO₄ and the tube contents. Tubes were then capped and inverted to mix reagents. Tubes were then immediately transferred to a COD digester (45600, HACH, London, ON). The COD digester was operated at 120 °C for at least two hours. Once digestion was done, the absorbance at 600 nm of the samples was measured with a tube spectrophotometer (333183000, Thermoscientific, Saint Laurent, QC) equipped with a red filter against the blank sample. COD calibration curve was prepared using known additions of glucose.

3.1.3.2 *DNA Extraction and Quantification*

DNA extraction was done using a commercial kit (12955-4, Qiagen, Montreal, QC) and following supplier instructions. Prior to DNA extraction, biomass samples were collected using 2 mL tubes.

These tubes were autoclave (2540E-B/L, Tuttnauer, Hauppauge, NY) sterilized. Biomass samples were centrifuged (75002437, ThermoScientific) and decanted to remove water content. As an alteration to the supplied instruction, beads were transferred directly to the collection tube as opposed to biomass being transferred to the beads tube. This was the only alteration done to the supplied protocol.

Quantification was done using Picogreen (P11496, ThermoScientific), and following the protocol corresponding to the plate reader (Molecular Probes Data Sheet MP 07581, 2005). The 1x TE buffer (10 mM Tris-HCl, 1mM EDTA, pH 7.5) was prepared using the 20x stock included in the kit and diluting in DNase-free water. Working solution of PicoGreen was prepared by diluting the included stock 200 times in 1x TE buffer. The solution contents were covered using aluminum foil to protect from the light. A 100- μ L sample to be tested was pipetted to a black 96-well plate (655096, Greiner Bio-One, Monroe, NC). Working solution (100 μ L) was then added and mixed by pipetting up and down. The plate was then incubated in the dark for five minutes. A calibration curve was prepared using the included DNA stock; the final concentrations prepared were 1 μ g/L, 100 ng/L, 10 ng/L and 1 ng/L for the high-range curve and 25 ng/L, 2.5 ng/L, 250 pg/L and 25 pg/L for the low-range curve. After incubation, the plates were transferred to the plate reader; fluorescence was measured using an excitation wavelength of 490 nm, emission wavelength of 525 nm and a cutoff of 515 nm.

3.1.3.3 Solids

Both suspended solids (SS) and total solids (TS) tests were done. For TS, the tests were conducted directly in porcelain plates (08-732-101, ThermoScientific). Prior to testing, the plates were primarily incubated overnight in an oven (51028112, Thermo Scientific) set at 103 °C. Following primary incubation, the plates were then ignited at 550 °C for 15 minutes in an incinerator. Then,

the plates were left to reach room temperature in a desiccator. Plates were then weighed using a high-precision scale capable of reporting mass to a four-decimal precision. A 20-mL sample was pipetted to each plate and the plates were incubated overnight to remove the water. Plates were then left to cool to room temperature in a desiccator and their mass was measured.

For the TSS tests, the tests were done with the retentate on 0.45 μm filters. Filters with their porcelain plates were prepared prior to testing. The filters were placed on the filtration apparatus and the Buchner funnel placed on top and clamped. 20 mL of ddH₂O was passed into each filter three times. The filters were then placed in a porcelain plate and labeled. The plates with their filters were then incubated overnight to remove the water. Plates were then left to reach room temperature in a desiccator and then weighed using a high-precision scale; this measurement was labeled as *A* (Equation 5).

The TSS test was done by filtering 20 or 30 mL of sample using the filtration apparatus described earlier. The Buchner funnels were rinsed to recover any particles stuck to the sides. Filters were then transferred back to their original plates and incubated at 103 °C overnight. After incubation, plates were allowed to reach room temperature in a desiccator and then they were weighed. This measurement is labeled as *B* (Equation 5).

$$TSS \left(\frac{mg}{L} \right) = \frac{B - A}{Volume\ filtered} \times 10^6 \quad (5)$$

The plates were then moved to the incinerator and combusted at 550 °C for 15 minutes. After ignition, plates were allowed to reach room temperature and then weighed. This measurement was labeled as *C* (Equation 6).

$$VSS \left(\frac{mg}{L} \right) = \frac{B - C}{Volume\ filtered} \times 10^6 \quad (6)$$

3.1.3.4 Phosphate

Ascorbic acid was used to quantify ortho-phosphate concentration. Sulfuric acid reagent (5 M) was prepared in a volumetric flask by slowly adding 70 mL of the acid to about 300 mL of ddH₂O. The contents of the flask were left to cool down to room temperature then the volume was adjusted to 500 mL with ddH₂O. Antimony potassium tartrate solution was prepared by dissolving 1.3715 g of K(SbO)C₄H₄O₆ to 400 mL ddH₂O in a volumetric flask. Then, the volume was readjusted to 500 mL and the flask was capped. Ammonium molybdate solution was prepared by dissolving 20 g of (NH₄)₆Mo₇O₂₄ in 500 mL of ddH₂O. 0.1 M ascorbic acid was prepared by dissolving 1.76 g of ascorbic acid in 100 mL of ddH₂O. This reagent was stored at 4 °C for a maximum of one week. Test reagent was prepared by mixing the prepared solutions in the following proportions: 5 mL sulfuric acid, 0.5 mL antimony potassium tartrate, 1.5 mL ammonium molybdate and 3 mL ascorbic acid; this solution is used within four hours of preparation. Soluble and total phosphate measurements were taken. For the soluble phosphorus measurement, a 2 mL raw sample was centrifuged for 10 minutes at maximum speed (20,000×g). Following centrifugation, 5 µL of the supernatant were added to 195 µL ddH₂O in the well of a 96-well analytical microplate (12565501, ThermoScientific). The well contents were pipetted up and down to mix properly. Test reagent (32 µL) was then added to each well. The plate was left to let the colour develop for at least 10 minutes but not more than 30 minutes. Absorbance at 880 nm was measured against a ddH₂O blank using a plate reader. For the total phosphorus measurement, 25 mL raw sample was digested prior to quantification. Digestion was done using persulfate pillows. A 25-mL sample was transferred to a 125-mL Erlenmeyer flask. The contents of one persulfate pillow were emptied and 2 mL of 5.25 N H₂SO₄ were added and the contents swirled to mix. ddH₂O was used to rinse the internal walls of the flask to ensure all the persulfate powder were in solution. The flask was then placed on a

hot plate set at 350 °C to digest. After 30 minutes, the contents of the flask turned clear. The volume was then raised to above 30 mL and the contents left to boil until volume dropped below 20 mL (but not completely boiled). This step was done to enhance phosphorus extraction. Once digestion was complete, the flask was left to cool down to room temperature. NaOH (2 mL, 5.25 N) was then added to neutralize the acid added before digestion. The volume of the contents was measured using a 50-mL graduated cylinder. The internal walls of the flask were rinsed with some ddH₂O, this mixture was used to readjust the volume in the cylinder to 25 mL. The phosphorus concentration was then measured accordingly.

3.1.3.5 *Bacteriochlorophyll a*

BChl-a was extracted using pure methanol (99.9%). A 2-mL biomass sample was centrifuged at maximum speed (20,000×g) for 30 minutes and the pellet was then resuspended in 1 mL of methanol. Samples were incubated in the dark for 30 minutes. Samples were then centrifuged again, methanolic supernatant transferred to a clean collection tube and the methanol extraction was done one more time on the original sample to ensure complete extraction. Methanolic extracts were then pooled in the same collection tube. 200 µL were transferred to a 96-well microplate (12565501, Fisherbrand, Ottawa, ON) and the absorbance was measured at 768 nm using a plate reader (SpectraMax M5, Molecular Devices, San Jose, CA). Absorbance measurements were done in triplicates.

Calibration curve was prepared using BChl-a (SLBW935, Sigma Aldrich, Oakville, ON) isolated from *Rhodospseudomonas sphaeroides*.

3.1.3.6 *Optical Density (OD)*

OD measurements were done in 96-well analytical plates (12565501, Fisherbrand). A 200-µL sample was transferred to each well in the plate. The plate was then placed in a plate reader

(SpectraMax M5, Molecular Devices) and the absorbance spectrum was recorded between 350 nm and 1000 nm with a step-size of 10 nm. All measurements were done in triplicates against a water blank.

3.1.3.7 Illuminance

Illuminance measurements were done using an IR probe connected to a radiometer (PMA2100, Solar Light, Mississauga, ON). The measurements were taken at the inner surface of the reactor facing the light source (influx) and the outer surface opposite to the source. The average is taken as the amount of irradiance exposed to the biomass. Measurements on both sides were taken at six different positions.

3.1.3.8 DAPI Staining and Fluorescence Microscopy

4',6-diamidino-2-phenylindole (DAPI) was used to visualize poly-P within the culture. Prior to staining, clean glass microscopy slides were prepared. Glass slides (351-2968, Tekdon Incorporated, Myakka, FL) were thoroughly washed with soap, rinsed with ddH₂O and then soaked in 1 M hydrochloric acid overnight. Slides were then rinsed with ddH₂O, soaked in 80% ethanol for a minute then left out to dry. Once dry, biomass samples were fixed into each well on the slide. Poly-L-lysine solution (3195820, Speciality Media, Montreal, QC) was used to coat the slides to enhance cell attachment. About 50 μ L of solution was pipetted into each well and left for five minutes. Excess solution was then discarded by tapping slides. Slides were transferred to a fume hood and left to dry completely. Centrifuge tubes (15-mL) were filled with biomass from the reactor. The sample was allowed to partially settle to increase the concentration of the biomass. A 15- μ L sample from the bottom of the tube was transferred to each well on the slide. The wells were then flushed with 50% ethanol followed by 80% ethanol. This step was done slowly as to not discard the biomass. Ethanol was discarded and the slides were left to dry. Once dry, 1x phosphate

buffer solution (PBS) solution was used to rinse the slides. Rinsing was done three times. DAPI solution was prepared using the contents of a DAPI vial (1890543A, Thermochemical). To create 14.3 nM stock solution (5mg/mL), 2 mL of ddH₂O was added to the vial. The stock was diluted down 300 nM in phosphate buffer solution (PBS). The wells were covered in 300 nM DAPI and incubated in the dark for five minutes. Stain was discarded and the slides rinsed with 1x PBS three times. Cover slip was added to the slide and sealed using nail polish. The slides are now ready for microscopy.

Microscopy was done using (U-RSL6EM, Olympus) microscope; excitation light was delivered using a fluorescence lamp (X-Cite 120PCQ, EXFO, Montreal, QC). 100x oil immersion objective was used to visualize. A drop of immersion oil was added to the slide; the slide platform was raised such that the objective lens was fully immersed. The focus was adjusted while viewing in phase contrast mode. Once focused, the slide was then excited. The filter for excitation used fluorescein isothiocyanate (FITC) while DAPI was used for emission. Images were taken using a mounted microscope camera (Retiga 2000DC, QIMAGING, Surrey, BC).

3.1.4 Bioinformatics Analysis

Bioinformatic analysis was done following 16S rRNA amplicon sequencing using 515f-806r as the primer pair. The analysis was done using QIIME 2 (Ver. 2018.6) (Bolyen et al., 2019) in a virtual box environment. QIIME commands used for the analysis are presented in APPENDIX C: QIIME 2 Sequences were imported in their FASTQ format, which allows for quality analysis of the sequences. Once imported, quality of the sequences with increasing sequence length were checked; sequences were trimmed to remove barcodes and to ensure a minimum sequence quality of 30%. Following demultiplexing, Illumina sequencing errors were corrected using DADA2 (Callahan et al., 2016). Reads were then classified using a pre-trained Green Genes (Ver. 13-5)

classifier (DeSantis et al., 2006). Alpha diversity was assessed by enumerating the number of observed operational taxonomic units (OTUs) defined at the 99% sequence identity level, calculating the Shannon index, Hill's number and through evenness. The Shannon index was calculated using Equation 7

$$H = \sum p_i \ln(p_i) \quad (7)$$

Where p is the OTU fraction of each organism in the sample.

Subsequently, Hill's number is calculated using Equation 8 (Kang et al., 2016).

$$N = e^H \quad (8)$$

Evenness was calculated using Equation 9.

$$E = \frac{e^H}{Q} \quad (9)$$

H is the Shannon index described earlier; Q is the species richness.

Beta diversity was assessed through principal coordinate analysis (PCoA) with sequencing depth of 47000 read per sample. This corresponds to the lowest number of reads in one of the reactors. PCoA was done using two different distance matrices, Jaccard and Bray Curtis (Legendre and Legendre, 2012). Two-dimensional plots were generated using the two dominant eigenvalues from the eigenvalue decomposition of the distance matrix used. PCoA decomposes the distance matrix used into its eigenvectors; the position of each reactor in the PCoA space is described by a linear combination of the eigenvectors (Legendre and Legendre, 2012).

Abundance analysis was done at the phylum level and the family level and visualized through bar graphs; this was done after filtering out any sequences that were under an abundance of 100 OTUs. BLAST (Altschul et al., 1990) was used on some OTUs to get a genus classification.

3.1.5 Statistical Methods

Analysis of variance (ANOVA) was done to assess the significance of the experimental treatment effects and interactions. Two-tailed test was conducted with $\alpha = 0.05$. Where significant differences (treatment or interaction) were recognized, least significant difference (LSD) test was done to identify which groups differ. LSD is calculated according to the following equation:

$$LSD_{A,B} = t_{0.025,DF} = \sqrt{MS_w \left(\frac{1}{n_A} + \frac{1}{n_B} \right)} \quad (9)$$

Where DF is the degree of freedom, MS_w is the mean square within and n_A and n_B are numbers of samples of A and B, respectively (Zar, 2007).

4 MAIN LARGE 4-L BIOMASS REACTOR

4.1 Introduction

A biomass reactor was developed serving as an initial proof-of-concept for wastewater treatment using PPB and as a standard source of biomass for subsequent experiments on PPB. Though the microbial composition is unlikely to be static, the variability is expected to be significantly lower than when dealing with an initial seed for each experiment. The reactor also serves as the basis for future engineering work.

Synthetic wastewater was used as the feed for the system. The use of synthetic wastewater over municipal wastewater allowed for a more controlled environment, which can lead to more reproducible results. It also facilitated access to the wastewater feed while the design and operation of the reactor were optimized. The wastewater composition was developed in 1998 (Nopens et al., 2001), and the recipe was used in multiple studies worldwide since then. Constituents were chosen to mimic the aggregate properties (COD, TP, TN) of municipal wastewater as well as the presence of specific chemicals (e.g. surfactants). Nitrogenous components also mimic urine additions to municipal wastewater. Finally, as an initial study, we hypothesized that using synthetic wastewater instead of actual municipal wastewater would increase the universality of the results because municipal wastewater is highly variable both spatially and temporally.

4.1.1 Objectives:

The biomass reactor is used to address the first objective described in Chapter 1, which is the construction of a first (in our lab) 4-L scale IR photobioreactor and the description of its basic operation, enriched microbial community and poly-phosphates accumulation. Additionally, the reactor will:

1. provide a source of biomass for downstream experiments on PPB (Chapter 5 and 6)
2. serve as an initial proof-of-concept for resource recovery using PBRs in a wastewater treatment setting.

4.2 Experimental Setup

4.2.1 Reactor Geometry and Design

The reactor frame was made using two stainless steel U-sections (McMaster-Carr, 1262T41). The sections were three feet long each with a wall thickness of 3/16 inches. The sections were cut at 45° angles to create the frame segments; measuring the long end, the channels were cut into two 20 cm pieces (side pieces) and one 30 cm piece (bottom piece). Stick electrodes (McMaster-Carr, 7973A204) were used to weld the three pieces together. Polyurethane (McMaster-Carr, 6937T5) was then added to the internal flanges, borosilicate sheets of the glass (McMaster-Carr, 8476K84) were then placed. The sheets were added one at a time with each sheet lying flat on the frame for three days. The reactor dimensions were 30 cm, 20 cm and 6 cm (Figure 4-1).

Reactor was operated on a bench at room temperature (Figure 4-1). The reactor was mixed using three magnetic stirrers. Reactor was subjected to IR from an infrared camera lamp (CM, IR-200); the lamp was placed at approximately six inches away from the reactor surface. SRT and HRT of the reactor was six days with a cycle time of two days; every two days, 1.2 L of the reactor's volume would be removed and replenished with fresh feed. The reactor was monitored during its steady-state through measuring COD, solids, phosphates and pH. These measurements are described in Chapter 3.

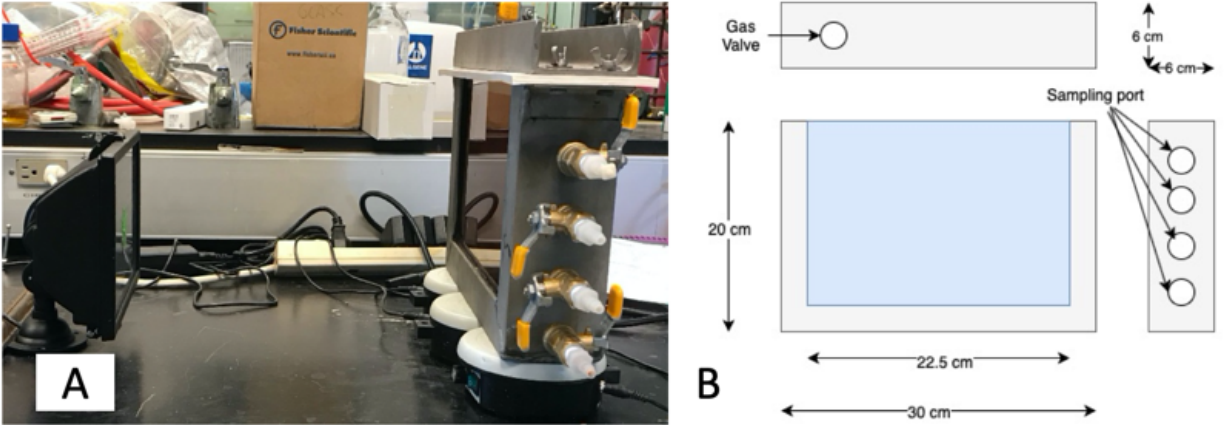


Figure 4-1: (A) Side view of the reactor setup. The lamp (850 nm IR source) is shown on the left with the reactor on the right. The distance between the lamp and the reactor is 30 cm. Three stirring plates can be seen underneath the reactor. During operation, a cardboard box is placed over the setup to block any external light from reaching the reactor. (B) Reactor schematic showing front, side and top views. Grey corresponds to the stainless steel and blue is the borosilicate glass.

4.3 Results and Discussion

4.3.1 Start-up of Reactor

Operation started by seeding a waste activated sludge sample (5 mL) into the reactor volume. The contents of the reactor were then flushed with nitrogen gas for 5 minutes. Following initial seeding, the reactor contents became turbid over the next two days; the initial color that developed was green-grey. Following that, red color started intensifying over time. Scum formed during initial operation of the reactor. Flocs formed during most of the reactor operation; this was apparently due to inadequate agitation provided by the stirring plates. This was remedied by manually agitating the reactor daily, which was when floc presence decreased.

4.3.2 Steady-state Analysis

During the last two months, the reactor operation was near steady-state and the illuminance was measured at that time. Illuminance was measured at the entrance and exit faces of the reactor; the average influx measured was 6.733 mW/cm^2 and at the exit was 1.645 mW/cm^2 . This indicates that the reactor managed to intercept 75.6% of the incoming energy indicating that this is a shallow reactor with respect to the energy (i.e. light reaches the entire depth). Average this result over the depth of the system, the average illuminance within the reactor was 4.189 mW/cm^2 .

Reactor operation was monitored by measuring COD (soluble and total), phosphorus (soluble and total), and solids (suspended and total) (Figure 4-2). The temporal profiles during the last two months of operation describe a near steady-state because the data are generally stable over the time period. The reactor consistently dropped the soluble chemical oxygen demand (sCOD) to less than 30 mg/L , which represents a 90% COD removal. The sCOD and solids data closely matched their respective temporal averages, indicated by a small standard deviation. More fluctuations were observed in the total chemical oxygen demand (tCOD), suspended solids and phosphorus measurements. The tCOD fluctuations can be due to floc formation, which might introduce error in the measurements. The soluble ortho-P trend appears to follow that of the total ortho-P, indicating the biomass is partitioning a proportion of it. This is inconsistent with the COD data, as the sCOD profile remains steady while the tCOD exhibits more fluctuations. Considering the feed had a COD of 430 mg/L , the tCOD observed in the reactor is about 315 mg/L and the sCOD $< 30 \text{ mg/L}$, this produces an average yield of 73% [COD-biomass/COD-substrate removed]. This yield is considerably higher than the typically observed yield in activated sludge of about 50% (Rittman and McCarty, 2012). While greater than the normally observed value in activated sludge, this value appears to be smaller than the typically reported literature value for PPB of about 1.1 [COD-

biomass/COD-substrate removed] (Puyol et al., 2017). This is likely due to carbon fixation in the presence of CO₂, which is not occurring in this reactor. This result is to be expected as the biomass produced in this reactor is less reliant on the substrate as an energy source. The yield is not 100% (meaning the entire feed is not converted to biomass) due to the substrate being used as an electron donor, decay, or COD loss to the headspace.

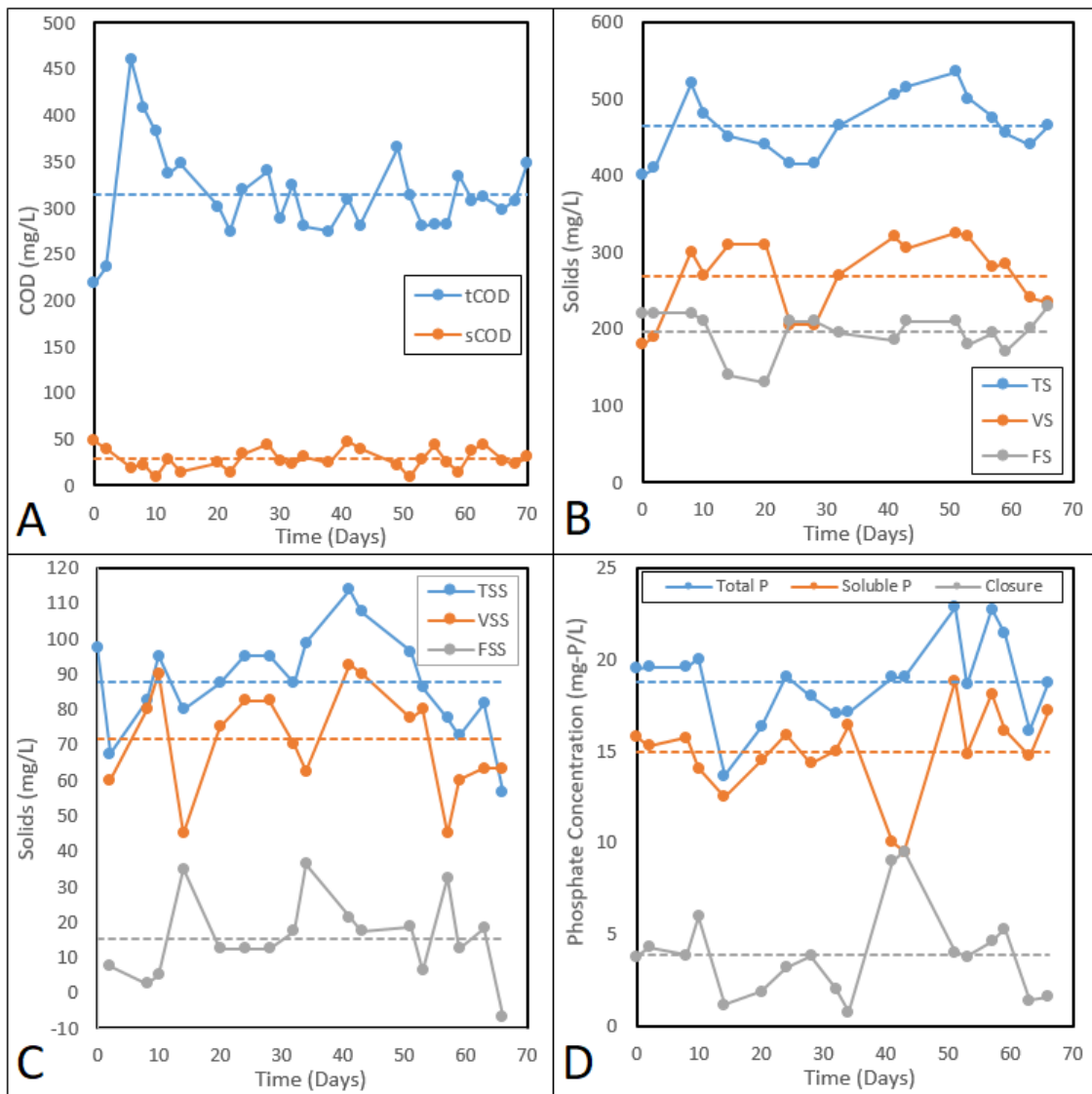


Figure 4-2: Reactor performance during steady-state operation. (A): COD profiles (soluble: sCOD and total: tCOD). (B): Total solids profiles (total: TS, volatile: VS and fixed: FS). (C): Suspended solids profiles (total: TSS, volatile: VSS and fixed: FSS). (D): Total phosphorus profiles. Day 0 corresponds to the measurement

taken on May 5th (three months after the start of the reactor). Dashed lines in the plots represent the average measurement over time. Standard error did not exceed 10% and was not shown for clarity.

The reactor removed between 1 and 10 mg-P/L (average of 4 mg-P/L). The reason of this variability is unclear. It appears that the amount of phosphorus removal depended on the available phosphates, with a higher removal achieved at high total P concentrations, the biomass removed more phosphate. This suggests that the biomass was reacting to the changing concentrations in the liquid implying a level of metabolic control. Normalizing with the VSS concentration (Figure 4-3), the biomass accumulated up to 11% of its dry weight. This is close to the presumed maximum of about 15% (Liang et al., 2010). Generally, the biomass P content was consistently above 2%, dipping once to 1%. According to the average biomass P content in wastewater treatment, any P content above 2% implies accumulative behavior (Rittman and McCarty, 2012). This mass balance suggests that the biomass enriched in this reactor was consistently accumulating phosphorus under the provided illumination and dosing conditions.

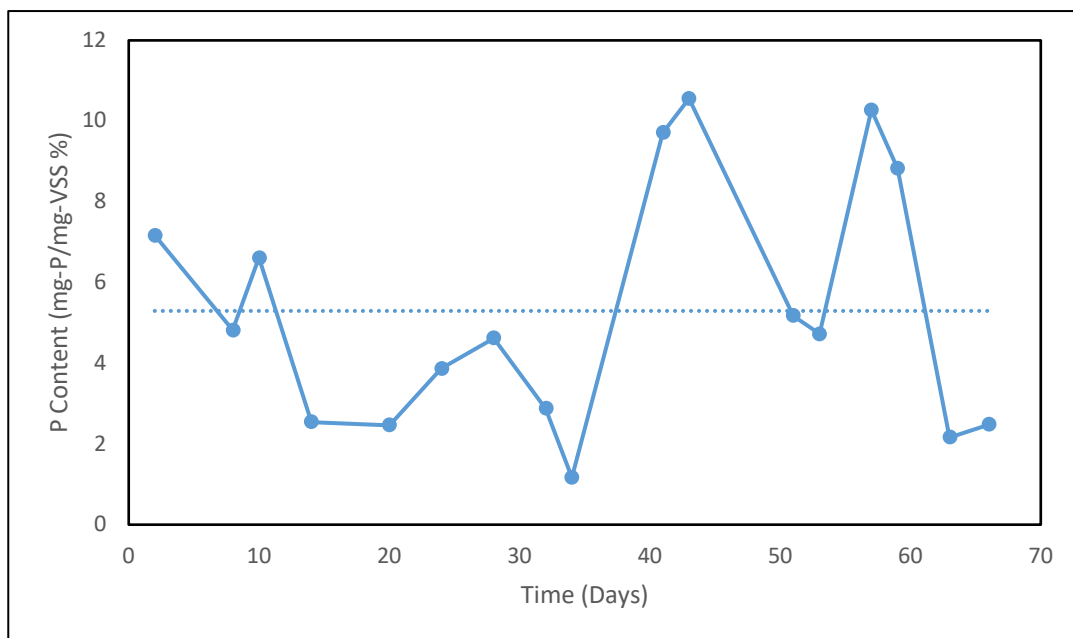


Figure 4-3: Presumed biomass phosphorus content. Calculation is done using phosphorus closure with respect to the VSS level.

4.3.3 DAPI Staining

The observation that the P content in the VSS were greater than 3%, we hypothesized that poly-P was accumulated. We investigated this hypothesis using fluorescent (excitation using 360 nm light) microscopy with DAPI. It can be seen from Figure 4-4 that yellow (emission of 550 nm light corresponding to poly-P) and blue regions (emission of 460 nm light corresponding to DNA) can be observed. The yellow regions are almost always longitudinal, which can suggest that longitudinal forms of poly-P are mainly produced. Another possibility is the DAPI-DAPI binding mediated by negatively charges polymers (Omelon et al., 2016). To reduce the likelihood of ions from the medium affecting the staining results, cell residue on slides was always washed with PBS.

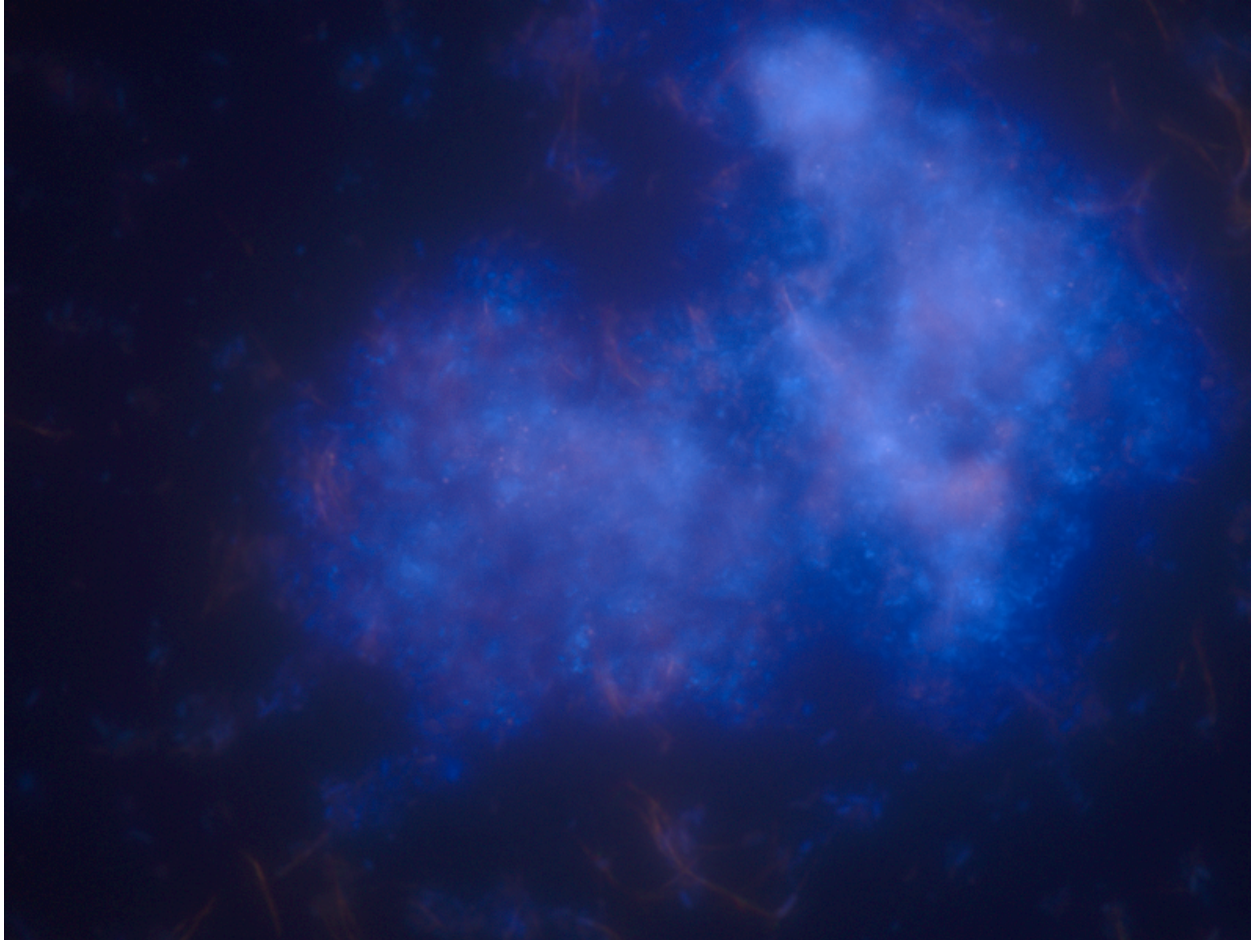


Figure 4-4: DAPI staining of the enriched biomass. Picture was taken using biomass from day 32. Blue regions correspond to fluorescence from DAPI-DNA interactions. Yellow regions are likely due to DAPI-poly-P fluorescence. Image was taken using a 100x objective.

4.3.4 Microbial Community Structure

The microbial community in the reactor was analysed by 16S rRNA gene amplicon sequencing (Figure 4-5). The analysis reveals dominance by three phyla, *Proteobacteria* (36%), *Firmicutes* (43%) and *Bacteroidetes* (15%). The family *Bradyrhizobiaceae* (Class: *Alphaproteobacteria*) accounted on average for 29%. This family is recognized to harbour several PNSB genera (Imhoff et al., 2017). Other families present in high relative abundance in the reactor were the *Enterobacteriaceae* (Class: *Gammaproteobacteria*), the *Veillonellaceae* (Phylum: *Firmicutes*) the *Prevotellaceae* (Phylum: *Bacteroidetes*) and the *Bacteroidaceae* (Phylum: *Bacteroidetes*). All the

families present were either obligate or facultative anaerobes. The *Veillonellaceae* family harbors mainly sugar-fermenting organisms (Marchandin and Jumas-Bilak, 2014) while the *Prevotellaceae* and *Bacteroidaceae* has protein and complex-carbohydrate fermenters (Brook, 2017; Rosenberg, 2014). These families are not known to harbour any known PNSB genera. Therefore, it would appear that community was structured around possible PNSB populations belonging to *Bradyrhizobiaceae* and fermentative populations belonging to the *Enterobacteriaceae*, *Veillonellaceae*, *Prevotellaceae* and *Bacteroidaceae* families.

A similar reactor configuration done by Hulsen et al. (2018) enriched for a microbial community that was dominated with the genera *Rhodobacter* and *Rhodopseudomonas*. Considering that *Rhodopseudomonas* belongs to the *Bradyrhizobiaceae* family, it is likely that similar PPB organisms were growing in both systems. Their reactor enriched for a higher proportion of PPB (40-90%) indicating that it was better at selecting for their growth as it had less fermentable substrates.

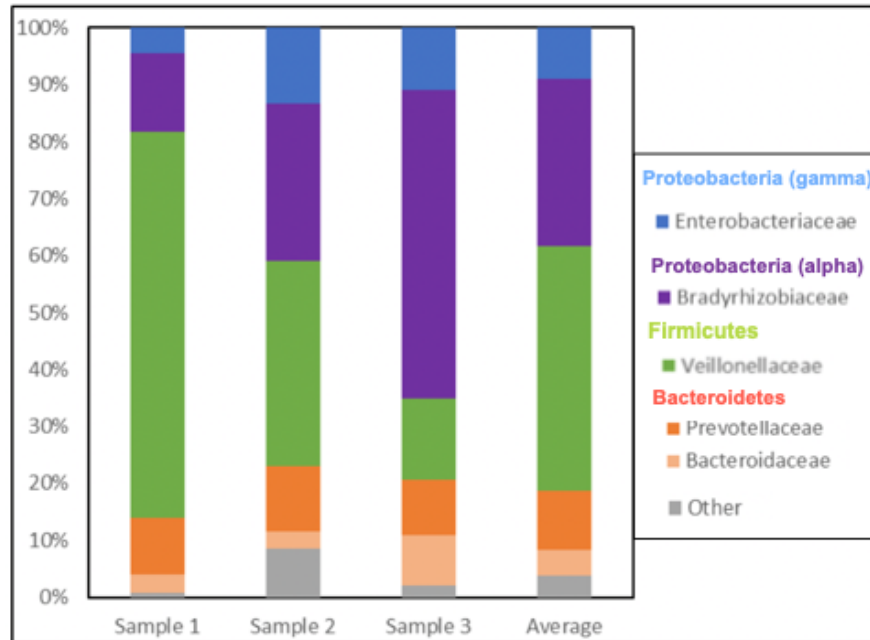


Figure 4-5: Family-level abundance. The major phyla represented were *Proteobacteria* (36%), *Bacteroidetes* (15%), and *Firmicutes* (43%). DNA from three samples taken at the same time was used to generate the plot.

4.4 Conclusions

Through this biomass reactor, we have witnessed the potential for poly-P accumulation under PPB-enriching conditions receiving synthetic wastewater as the feed. The accumulation was achieved under unoptimized conditions (parameter choices were arbitrary rather than carefully selected); this initial proof-of-concept serves as the basis for further poly-P recovery from wastewater research. The main questions that remain unanswered are a) which microbial population is responsible for recovery, b) what is influencing recovery and c) how to properly engineer the process to maximize recovery yield. Fundamentally, all three questions are targeting different areas of optimization. The microbial population recovering poly-P is hypothesized to be composed of PPB as these are the organisms receiving most of the energy; proper knowledge of which organism(s) is responsible for most of the accumulation introduces the avenue to increase recovery

by selecting for these organism(s). The second question relies on better understanding of the metabolic control of the accumulating organisms; again, introducing another optimization angle. The third relies on the actual engineering of the entire process, which is bringing in the elements of microbial selection, metabolic control and engineering technicalities to maximize recovery.

5 ENRICHMENT EXPERIMENT IN SMALL 60-ML REACTORS

5.1 Introduction

Starting from the biomass enriched in the 4-L reactor (Chapter 4) and knowing the microbial community has a significant abundance of PPB (about 30%), we now ask the question on how the enriched microbial community is structured around the presence of PPB. In other words, to what extent does the community rely on each other for completely degrading wastewater? In this chapter, PPB from the 4-L reactor described earlier is seeded into serum bottle photobioreactors and cultivated under similar conditions to those in the main reactor (Chapter 4). Two factors that are likely to drive PPB selection and the structure of microbial community were investigated: a) the carbon sources in wastewater and b) the wavelength of the incident IR light. To address the first factor, the photobioreactors were fed with only one major carbon source (acetate, starch, milk or glycerol) from Syntho. The second factor was tested by subjecting each reactor to either 850 nm or 940 nm IR. The design of the experiment allows us to answer the question regarding which organisms are the primary consumers of each substrate as well as check for any similarities between microbial compositions under different conditions (carbon source or light).

This experiment addresses the second, third and fifth thesis objectives restated here:

1. Description of the microbial populations that grow on each of the carbonaceous components of synthetic wastewater (Syntho) as sole carbon sources.
2. Determination of the capacity to predict the synthetic wastewater community based on the independent results of individual carbon sources.
3. Investigation of the effect of changing IR wavelength (850 nm and 940 nm) on the microbial community.

5.2 Experimental Setup

The experiment was conducted in 60 mL glass serum vials. The vials were thoroughly cleaned with soap to remove any trace organics and soaked in bleach overnight to disinfect, then, the vials were rinsed with ddH₂O and left to dry. The vials were each filled with 40 mL of synthetic wastewater medium that was altered to only have one carbon source in addition to an unaltered one serving as a positive control. The carbon sources in the media used were sodium acetate, starch, milk powder or glycerol. The COD in the feed of all reactors was adjusted to be around 400 mg-COD/L. Each reactor was then seeded with 1 mL of biomass from the 4-L reactor. The reactors were then sealed with a rubber stopper and a crimped aluminum cap. Once capped, the reactor headspace was flushed with nitrogen gas for one minute each. The reactors were then transferred to a shaker and illuminated with either 850 or 940 nm IR. Each reactor was done in triplicates with a reactor placed in the dark used as a light negative control.

All reactors were first incubated under the previous conditions for five days (batch phase). The positions of the reactors in the shaker was randomized daily to avoid an illumination bias. Once the batch phase was done, the reactors were then operated as sequencing batch reactors (SBRs) with a retention time of 8 days (HRT = SRT) and a cycle time of 2 days. The biomass extracted from these reactors was stored for future DNA analysis. For analytical methods and the bioinformatic analysis, refer to chapter 3.

5.3 Results

5.3.1 Temporal Dynamics of the Biomass

Over the course of the experiment, the optical density at 600 nm (OD₆₆₀) was monitored to estimate the level of biomass in the reactors (Figure 5-1). OD₆₆₀ is typically only affected by

light-scattering (minimal absorption at that range), as such, it is a useful indicator of biomass growth over time. Greatest changes in the OD660 appeared during the first 1.5-2 HRTs of the sequencing batch phases of the experiment. During this phase, OD660 generally decreased in most reactors, except in reactors receiving only acetate and illuminated at 850 and ones receiving glycerol and illuminated at 940 nm where the biomass exhibited a peak of OD660 around 1 HRT (Figure 5-1). From the OD660 values, it appears from the profiles that the biomass levels in all reactors were similar towards the end of the experiment except for the reactors receiving acetate and illuminated at 850 nm (Figure 5-1a).

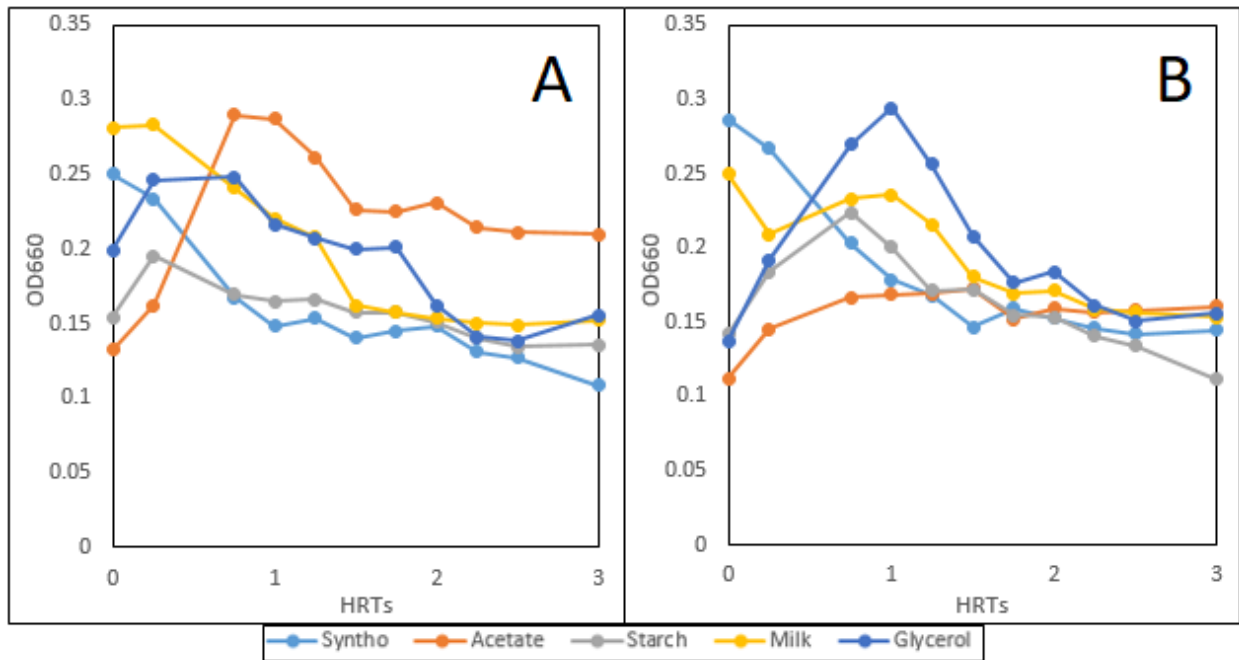


Figure 5-1: OD660 time series for (A): 850 nm reactors and (B): 940 nm reactors during the SBR operation. Horizontal axis expressed in dimensionless time (t/HRT) with $\text{HRT} = 8$ days. OD660 is used as an estimator for biomass concentration. Time 0 corresponds to the end of batch operation (8 days) and start of SBR operation. Measurements were taken in triplicates. Standard error was less than 10% in all cases and was not shown to improve clarity.

The temporal profiles (Figure 5-3 and Figure 5-4) show how the BChl-a content evolved over time after the batch incubation. The OD was measured at 810 and 870 nm, which corresponds to the absorption peaks of the pigment within the cell's membrane (Figure 5-2). Under both illumination regimes (850 nm or 940 nm) these two peaks were the only clearly distinguished from the absorption spectra taken over the range 350 – 1000 nm.

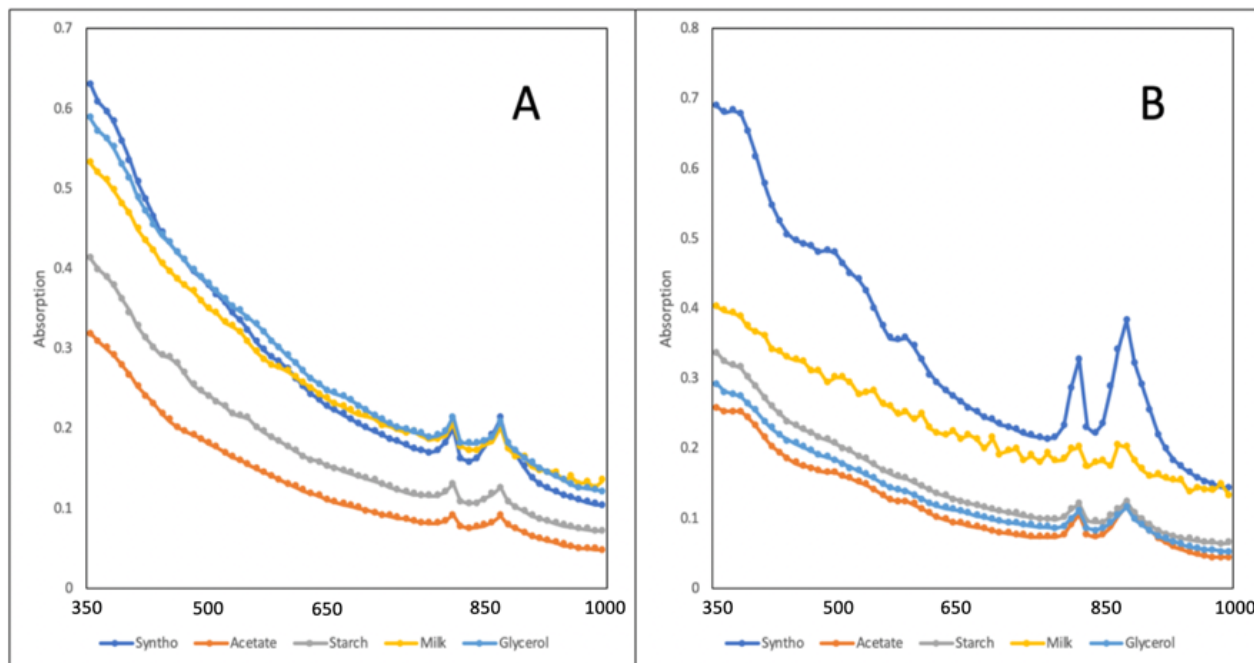


Figure 5-2: Absorption spectra over the range 350 - 1000 nm. (A) Spectra for reactors receiving 850 nm IR. (B) Spectra for reactors receiving 940 nm IR. Within the IR range (700 - 1000 nm), two distinct peaks develop corresponding to BChl-a. Plot was generated using data from Day 0.

The absorption values were normalized by OD660 to give the pigment content per unit biomass. Syntho reactors consistently produced the highest biomass-specific pigment content. 940 nm reactors had a higher OD ratio than 850 nm. Substrate profiles between both light sources were closely comparable for the acetate systems. During the SBR operation, there is a general decrease

in the OD ratio. The most pronounced decrease was with the acetate and Syntho reactors illuminated under 940 nm IR; the decrease was more significant for OD870/OD660.

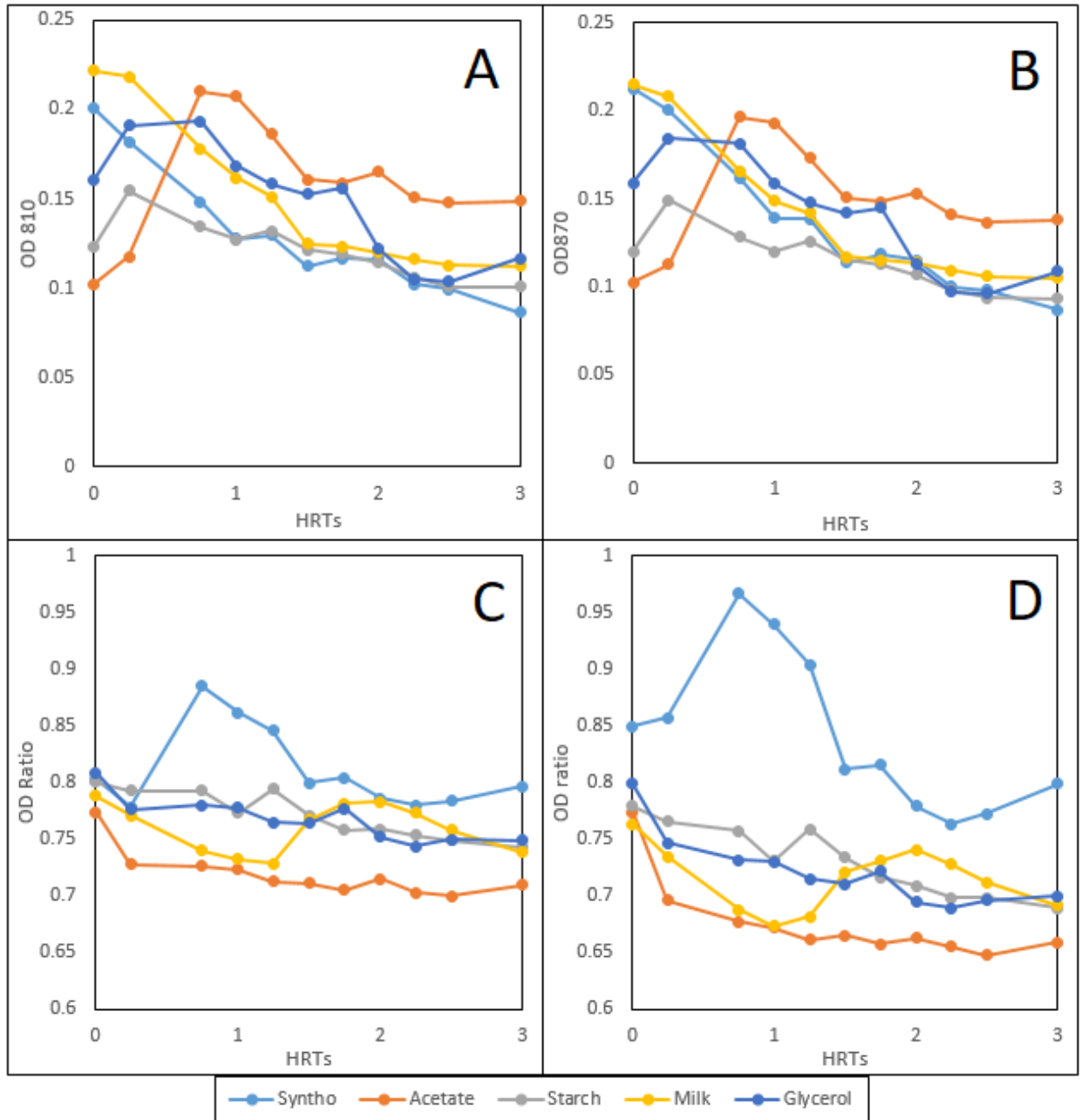


Figure 5-3: OD810 and OD870 temporal profiles for the reactors illuminated at 850 nm. (A): OD810 corresponding to the pigment content of the light-harvesting complexes. (B) OD870 corresponding to the

pigment content of the reaction center. (C) OD810/OD660 ratio. (D): OD870/OD660 ratio. Plots C and D were magnified by starting the vertical axis at 0.6. Horizontal axis expressed in dimensionless time (t/HRT) with $\text{HRT} = 8$ days. Time 0 corresponds to the end of the batch operation (8 days) and start of SBR operation. Measurements were taken in triplicates. Standard error was less than 10% in all cases and was not shown to improve clarity.

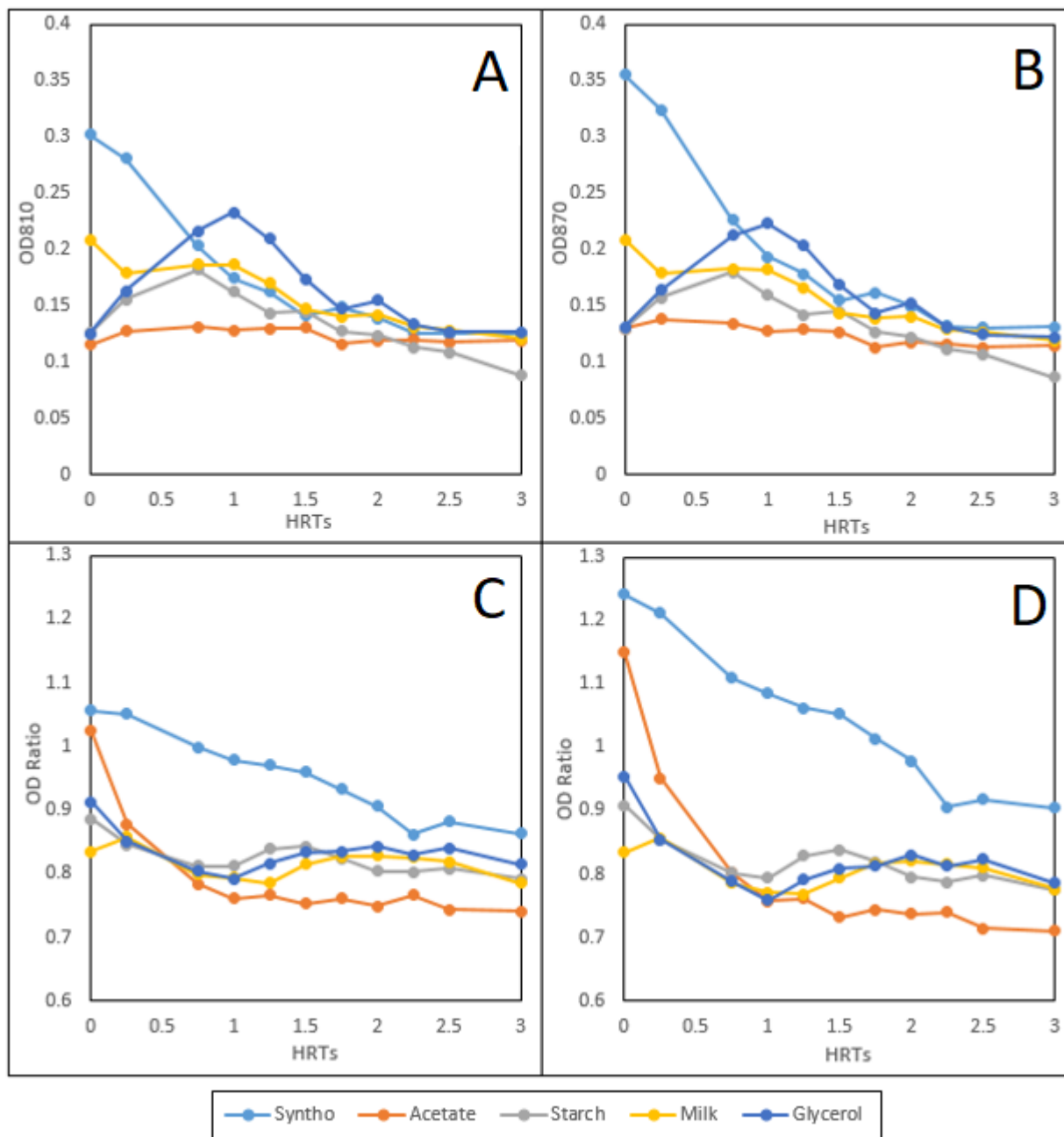


Figure 5-4: OD810 and OD870 temporal profiles for the reactors illuminated at 940 nm IR. (A): OD810 corresponding to the pigment content of the light-harvesting complexes. (B) OD870 corresponding to the

pigment content of the reaction center. (C) OD810/OD660 ratio. (D): OD870/OD660 ratio. Plots C and D were magnified by starting the vertical axis at 0.6. Horizontal axis expressed in dimensionless time (t/HRT) with $\text{HRT} = 8$ days. Time 0 corresponds to the end of the batch operation (8 days) and start of SBR operation. Measurements were taken in triplicates. Standard error was less than 10% in all cases and was not shown to improve clarity.

5.3.2 Biomass at the End of the Experiment

For a biomass measurement, VSS content of the reactors at the end of the operation was measured. Reactors had a TSS content between 63 and 85 mg/L (Figure 5-5). The highest VSS content was with the reactors receiving glycerol under either wavelength (Figure 5-5). While Syntho appeared to have a comparable VSS content to the other systems, the wavelength did not have a significant effect on VSS concentration ($p\text{-value} = 0.20$).

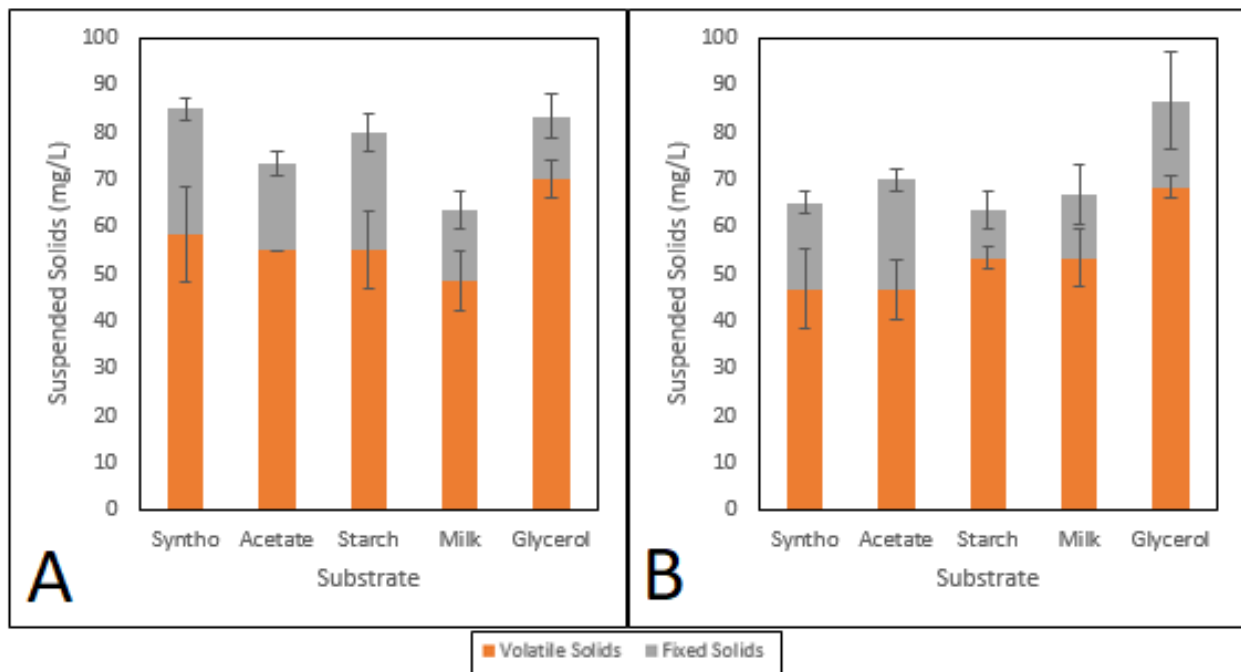


Figure 5-5: Suspended solids measurements. Height of the combined bars corresponds to total solids. Measurement represents average of the triplicates; error bars represent standard error ($n = 3$). (A): Data for 850 nm reactors. (B): Data for 940 nm reactors. Two-way ANOVA was done to test the significance of the substrate main effect ($p\text{-value} = 0.002$), wavelength main effect ($p\text{-value} = 0.20$) and substrate-wavelength interactions ($p\text{-value} = 0.39$). Glycerol was the only group that is different from the rest identified by the least square difference.

BChl-a content of each reactor at the end of the SBR operation was measured (Figure 5-6) to assess PPB presence and light harvesting activity. The data on the biomass demonstrated that variations in carbon sources and the illumination source changed the BChl-a content of the biomass, with the highest BChl-a associated with the complete Syntho and 940-nm illumination (Figure 5-6).

The substrate had a significant effect on BChl-a content (p -value = 0.023). The Syntho reactors produced the highest BChl-a concentrations, 31 and 60 ng/kg for the 850 and 940 nm reactors, respectively. Acetate resulted in the lowest concentrations. These results appear to be consistent with the OD810/OD660 (Figure 5-3) and the OD870/OD660 data (Figure 5-4).

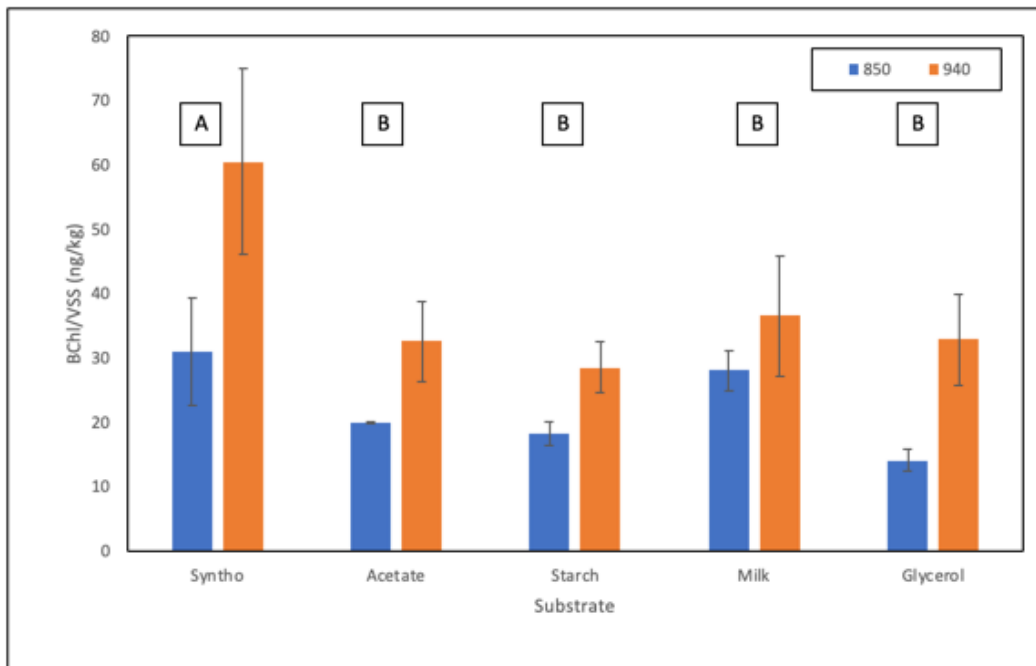


Figure 5-6: Bacteriochlorophyll a content measured at the of the SBR operation. Measurements corresponds to the average of the three replicates normalized per unit VSS. Error bars represent standard error (n=3). Two-way ANOVA was done to test the significance of the substrate main effect (p -value = 0.023), wavelength main

effect (p-value = 8E-4) and substrate-wavelength interactions (p-value = 0.69). Letters indicate substrate conditions with non-significant differences identified by the least square difference.

5.3.3 Structures of the Communities Enriched under Different Reactor Conditions

This section investigates if these differences are related to the structure of the community enriched under each condition. Specific questions ask are: which populations are responsible for the removal of each COD component? Are the microbial community structures reproducible between reactors? And what are the possible niches developed by the consumption of Syntho? Two main sub-sections are presented. First, the within reactors diversity (i.e., alpha diversity) is assessed. Second, the differences in community structures between reactors (i.e., beta diversities) is described. The basic unit of community structure used was the operational taxonomic unit (OTU) defined at the 99% sequence identity level.

5.3.3.1 *Alpha Diversity*

Alpha diversity is the diversity in each isolated reactor at a given sampling time. The species richness (Figure 5-7) is the number of unique OTUs present in the reactor. Syntho reactors achieved the lowest richness for both 850 and 940 nm reactors. This was opposite to what was expected for Syntho as it is composed of the highest number of individual carbon sources, and as such would would have the highest number of available resource niches. The reactors achieving the highest richness were the ones fed with starch, milk or glycerol (the fermentable substrates). The effect of wavelength on species richness was insignificant (p-value = 0.56). However, the interactions between substrate and wavelength were significant (p-value = 0.045).

The species richness is not the only aspect of diversity that should be considered. The relative proportion of each OTUs is also important as a community structure with equally abundant

populations (more even) is more diverse than one with a few highly abundance populations and the others at low populations. The biomass growing using Syntho exhibited the lowest Hills number derived from the Shannon index (Figure 5-8) because these communities also exhibited the lowest evenness (Figure 5-9). This shows that these communities were dominated by a few OTUs to fully degrade the substrate as opposed to requiring more different organisms. In contrast, acetate and milk feed resulted in communities with the greatest evenness.

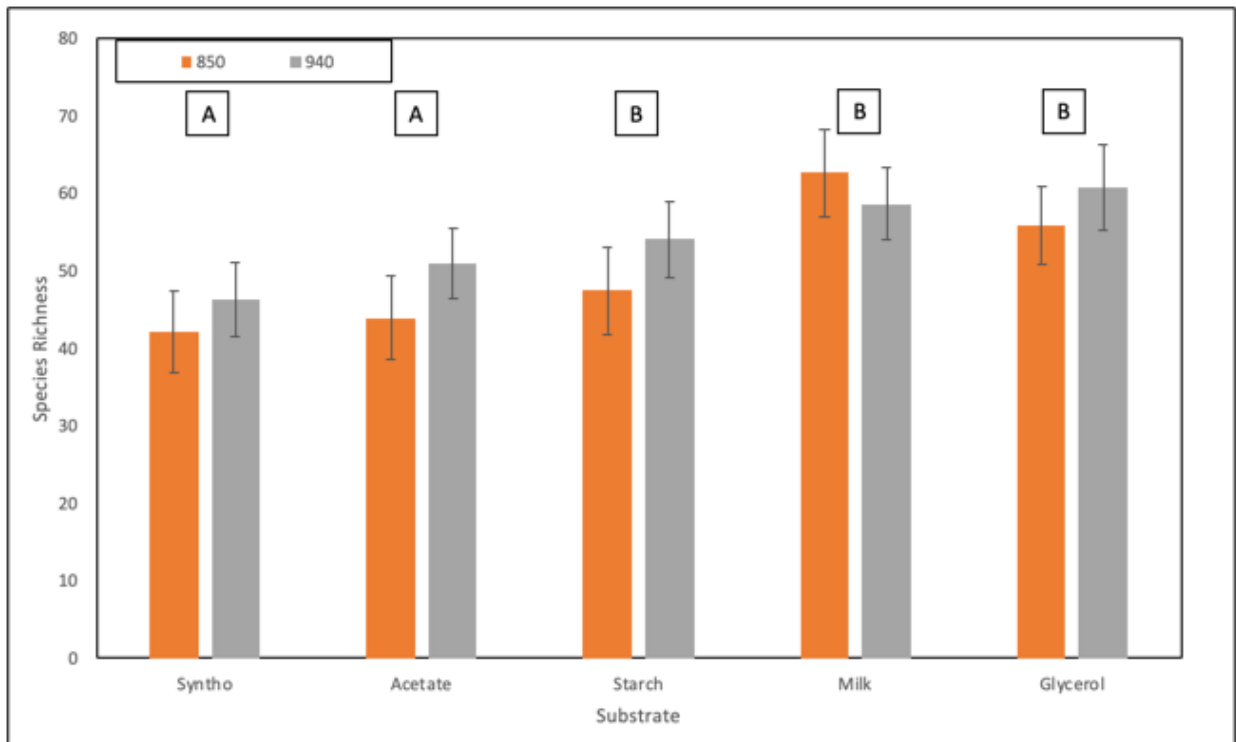


Figure 5-7: Species richness plot. Measurements correspond to the average number of observed OTUs. Error bars represent standard error ($n = 3$). Two-way ANOVA was done to test the significance of the substrate main effect (p -value = $3E-6$), wavelength main effect (p -value = 0.55) and substrate-wavelength interactions (p -value = 0.045). Letters indicate substrate conditions with non-significant differences identified by the least square difference.

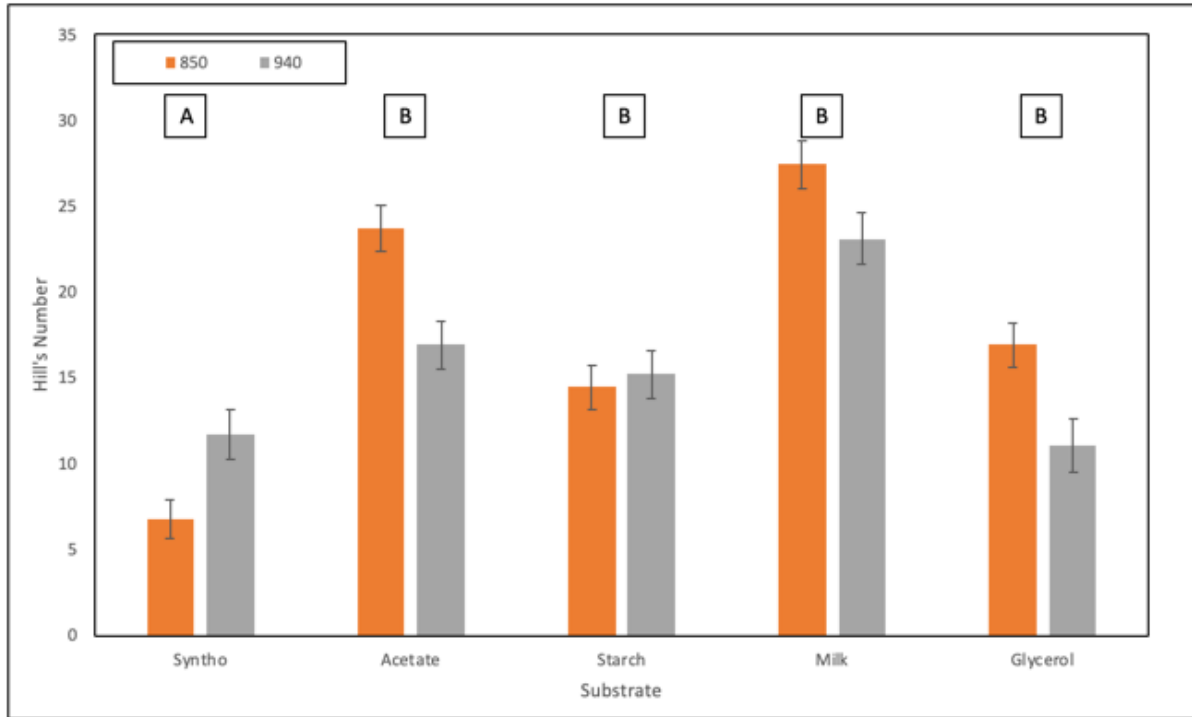


Figure 5-8: Average Hill's number from the Shannon index. Measurements correspond to the average Hill's number. Error bars represent standard error (n = 3). Two-way ANOVA was done to test the significance of the substrate main effect (p-value = 7E-6), wavelength main effect (p-value =0.12) and substrate-wavelength interactions (p-value = 0.49). Letters indicate substrate conditions with non-significant differences identified by the least square difference.

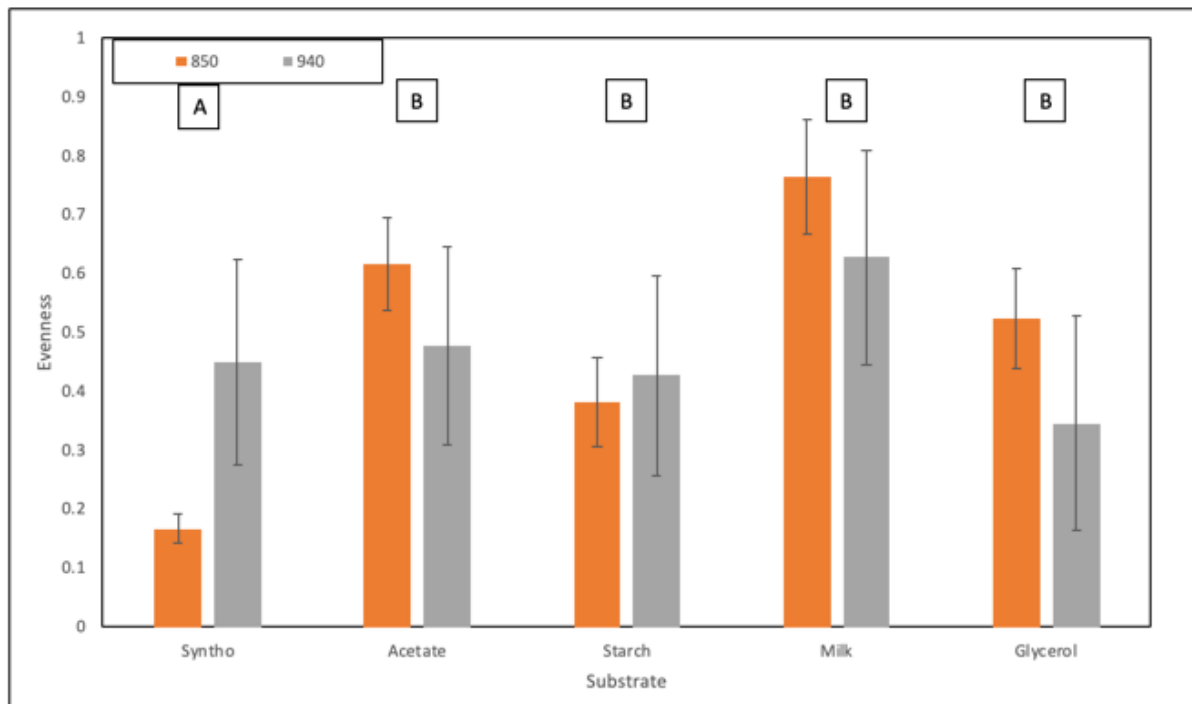


Figure 5-9: Evenness plot. Evenness was calculated by taking the exponential of the Shannon index and dividing that by the richness. Measurements correspond to the average. Error bars represent standard error ($n = 3$). Two-way ANOVA was done to test the significance of the substrate main effect (p -value = $7E-6$), wavelength main effect (p -value = 0.12) and substrate-wavelength interactions (p -value = 0.49). Letters indicate substrate conditions with non-significant differences identified by the least square difference.

5.3.3.2 Overall Community Variations between the Reactor Conditions

The principal coordinate analysis (PCoA) plot was used to visualize the variations in community structure using the Jaccard dissimilarity (presence or absence) (Figure 5-10) and Bray-Curtis (quantitative) (Figure 5-11).

The Jaccard dissimilarity revealed that the batch incubation (plotted as Start of SBR phase) clustered the microbial community structures in three carbon source groups: north-west for communities grown on acetate, south-west for those grown on Syntho and south-east for those on milk, glycerol and starch (fermentable substrates). During the SBR incubation, the communities

grown on acetate retained similar structures, while the one grown on the other carbon sources moved in the north-east direction (Figure 5-10). The two illumination wavelengths appeared to have had the same effect on the microbial composition in term of the Jaccard dissimilarity (Figure 5-10). Thus, change of operation from batch to SBR appears to affect the presence of some OTUs present in the communities fed with Syntho, milk, glycerol, and starch (i.e., the fermentable substrates). It is worth noting that the seed and Syntho reactors at the end of the experiment are apparently close, which indicates that the same OTUs were present in the two communities.

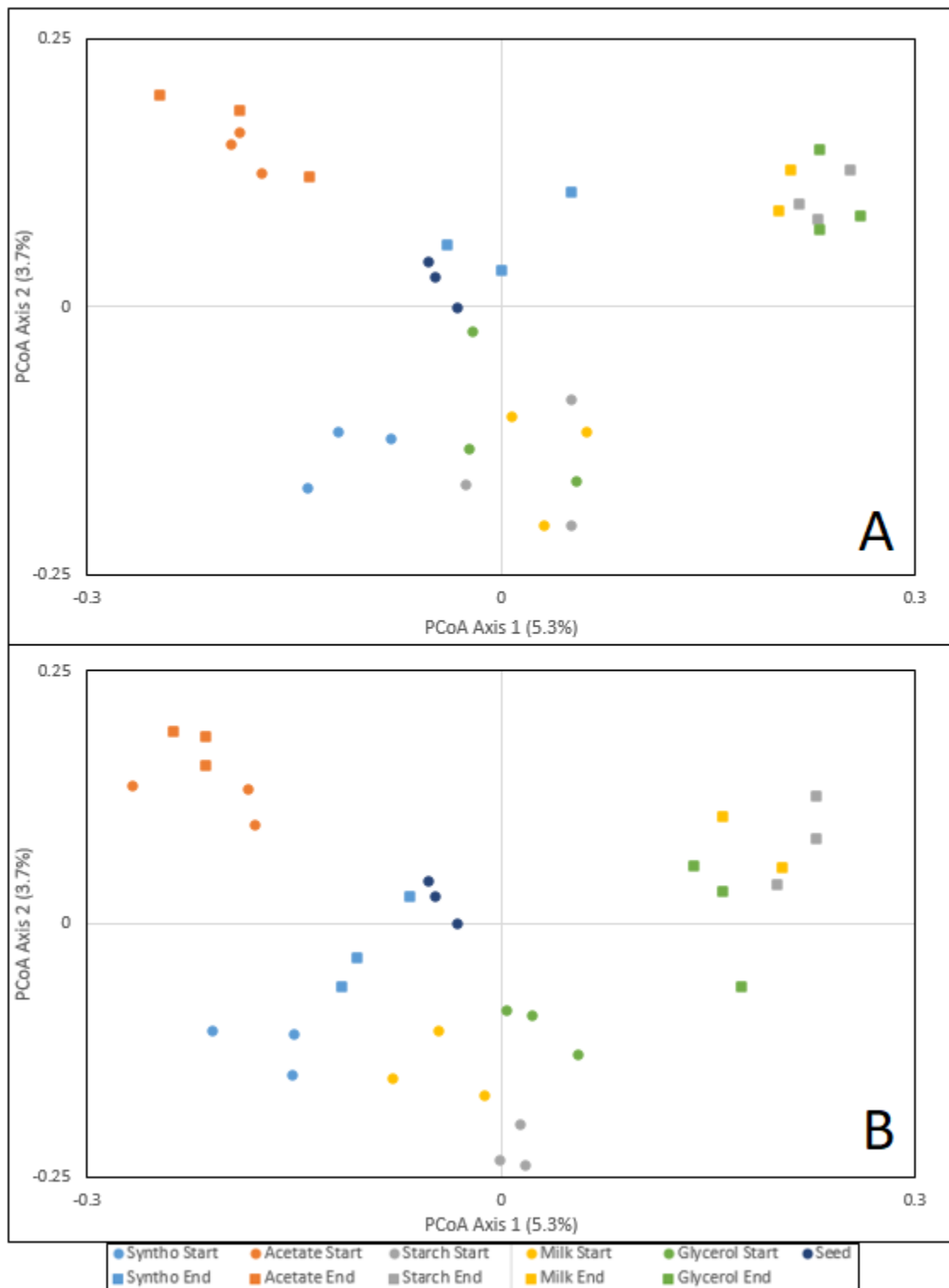


Figure 5-10: PCoA plot using Jaccard dissimilarity to visualize the differences in OTU community structures grown one different carbon sources and illuminated at (A) 850 nm and (B) 940 nm. Panel A and B depict the same plane of data, but the points were separated in two plots for clarity. Percentages on the axes represent the

proportion of variation represented by the PCoA axis. Start (circles) means at the start of the SBR incubation (end of batch incubation) and End (squares) means the end of the SBR incubation. Seed is the community structure of the inoculum from the 4-L biomass reactor.

Similarly to the Jaccard PCoA, clustering of communities grown on acetate were observed again when community dissimilarities were calculated with Bray-Curtis with almost no displacement in the PCoA during the SBR operation and positioned similarly for both 850 and 940 nm reactors (Figure 5-11). However, there does not seem to be a clear cluster formation for the other substrates. Instead, a gradient forms across the observations. This shows that, in the case of fermentable substrates (milk, glycerol, and starch), the resulting microbial composition was more variable than when the carbon source was only acetate. The Syntho clusters showed an eastbound transition under both lighting conditions; the direction of transition appears to be opposite to the fermentable substrates, each of which transitioned to the left. These were probably related to the increase in abundance of the *Enterobacteriaceae* in the communities receiving Syntho and their decrease in the others (next section).

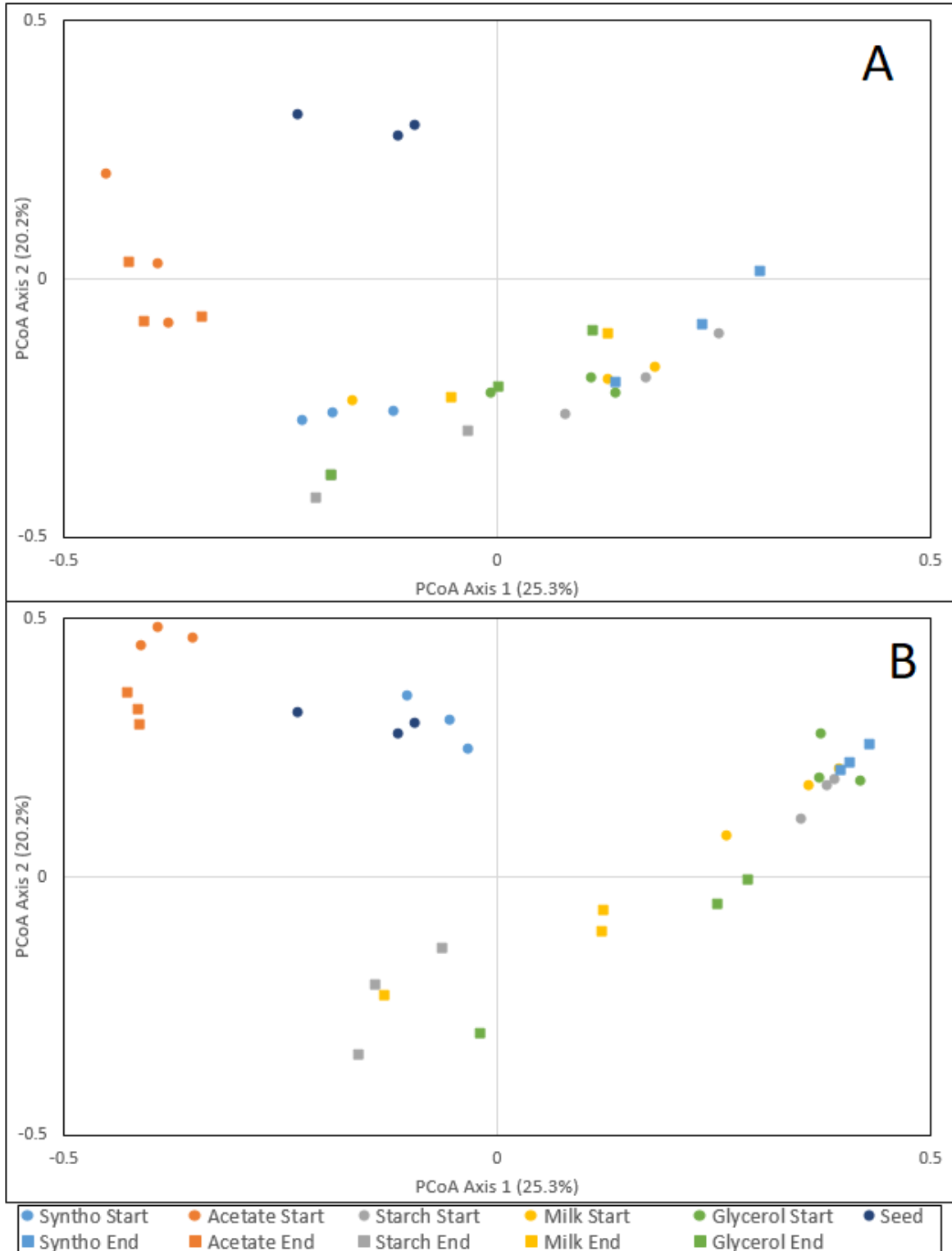


Figure 5-11: PCoA plot using Bray-Curtis distance matrix to visualize the differences in OTU community structures grown one different carbon sources and illuminated at (A) 850 nm and (B) 940 nm. Panel A and B depict the same plane of data, but the points were separated in two plots for clarity. Percentages on the axes

represent the proportion of variation represented by the PCoA axis. Start (circles) means at the start of the SBR incubation (end of batch incubation) and End (squares) means the end of the SBR incubation. Seed is the community structure of the inoculum from the 4-L biomass reactor.

5.3.3.3 Variations in the Abundance of Certain Populations

In order to get a better perspective on the diversity as well as the various functionalities introduced by the different organisms, abundance analysis was conducted starting at the phylum-level (Figure 5-12). *Proteobacteria* were the most abundant under all settings. The reactors containing acetate created the highest abundance of *Proteobacteria*. Knowing all PPB are members of *Proteobacteria* and their preference towards simple substrates (i.e. acetate), the increased abundance of *Proteobacteria* possibly attributable to a higher relative abundance of PPB. This is coupled with a decrease in abundance of the fermenters (*Bacteroidetes*, *Verrucomicrobia* and *Cyanobacteria*). While *Bacteroides* appeared in most reactors (including acetate), the abundance of *Verrucomicrobia* and *Cyanobacteria* was only significant in starch, milk and glycerol at the end of SBR incubation with the exception of glycerol-fed reactors illuminated at 940 nm. Syntho reactors showed some *Verrucomicrobia* presence but did not show any *Cyanobacteria*. It appears that *Proteobacteria* are better selected for through batch operation as opposed to the sequencing batch. Comparing the abundance results with our analysis of alpha diversity, the results appear to corroborate the initial interpretation (care should be taken as these results are taken at the phylum level while alpha diversity was done at the OTU level); a variety of phyla are represented under starch, glycerol and milk, which would lead to a higher richness.

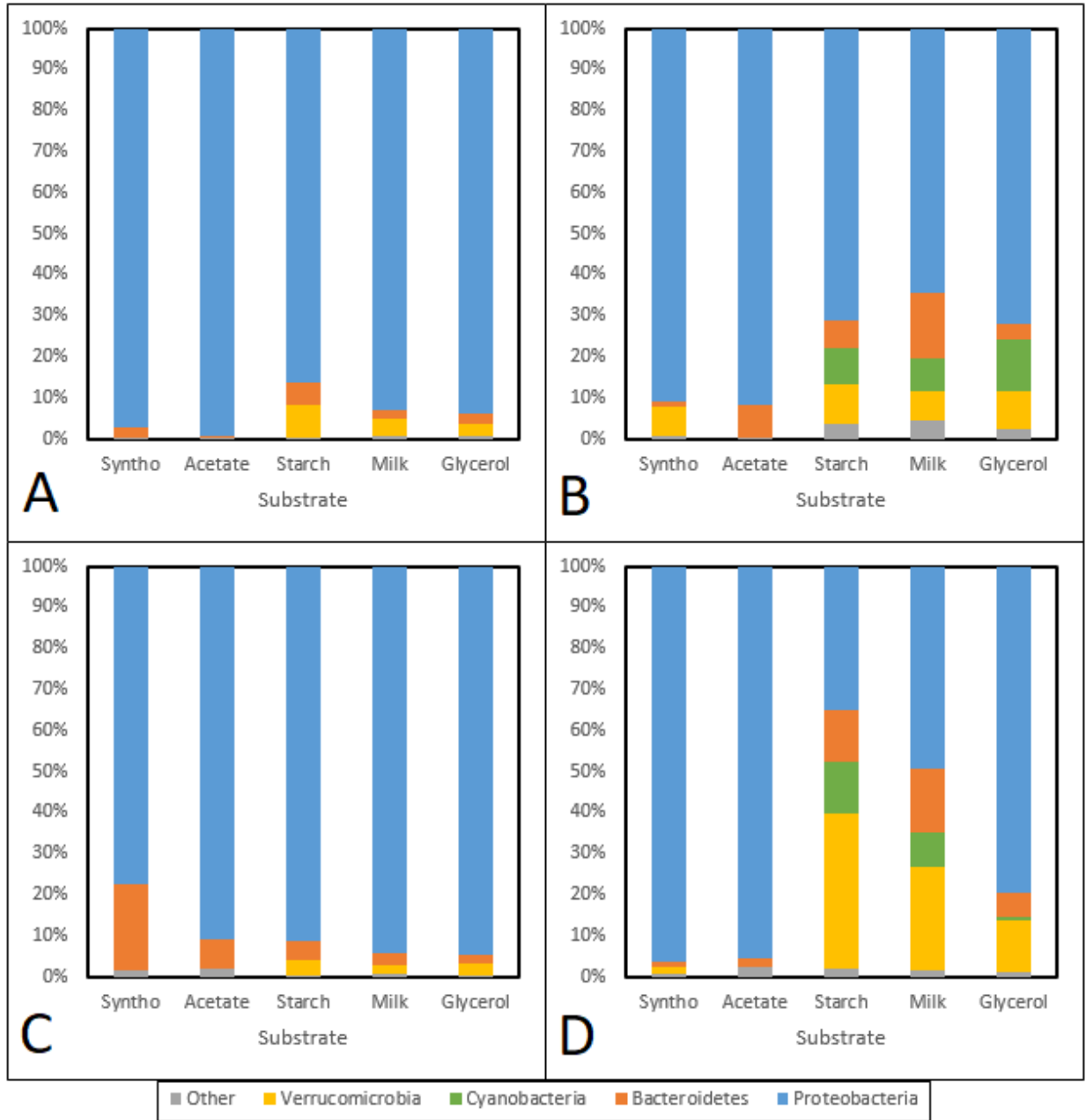


Figure 5-12: Phylum-level abundance of the classified OTUs at the beginning and end of the SBR operation. 850 nm reactors at the start (A) and at the end (B). 940 nm reactors at the start (C) and at the end (D).

Continuing the abundance analysis, the *Proteobacteria* phylum is broken down into *Alphaproteobacteria*, *Betaproteobacteria* and *Gammaproteobacteria* (

Figure 5-14). *Deltaproteobacteria* were virtually absent from the reactors. PPB are known to be subsets of *Alphaproteobacteria*, *Betaproteobacteria* and *Gammaproteobacteria*; the former two house PNSB while PSB are under the latter. Generally, *Alphaproteobacteria* appears to be least represented; their greatest relative abundance was under acetate-fed reactors. *Alphaproteobacteria* were mainly broken down into three families: *Caulobacteriaceae*, *Bradyrhizobiaceae* and *Rhodobacteraceae* (Imhoff et al., 2017). The three families house PNSB under some of their genera. The *Betaproteobacteria* represented by *Commamonadaceae* were significantly abundant under all conditions except during the batch incubation for the reactors illuminated at 940 nm. During these conditions, the *Gammaproteobacteria* were the most abundant, which were represented by *Xanthomonadaceae* when acetate was present or *Enteriobacteriaceae* when fermentable substrate was present.

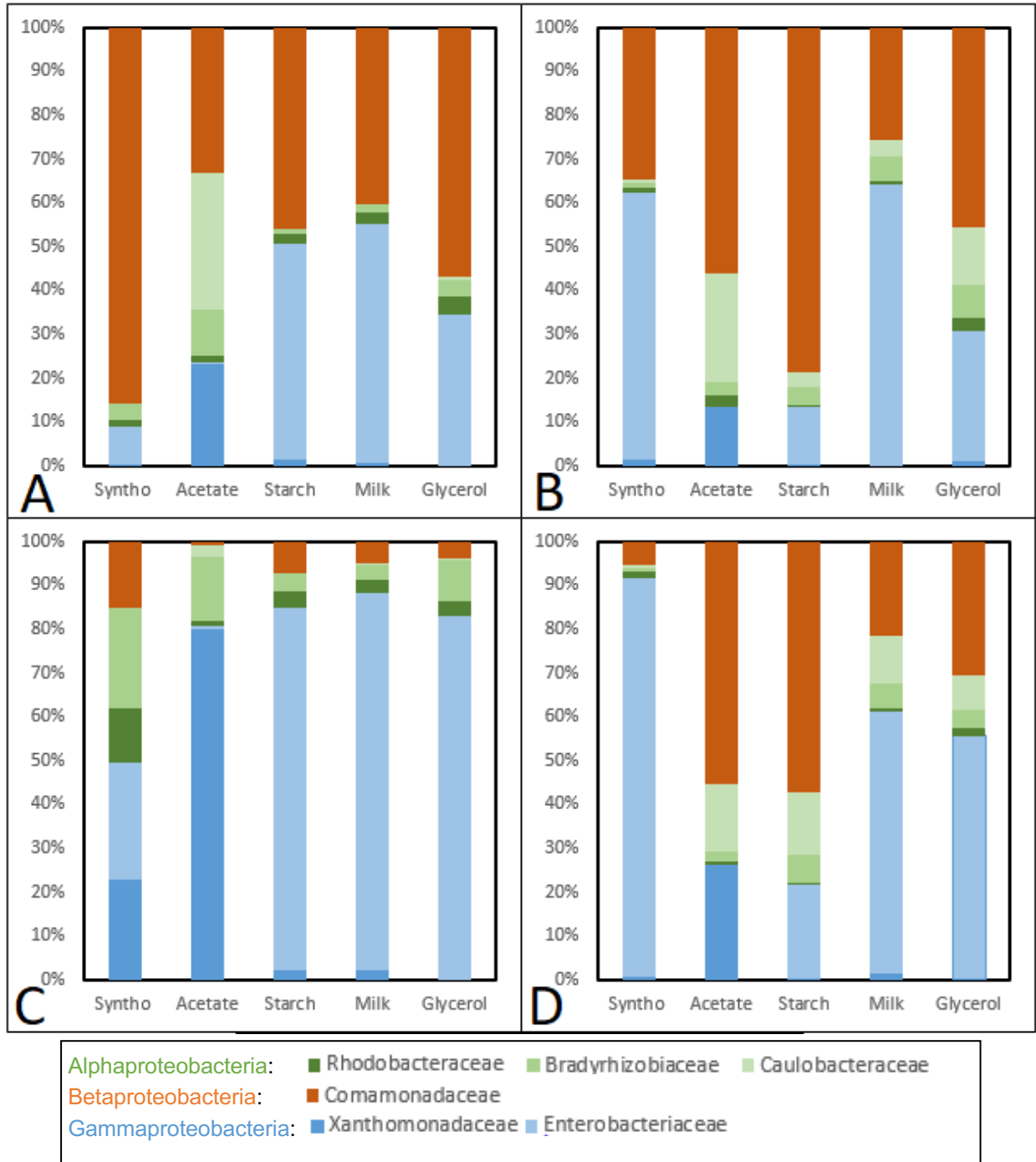


Figure 5-13: Abundance of different families within the *Proteobacteria*. Blue bars represent *Gammaproteobacteria*. Green bars represent *Alphaproteobacteria*. Red bars represent *Betaproteobacteria*. 850 nm reactors at (A) Start and (B) end. 940 nm reactors at (C) start and (D) end.

Following the classifications documented by Imhoff et al. (2017), the families *Caulobacteraceae*, *Bradyrhizobiaceae*, *Rhizobiaceae*, *Methylocystaceae*, *Rhodobacteraceae*, *Acetobacteraceae*, *Rhodospirillaceae*, *Comamonadaceae* and *Rhodocyclaceae* were classified as PPB (

Figure 5-14). None of the *Gammaproteobacteria* present incorporated any PSB.

850 nm light generally resulted in more PPB abundance compared to 940 nm. In most cases, there was a decrease in abundance during the SBR operation. The opposite trend is observed with acetate where the abundance in the 850 nm samples remained similar while the 940 nm samples experienced a considerable increase. Abundance of PPB in starch reactors also increased during SBR operation. The most considerable decrease was with the Syntho reactors subjected to 940 nm; the abundance decreased from 42% to just 8%. It appears that under complex media (Syntho and milk) the abundance of PPB is considerably lower than with simpler ones like acetate and glycerol.

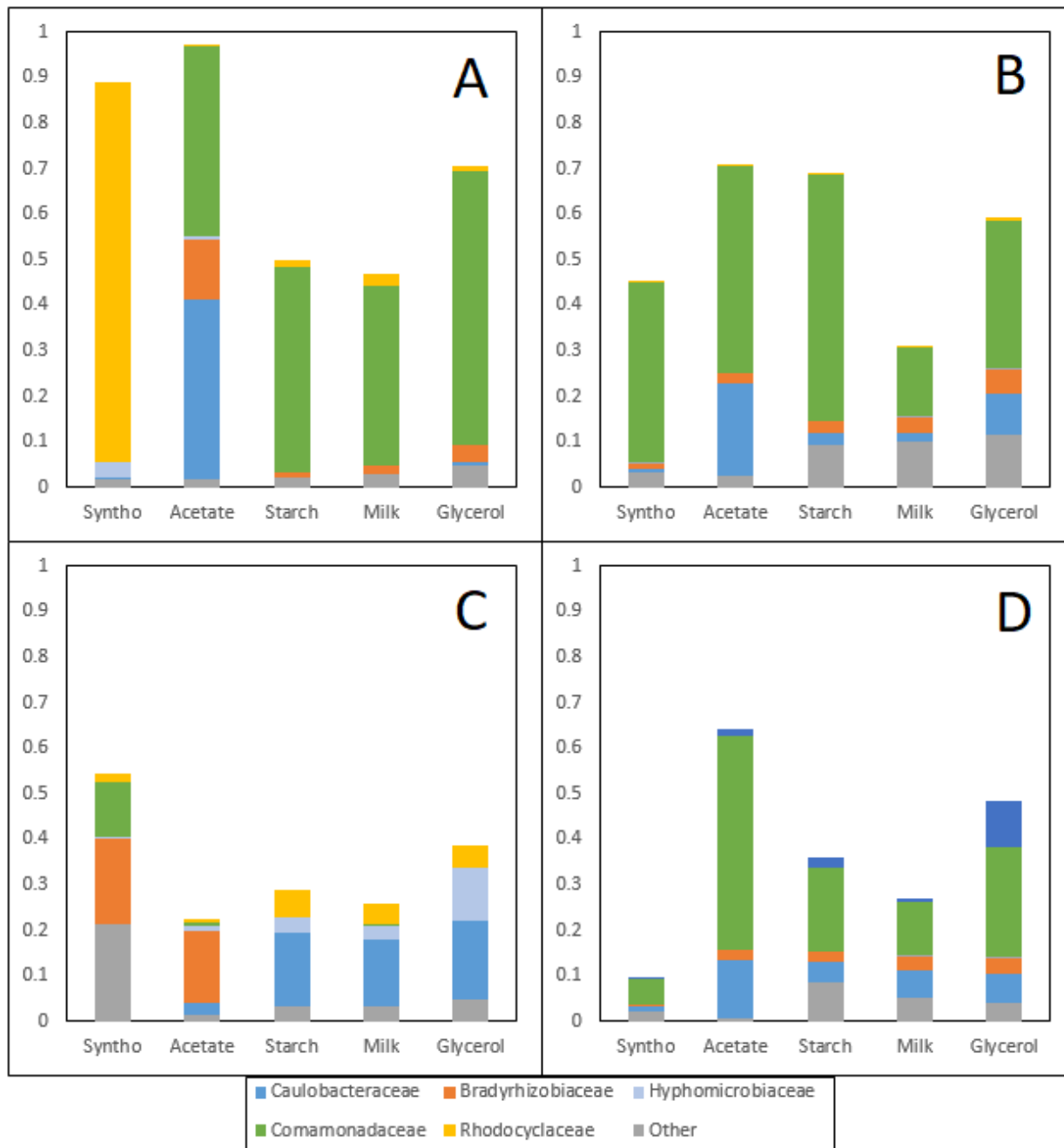


Figure 5-14: Abundance of PPB for the 850 nm reactors at (A): start and (B): end and for the 940 nm reactors at (C): start and (D): end. Enumeration was done on family level. Data from the three replicates were averaged.

5.4 Discussion

5.4.1 Biomass Yield and Bacteriochlorophyll Content

Comparing the VSS levels between reactors, the only significant difference was between reactors fed with glycerol and the others. The glycerol-fed reactors produced much more VSS. Knowing that all reactors were receiving similar amounts of COD (400 mg/L), the difference implies that there was less COD loss to the headspace in the glycerol-fed reactors. This could be coupled with a higher lipid accumulation in those reactors as it is common that glycerol metabolism leads to lipid accumulation within the cells. This observation also applies under anaerobic conditions (Xue et al., 2017).

Samples from reactors subjected to 940 nm IR exhibited a significant increase in BChl-a concentration. This either means that the biomass is producing more pigment to extract more light or that the 850 nm light source is emitting too much light, which might result in photobleaching of BChl-a. Photobleaching is unlikely under the current lighting conditions (Basak et al., 2014). The 850 nm reactors are receiving about 200 W/m² of IR, which has been shown to be below the turning point, which would cause a decrease in biomass content (Carlozzi et al., 2010; Uyar et al., 2009). It is more plausible that the increase is an adaptive measure to the lower energy flux from the 940 nm lamp (70 W/m²). A study on the effect of different visible light wavelengths showed that when there is less red light available, the PPB produce more BChl (Zhou et al., 2015). In their experiment, the pigment content was about 100 times higher than the one observed in this work. However, their study used a much more concentrated feed (COD of 6000 mg/L) and was illuminated using light in visible spectrum (400-700 nm), which is more ideal for carotenoid absorption rather than BChl absorption. The higher BChl content could be an adaptive mechanism to support the higher energy demands to fully degrade the concentrated wastewater. The fact that

the 940 nm samples showed more pigment while the abundance analysis shows lower PPB presence suggests that the enriched PPB under 940 nm produced more pigment rather than more cells. Crosschecking the families present in the abundance with those presented in Stomp et al. (2007), it appears that the enriched PPB were exhibiting BChl-a, which is the pigment we are mainly extracting. It appears that the PPB abundance is in complete disagreement with BChl-a content. In all cases, the 940 nm reactors produced more pigment per VSS but when looking at the PPB abundance, the 850 nm reactors enriched for more PPB. This might be due to a combination of the following reasons: a) that not all the PPB enumerated produced BChl-a, b) not all the enumerated organisms were PPB or c) some organisms managed to produce more pigment than others. The latter seems more likely considering the very low abundance of PPB under 940 nm (less than 10%), which was coupled with the highest BChl-a content.

5.4.2 Diversity

Comparing the effects of substrates on diversity, the reactors receiving milk as the carbon source resulted in the highest Hill's number for both 850 and 940 nm reactors, which was coupled with the highest evenness. Surprisingly, the Syntho reactors created the least diverse communities as indicated by the Hill's number and evenness; this goes against our initial assumption that a more complex feed would lead to a more diverse community. This suggests that a single carbon source was capable of supporting the growth of multiple organisms not just the most competitive one. Contrasting Syntho, milk and glycerol achieved the highest richness which could be explained knowing these substrates can support multiple levels of fermentation and in turn multiple organisms. Milk powder used was mainly composed of maltose and oligosaccharides. Trace amounts of mono- and diglycerides were present (less than 2%). As such, milk has similar components to starch and glycerol. Fermentation of these substrates yields either ethanol or VFAs

(Voet et al., 2006) which are readily consumed by PPB. As such, the dominance by PPB in all reactors and the high diversity observed in reactors receiving milk is to be expected.

The distinction between substrates appears to be the underlying reason for the isolated clusters in the PCoA. The Syntho reactors, composed of both acetate and fermentable substrates, is positioned between the acetate and fermentable substrates clusters. This implies some level of predictability on the enriched Syntho community. The deviation between the prediction and the actual observation can be attributed to microbial interactions, either direct (microbe directly influences other microbe) or indirect (microbe influences environment, which then influences another microbe).

5.4.3 PPB Population

The *Commamonadaceae* were the most abundant PPB family under many reactor conditions especially towards the end of the SBR incubation. Surprisingly, these organisms possess a respiratory-type metabolism. Most members of the family are described as poly-hydroxybutyrate-co-hydroxyvalerate (PHBV) degraders. An observation that is based on isolation from activated sludge reactors (Khan et al., 2002). This suggests that PHBV might be accumulated in the reactors which is sustaining the growth of the *Commamonadaceae*.

Hyphomicrobiaceae were only present in the 940 nm at the start of the SBR incubation. The family houses some facultative photoheterotrophs, mainly the *Blastochloris*, the *Rhodomicrobium* and the *Rhodoplanes* genera (Oren and Xu, 2014). Upon closer inspection of the OTUs sequenced, the family was represented purely by *Rhodoplanes elegans*, a PNSB. These PNSB develop pink cultures (Hiraishi and Ueda, 1994), which could explain the slight variations in colour of the reactors (APPENDIX B: Enrichment Reactor Images). Another characteristic is their ability to undergo complete denitrification (Hiraishi and Ueda, 1994). The abundance of these organisms

appears to be positively correlated with *Rhodocyclaceae* (starch milk and glycerol) and negatively with *Comamonadaceae* and *Bradyrhizobiaceae* (Syntho and acetate). The major genera present under *Rhodocyclaceae* were the *Rhodocyclus*, *Dechloromonas* and *Zooglea*; the first one is a PNSB while the latter two are chemoorganoheterotrophs strictly exhibiting a respiratory type of metabolism (Oren, 2014). Furthermore, reactors receiving 850 nm IR also show a greater proportion of *Proteobacteria* which could indicate that the higher energy of the light was better at enriching for PPB. It is still perplexing that a lot of the PPB observed in the reactors were those exhibiting respiratory metabolisms.

5.4.4 Fermenter Population

The community structure analysis corroborates our statement regarding the emergence of fermenting populations with reactors fed with starch milk or glycerol. Non-proteobacteria were observed at about 30% in reactors receiving 850 nm IR and 60% in reactors receiving 940 nm IR. Further inspection of the phyla present showed that the entire abundance of *Verrucomicrobia* was represented by the family *Opitutaceae*. The family is composed of microaerophiles, facultative and obligate anaerobes. The organisms are generally neutrophiles. The *Verrucomicrobia*, specifically *Opitutaceae*, are distinguished by their ability to consume methane (methanotrophy). The genome of a bacterial strain belonging to the family revealed the presence of genes involved in cellulose hydrolysis and metabolism of subsequent products (Kotak et al., 2015). Starch and cellulose are polymers of glucose, which could explain why *Verrucomicrobia* abundance are highest in starch reactors. Cyanobacteria were also present in reactors fed with fermentable substrate. This is a common observation as a similar reactor fed with dairy wastewater also showed a significant Cyanobacteria presence (Hulsen et al., 2018). Going deeper into the phylum, the only organisms present within *Cyanobacteria* were *Melainabacteria*. Unlike most members of the

phylum, these bacteria are characterized as strictly anaerobes which is to be expected considering the reactors are completely flushed with nitrogen gas. Genome inspection of some members of the family reveals the ability to metabolize simple carbohydrates through the EMP pathway (Soo et al., 2014).

In most reactors except the acetate-fed ones, the *Gammaproteobacteria* were represented by *Enterobacteriaceae*. The family constitutes facultative anaerobes capable of fermenting sugars (Paterson, 2012). In acetate-fed reactors, *Xanthomonadaceae* represented all of the *Gammaproteobacteria*. The primary genus with the family was *Stenotrophomonas*. Phenotypic studies on the genus have shown that they have limited capacity to utilize sugars, only growing on maltose or fructose. They also lack the ability to degrade alcohols (Assih et al., 2002). *Stenotrophomonas maltophilia MK2* was reported to exhibit both aerobic and anaerobic metabolisms with the anaerobic metabolism relying on amino acid fermentation (Venkidusamy and Megharaj, 2016). Amino acids were not directly fed into the reactors, but they could be byproducts of the other organisms' fermentative growth. This might explain why they are only present in acetate environments but not milk, starch or glycerol.

5.5 Conclusions

The literature describes PPB as organisms with a limited capacity for the consumption of sugars while growing photoheterotrophically. Consequently, fermenters would likely have a more efficient access to sugars than PPB. The experiment presented here further evidenced this distinction between PPB and fermenters under varying carbon-sources. While the selection of PPB under IR in anaerobic environments is very consistent, the presence of fermentable substrate will inevitably lead to a significant fermenting population. This intimate coexistence of PPB and fermenting organisms is critical to optimizing the wastewater treatment operation with resource

recovery as our objective. VFAs are the preferred substrates for PPB which was either directly present in the medium or produced as a fermentation by-product; as such, a proper understanding of the carbon flow between these two populations is of great importance.

6 INTERMITTENT IR ILLUMINATION AS A SELECTIVE PRESSURE FOR POLY-P ACCUMULATORS

6.1 Introduction

Phosphorus as a resource is critical to the agricultural industry. While agricultural needs keep increasing, our natural phosphorus reserves are steadily depleting (Sattari et al., 2012). Most of the phosphorus used in North America is currently imported. Wastewater naturally contains significant levels of phosphorus, which can be leveraged to reduce dependence on imports.

Phosphorus recovery from wastewater relies on chemical and biological processes. The recovered phosphorus in the form of precipitate or biomass can later be used as a fertilizer. Focusing on biological processes, phosphorus can be removed from the wastewater by assimilation or the production of phosphorus storage polymers (poly-P). First, as microorganisms grow, they assimilate phosphorus into biomass. However, because phosphorus assimilation into biomass accounts for less than 3% of the biomass's dry weight, this low level of assimilation is insufficient for complete phosphorus recovery.

To complement assimilative uptake, enhanced biological phosphorus removal (EBPR) is usually employed. EBPR relies on developing an ecological niches in the wastewater community that favors the production of phosphorus storage polymers (poly-P). EBPR relies on phosphate accumulating organisms (PAOs) that accumulate poly-P to store energy while under aerobic conditions to be able to gain preferential access to their substrate under anaerobic conditions. This metabolism allows PAOs to sequester the phosphorus from the water, which can be leveraged to create a concentrated phosphate stream for recovery. The EBPR process is a good example of a

design that creates a specific ecological niche (i.e, the one of the PAOs) that can be engineered and exploited to achieved specific goals.

Inspired by EBPR, we aimed at doing the same here with PPB by generating a niche for poly-P accumulation. We also hypothesize that poly-P is used as excess energy storage by PPB. Therefore, as opposed to EBPR, cycling between aerobic and anaerobic environments to create the energy cycle, cycling between light and dark environments was hypothesized to select for poly-P accumulating PNSBs. The potential for using microbial communities dominated by PPBs was evaluated as a method to accumulate phosphorus in a wastewater treatment scenario. The cultures grown were taken from a 4-L reactor (Chapter 4). The cultures were fed with synthetic wastewater and were subjected to an intermittent lighting regime (8 hours dark, 16 hours light). The light sources were either 850 nm or 940 nm IR.

This experiment addresses the fourth and fifth thesis objectives restated here:

1. Comparison of the level poly-phosphate accumulation between reactors subjected to intermittent and continuous illumination.
2. Investigation of the effect of changing IR wavelength (850 nm and 940 nm) on poly-P accumulation.

6.2 Experimental Design

6.2.1 Experimental Setup

Serum bottles of 500 mL were operated as reactors with a working volume of 400 mL and fed with synthetic wastewater (Chapter 3). The reactors were inoculated with 1 mL solids from the 4-L reactor. The reactors were operated as SBRs with a retention time of four days and a cycle time of one day. The reactors were exposed to either 850 or 940 nm light intermittently (8 hours dark, 16

hours light). Continuously illuminated reactors were used as light controls. Additionally, reactors kept in a dark environment were used as dark controls. The reactors' positions were switched daily to avoid an illumination bias. The reactors were mixed using magnetic stirrers. Each reactor configuration was duplicated and operated for at least 3 SRTs to reach steady-state. Finally, COD, P, solids and pH were measured over the course of the experiment (Chapter 3).

6.3 Results and Discussion

Over the course of the operation (3 HRTs), the COD was recorded

Figure 6-1). The total COD for all the reactors appeared to be following the same trend. All reactors except 850 C2 started with a COD around 450 mg-COD/L and it decreased overtime reaching around 350 mg-COD/L. This trend in the total COD profile was consistent with our profile for 4-L biomass reactor. The COD in the feed was kept relatively constant, which means that the decrease in total COD overtime indicates COD loss to the headspace. The concentration of soluble COD in the reactors also decreased overtime reaching around 20-40 mg-COD/L at the end, while the soluble COD in the dark control reactors stabilized at 100 mg-COD/L towards the end.

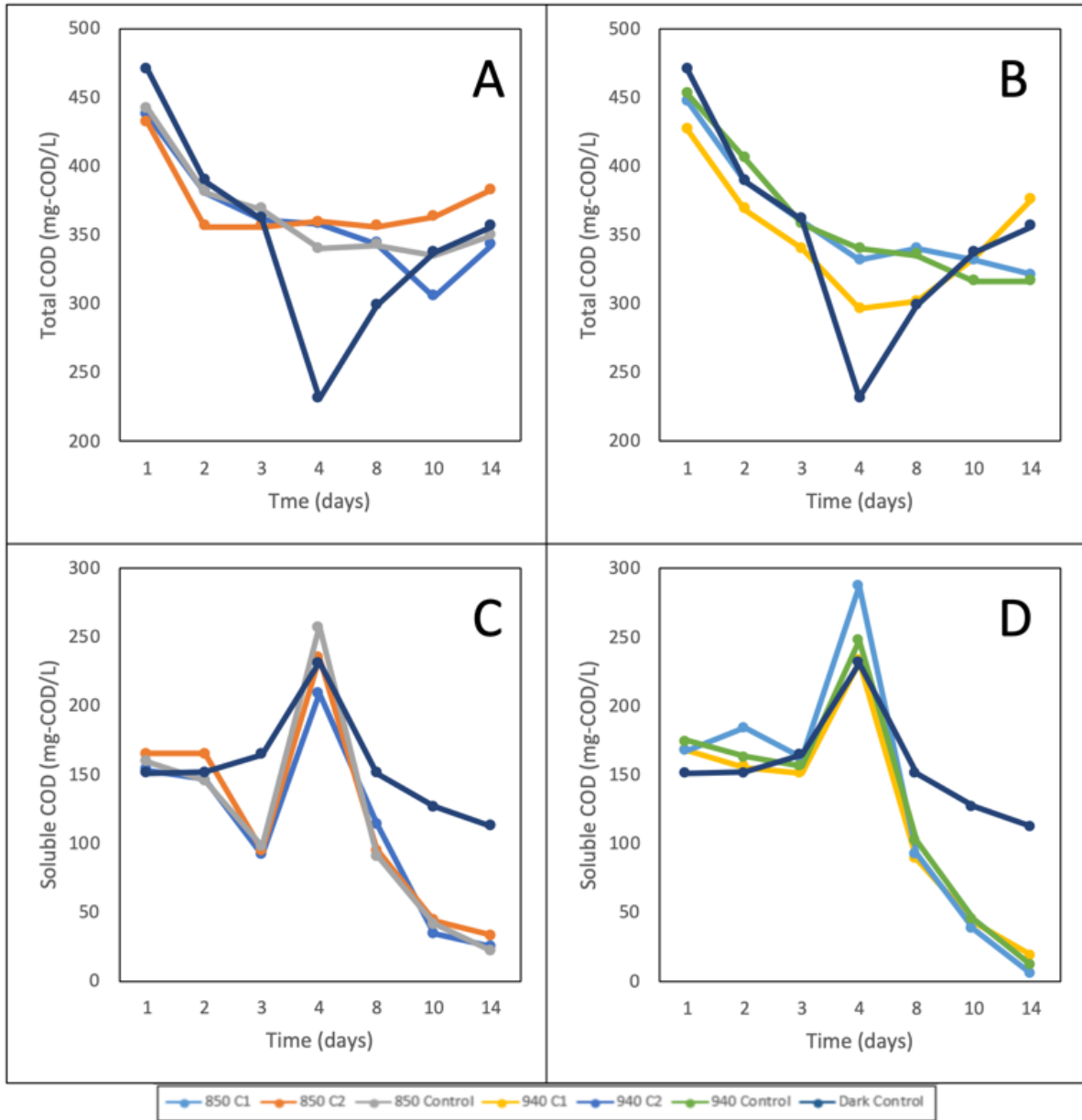


Figure 6-1: COD profiles over time. (A) Total COD for 850 nm reactors. (B) Total COD for 940 nm reactors. (C) Soluble COD for 850 nm reactors. (D) Soluble COD for 940 nm reactors.

Starting with an initial phosphate concentration of about 12 mg-P/L, all reactors (except the dark control) managed to drop the concentration down to about 10 mg-P/L. This removal was due to biomass growth. Following the growth phase, there was a steady decline in phosphate

concentration for reactors illuminated with the 850 nm. However, one of the reactors started exhibiting the opposite trend after nine days. All the reactors illuminated with 940 nm IR generally showed a declining trend over time. From the phosphate profiles over time, it is unclear if intermittent lighting in this experiment had an effect on accumulation of poly-P. Under 940 nm illumination the difference was found to be insignificant through two-way ANOVA. More pronounced differences from the control were observed in the reactors receiving 850 nm IR. Only one of reactors illuminated with 940 nm IR managed to accumulate more phosphorus than the control. In all cases, the reactors outperformed the dark control. This is expected since the dark control reactors did not fully utilize the COD thus, the growth-related assimilative uptake was reduced. Inadequate illumination also limits the amount of energy the microorganisms had access to which would limit accumulative uptake in the dark control reactors.

The experiment was conducted for three retention times, which might have been not long enough for a selective pressure to promote the growth of phosphate accumulators or it might not have been long enough to establish a steady-state. It is worth noting that the reactors appeared to still be removing phosphates and COD towards the end of the experiment. Alternatively, phosphate accumulators under both illumination regimes might have been operating at near capacity and the slight differences are due to random error in measurements.

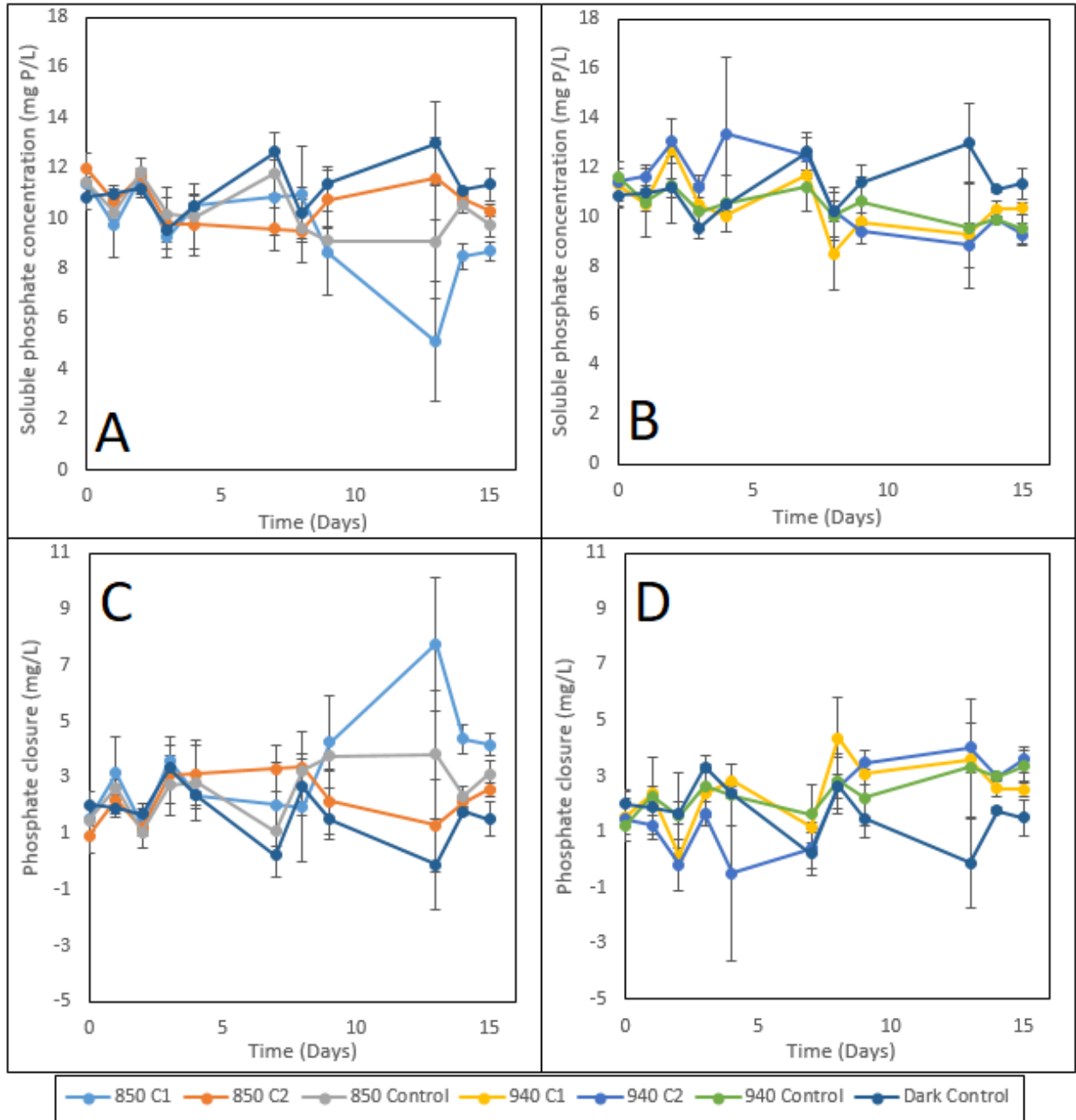


Figure 6-2: Phosphate profile over time. Measurements correspond to the average of four replicates; error bars represent one standard deviation. (A): Soluble phosphate profile for 850 nm reactors. (B): Soluble phosphate profile for the 940 nm reactors. (C): Difference between total phosphate and soluble phosphate measurement for 850 nm reactors. (D): Difference between total phosphate and soluble phosphate for 940 nm reactors. Two-way ANOVA was done to assess significance of the substrate main effect, wavelength main effect and substrate-wavelength interactions. Results indicate that none of parameters were significant.

In all reactors other than the dark control, a clear and significant increase in the pH was noted (Figure 6-3). The pH of the systems started at near neutral levels (about 7.5) and increased up to a maximum of about 9 for some of them. The two 940 nm reactors appeared to have a similar increase in pH to each other. In the case of 850 nm reactors 850-C2 and the 850-Control had the greatest increase. However, 850-C1 had a lower pH towards the end than the reactors illuminated at 940 nm. The pH of the dark control did not change significantly during this experiment.

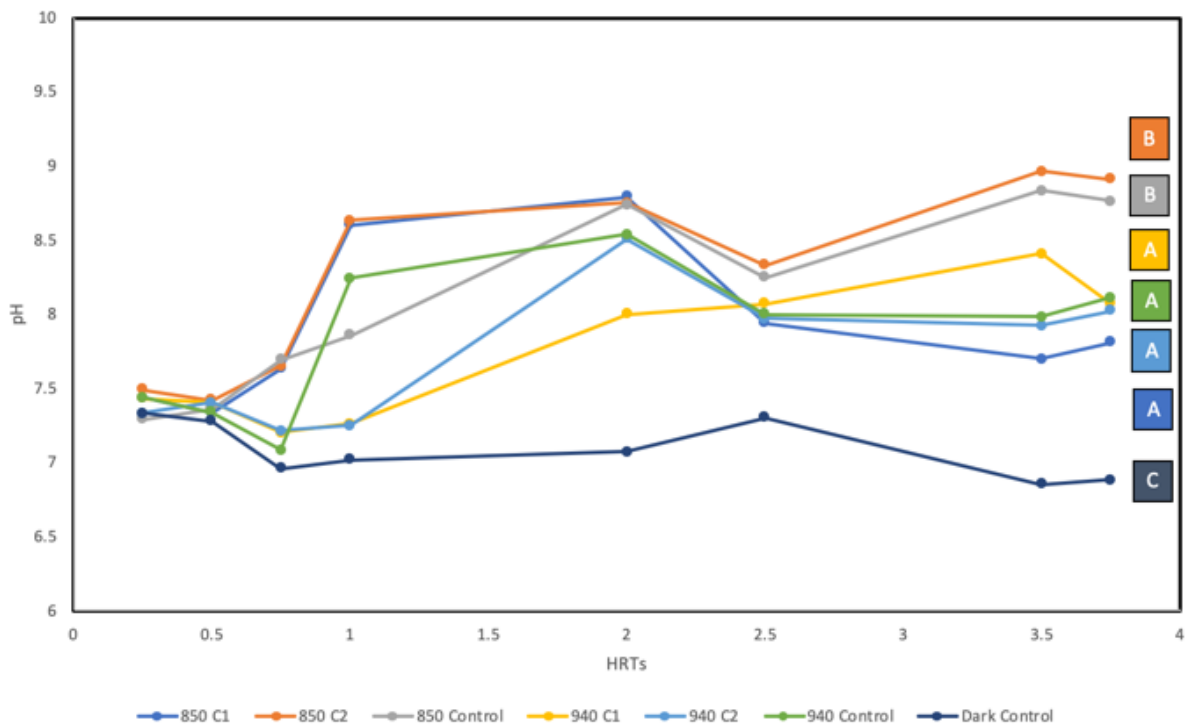


Figure 6-3: pH profile over time for the batch reactors. Horizontal axis represents dimensionless time in multiples of HRT. Vertical axis is magnified (starting at 6) to highlight differences between reactors. One-way ANOVA was done to assess the significance of the differences using data after 2.5 HRTs. Letters indicate reactors with non-significant differences identified by the least square difference.

The pH increase could be evident of a proton uptake processes (Trchounian, 2015) leading to hydrogen production. While the exact nature of the uptake is not clear, a possible reason for it

could be due to nitrogenase activity rather than hydrogenase activity. Nitrogenase is generally expressed when the medium is insufficient in nitrogen. Knowing that the synthetic wastewater used had about 45 mg-N/L and the enriched VSS has about 10 mg-N/L, it is reasonable to exclude nitrogenase as the reason for the pH increase. Alternatively, the pH increase in the reactor could have led to poly-P breakdown as a means to regulate pH. In an experiment investigating the benefits of buffering the growth medium at around neutral levels on poly-P accumulation, it was observed that when the system was unbuffered, the poly-P reserves decreased to help mediate pH changes (Liang et al., 2010). Changes in pH can also be attributed to variations in the partial pressure of CO₂. Contrary to the 4-L biomass reactor, which remained neutral over the course of the operation, the bottles in this experiment had a considerably larger headspace than the main reactor. The larger headspace in the serum bottles makes it more difficult to increase the partial pressure of CO₂ in the headspace, which could explain why there is a significant increase in the pH in the serum bottles but not in the 4-L reactor.

6.4 Conclusions

The design of this experiment has to be reviewed. It is unclear whether there is a difference between continuous and intermittent illumination. The revised experiment would have to consider a) an extended experimental duration such that the phosphate profiles appear to be steady and b) a comparison between unbuffered and buffered conditions. In the case where the current results are indicative of what is truly happening, we suggest that proton uptake (possibly due to nitrogenase) would be the next step for optimization of poly-P accumulation. However, a nitrogen balance or nitrogenase assay would have to be incorporated before we can confidently conclude that nitrogenase activity is affecting poly-P accumulation.

7 CONCLUSIONS AND FUTURE WORK

7.1 Conclusions

This work aims to bridge some of the gaps between the metabolically versatile and ubiquitous PPB that possess attractive properties for resource-recovery applications and the design of complex wastewater treatment reactors. A 4-L flat-panel photoreactor was built and operated anaerobically with IR illumination. The biomass enriched in this reactor appeared capable to accumulate Poly-P under unoptimized conditions (Chapter 4). From this initial result, two additional questions were raised. (A) What are the main ecological functions developed in photobioreactors fed with Syntho, and what are the populations responsible? (B) Is it possible to identify operation conditions to promote the Poly-P accumulation. The enrichment experiment identified two major guild (functional populations) populations when the carbon sources used in Syntho were separated: fermenters and PPB population (Chapter 5). The emergences of fermenters were due to presence of fermentable substrate such as sugars (glycerol, starch, and sugars in milk powder) or the formation of fermentable byproducts from the growth of PPB. These results highlight two aspects of PPB biotechnology, a) PPB appear to lose competition over fermentable substrate and b) the relationship between fermenters and PPB is critical to analysis of the process. Incidentally, the dominant PPB populations did not appear to be the same in the 4-L reactor and the 60-mL serum-bottle reactors, and it remained unclear what was the cause for these differences. With the second experiment, we attempted to address the second question raised by the 4-L reactor operation (Chapter 4). The effect of the illumination regime was hypothesized to have an effect on the accumulation of the reactors, either through variations in microbial community or through changes in the organisms' behavior under these conditions. The engineering implications of illumination regimes were unfortunately inconclusive as the reactors attempting to accumulate Poly-P did not

differ significantly under the two wavelengths tested and the two illumination regimes (continuous vs. 16 hours light/8 hours dark). The experimental design should be reviewed, and additional scrutiny should be used to formulate the hypothesis that poly-P is mainly used as an energy storage. This is done either through consideration of other metabolic regulators on the polymer's accumulation or through revision of the experiment's design. The possible revisions of the experimental design could include through the light:dark ratio or through the experiment's length. The most pronounced effect of the IR wavelength was observed in the pigment concentration.

In conclusion, evidence of the accumulation of poly-P in a wastewater treatment setting was provided and the impact of carbon substrate on the community structure was demonstrated. However, the capacity of the reactor to fully remove all the phosphates appear to be insufficient at the moment, and the reasons will need to be addressed in future research.

7.2 Future Work

4-L Reactor

The biomass reactor is planned to be upscaled to a 10 L. The increased volume will allow for an easier operation of a continuous system and the increased depth of the reactor will allow it to intercept more of the light. Nitrogen balance will be added to account for nitrogen fixation. The balances will be extended to the headspace to account for any COD loss.

Enrichment Experiment

Further bioinformatic analysis will be conducted. The results of this experiment will be extended to better understand the extent of intermicrobial interactions and their effect on the resulting microbial community. Keeping the same premise, the permutations of synthetic wastewater

components. This will be coupled with an increase in sample size of each configuration. This will all be achieved by operating the reactors in 96-well plates.

LIST OF REFERENCES

- Albi, T. and Serrano, A. 2016. Inorganic polyphosphate in the microbial world. Emerging roles for a multifaceted biopolymer. *World J Microbiol Biotechnol* 32(2), 27.
- Albuquerque, M.G., Martino, V., Pollet, E., Averous, L. and Reis, M.A. 2011. Mixed culture polyhydroxyalkanoate (PHA) production from volatile fatty acid (VFA)-rich streams: effect of substrate composition and feeding regime on PHA productivity, composition and properties. *J Biotechnol* 151(1), 66-76.
- Altschul, S.F., Gish, W., Miller, W., Myers, E.W. and Lipman, D.J. 1990. Basic local alignment search tool. *J. Mol. Biol.* 215(3), 403-410.
- APHA (2012) Standard methods for the examination of water and wastewater (22nd Edition), American Public Health Association (APHA), American Water Works Association (AWWA) and Water Environment Federation (WEF), Washington, D.C., USA.
- Assih, E.A., Ouattara, A.S., Thierry, S.b., Cayol, J.-L., Labat, M. and Macarie, H. 2002. *Stenotrophomonas acidaminiphila* sp. nov., a strictly aerobic bacterium isolated from an upflow anaerobic sludge blanket (UASB) reactor. *INT J SYST EVOL MICR* 52, 559-568.
- Basak, N., Jana, A.K., Das, D. and Saikia, D. 2014. Photofermentative molecular biohydrogen production by purple-non-sulfur (PNS) bacteria in various modes: The present progress and future perspective. *Int J Hydrogen Energy* 39(13), 6853-6871.
- Bolyen, E., Rideout, J.R., Dillon, M.R., Bokulich, N.A., Abnet, C.C., Al-Ghalith, G.A., Alexander, H., Alm, E.J., Arumugam, M., Asnicar, F., Bai, Y., Bisanz, J.E., Bittinger, K., Brejnrod, A., Brislawn, C.J., Brown, C.T., Callahan, B.J., Caraballo-Rodriguez, A.M., Chase, J., Cope, E.K., Da Silva, R., Diener, C., Dorrestein, P.C., Douglas, G.M., Durall, D.M., Duvallet, C., Edwardson, C.F., Ernst, M., Estaki, M., Fouquier, J., Gauglitz, J.M., Gibbons, S.M., Gibson, D.L., Gonzalez, A., Gorlick, K., Guo, J., Hillmann, B., Holmes, S., Holste, H., Huttenhower, C., Huttley, G.A., Janssen, S., Jarmusch, A.K., Jiang, L., Kaehler, B.D., Kang, K.B., Keefe, C.R., Keim, P., Kelley, S.T., Knights, D., Koester, I., Kosciolk, T.,

Kreps, J., Langille, M.G.I., Lee, J., Ley, R., Liu, Y.X., Loftfield, E., Lozupone, C., Maher, M., Marotz, C., Martin, B.D., McDonald, D., McIver, L.J., Melnik, A.V., Metcalf, J.L., Morgan, S.C., Morton, J.T., Naimey, A.T., Navas-Molina, J.A., Nothias, L.F., Orchanian, S.B., Pearson, T., Peoples, S.L., Petras, D., Preuss, M.L., Pruesse, E., Rasmussen, L.B., Rivers, A., Robeson, M.S., 2nd, Rosenthal, P., Segata, N., Shaffer, M., Shiffer, A., Sinha, R., Song, S.J., Spear, J.R., Swafford, A.D., Thompson, L.R., Torres, P.J., Trinh, P., Tripathi, A., Turnbaugh, P.J., Ul-Hasan, S., van der Hooft, J.J.J., Vargas, F., Vazquez-Baeza, Y., Vogtmann, E., von Hippel, M., Walters, W., Wan, Y., Wang, M., Warren, J., Weber, K.C., Williamson, C.H.D., Willis, A.D., Xu, Z.Z., Zaneveld, J.R., Zhang, Y., Zhu, Q., Knight, R. and Caporaso, J.G. 2019. Reproducible, interactive, scalable and extensible microbiome data science using QIIME 2. *Nat. Biotechnol.* 37(8), 852-857.

Brook, I. (2017) *Infectious Diseases*, pp. 1628-1644, Elsevier, Amsterdam.

Callahan, B.J., McMurdie, P.J., Rosen, M.J., Han, A.W., Johnson, A.J. and Holmes, S.P. 2016. DADA2: High-resolution sample inference from Illumina amplicon data. *Nat Methods* 13(7), 581-583.

Carlozzi, P., Pintucci, C., Piccardi, R., Buccioni, A., Minieri, S. and Lambardi, M. 2010. Green energy from *Rhodospseudomonas palustris* grown at low to high irradiance values, under fed-batch operational conditions. *Biotechnol Lett* 32(4), 477-481.

Cogdell, R.J. and Frank, H.A. 1987. How Carotenoids Function in Photosynthetic Bacteria. *Biochim Biophys Acta* 895(2), 63-79.

Cogdell, R.J., Isaacs, N.W., Freer, A.A., Arrelano, J., Howard, T.D., Papiz, M.Z., Hawthornthwaite-Lawless, A.M. and Prince, S. 1997. The structure and function of the LH2 (B800-850) complex from the purple photosynthetic bacterium *Rhodospseudomonas acidophila* strain 10050. *Prog Biophys Mol Biol* 68(1), 1-27.

DeSantis, T.Z., Hugenholtz, P., Larsen, N., Rojas, M., Brodie, E.L., Keller, K., Huber, T., Dalevi, D., Hu, P. and Andersen, G.L. 2006. Greengenes, a chimera-checked 16S rRNA gene database and workbench compatible with ARB. *Appl Environ Microbiol* 72(7), 5069-5072.

- Ghimire, A., Valentino, S., Frunzo, L., Pirozzi, F., Lens, P.N. and Esposito, G. 2016. Concomitant biohydrogen and poly-beta-hydroxybutyrate production from dark fermentation effluents by adapted *Rhodobacter sphaeroides* and mixed photofermentative cultures. *Bioresour Technol* 217, 157-164.
- Ghosh, S., Dairkee, U.K., Chowdhury, R. and Bhattacharya, P. 2017. Hydrogen from food processing wastes via photofermentation using Purple Non-sulfur Bacteria (PNSB) – A review. *Energy Convers. Manag.* 141, 299-314.
- Guerra-Blanco, P., Cortes, O., Poznyak, T., Chairez, I. and García-Peña, E.I. 2018. Polyhydroxyalkanoates (PHA) production by photoheterotrophic microbial consortia: Effect of culture conditions over microbial population and biopolymer yield and composition. *European Polymer Journal* 98, 94-104.
- Hiraishi, A. and Kitamura, H. 1985. Changes in the polyphosphate content of photosynthetically grown *Rhodobacter sphaeroides* due to nutrient limitation. *Agric. Biol. Chem.*, 49.
- Hiraishi, A. and Ueda, Y. 1994. *Rhodoplanes* gen-nov, a new genus of phototrophic bacteria Including *rhodopseudomonas-rosea* as *rhodoplanes-roseus* comb-nov and *rhodoplanes-elegans* sp-nov. *Int J Syst Bacteriol* 44(4), 665-673.
- Hiraishi, A., Yanase, A. and Kitamura, H. 1991. Polyphosphate accumulation by *Rhodobacter sphaeroides* grown under different environmental conditions with special emphasis on the effect of external phosphate concentrations. *JSME* 6(1), 25-32.
- Hu, X., Ritz, T., Damjanovic, A., Autenrieth, F. and Schulten, K. 2002. Photosynthetic apparatus of purple bacteria. *Q Rev Biophys* 35(1), 1-62.
- Hulsen, T., Hsieh, K. and Batstone, D.J. 2019. Saline wastewater treatment with purple phototrophic bacteria. *Water Res* 160, 259-267.
- Hulsen, T., Hsieh, K., Lu, Y., Tait, S. and Batstone, D.J. 2018. Simultaneous treatment and single cell protein production from agri-industrial wastewaters using purple phototrophic bacteria or microalgae - A comparison. *Bioresour Technol* 254, 214-223.

- Imhoff, J.F., Rahn, T., Kunzel, S. and Neulinger, S.C. 2017. Photosynthesis is widely distributed among Proteobacteria as demonstrated by the phylogeny of PufLM reaction center proteins. *Front. Microbiol.* 8, 2679.
- Kang, S., Rodrigues, J.L., Ng, J.P. and Gentry, T.J. 2016. Hill number as a bacterial diversity measure framework with high-throughput sequence data. *Sci Rep* 6, 38263.
- Khan, S.T., Horiba, Y., Yamamoto, M. and Hiraishi, A. 2002. Members of the family Comamonadaceae as primary poly(3-hydroxybutyrate-co-3-hydroxyvalerate)-degrading denitrifiers in activated sludge as revealed by a polyphasic approach. *Appl Environ Microbiol* 68(7), 3206-3214.
- Kotak, M., Isanapong, J., Goodwin, L., Bruce, D., Chen, A., Han, C.S., Huntemann, M., Ivanova, N., Land, M.L., Nolan, M., Pati, A., Woyke, T. and Rodrigues, J.L. 2015. Complete genome sequence of the opitutaceae bacterium strain TAV5, a potential facultative methylotroph of the wood-feeding termite *reticulitermes flavipes*. *Genome Announc* 3(2).
- Kuo, F.S., Chien, Y.H. and Chen, C.J. 2012. Effects of light sources on growth and carotenoid content of photosynthetic bacteria *Rhodospseudomonas palustris*. *Bioresour Technol* 113, 315-318.
- Larimer, F.W., Chain, P., Hauser, L., Lamerdin, J., Malfatti, S., Do, L., Land, M.L., Pelletier, D.A., Beatty, J.T., Lang, A.S., Tabita, F.R., Gibson, J.L., Hanson, T.E., Bobst, C., Torres, J.L., Peres, C., Harrison, F.H., Gibson, J. and Harwood, C.S. 2004. Complete genome sequence of the metabolically versatile photosynthetic bacterium *Rhodospseudomonas palustris*. *Nat Biotechnol* 22(1), 55-61.
- Legendre, P. and Legendre, L.F. (2012) *Numerical ecology* (3rd Edition), Elsevier, Amsterdam.
- Liang, C.M., Hung, C.H., Hsu, S.C. and Yeh, I.C. 2010. Purple nonsulfur bacteria diversity in activated sludge and its potential phosphorus-accumulating ability under different cultivation conditions. *Appl Microbiol Biotechnol* 86(2), 709-719.
- Madigan, M.T. and Jung, D.O. (2009) *The Purple Phototrophic Bacteria*, pp. 1-15, Springer.

- Madigan, M.T., Martinko, J.M., Bender, K.S., Buckley, D.H. and Stahl, D.A. (2015) Brock biology of microorganisms, Pearson, New York.
- Marchandin, H. and Jumas-Bilak, E. (2014) The Prokaryotes: Firmicutes and Tenericutes. Rosenberg, E., DeLong, E.F., Lory, S., Stackebrandt, E. and Thompson, F. (eds), pp. 433-453, Springer Berlin Heidelberg, Berlin, Heidelberg.
- McCarty, P.L., Bae, J. and Kim, J. 2011. Domestic wastewater treatment as a net energy producer--can this be achieved? *Environ Sci Technol* 45(17), 7100-7106.
- Metcalf and Eddy (2003) Wastewater engineering : treatment and reuse, Fourth edition / revised by George Tchobanoglous, Franklin L. Burton, H. David Stensel. Boston : McGraw-Hill.
- Molecular Probes Data Sheet MP 07581 2005. Quant-iT PicoGreen dsDNA reagent and kits. Cathy Olsen, Sunnyvale.
- Nopens, I., Capalozza, C. and Vanrolleghem, P.A. 2001. Stability analysis of a synthetic municipal wastewater. Department of Applied Mathematics Biometrics and Process Control, University of Gent, Belgium.
- Omelon, S., Georgiou, J. and Habraken, W. 2016. A cautionary (spectral) tail: red-shifted fluorescence by DAPI-DAPI interactions. *Biochem Soc Trans* 44(1), 46-49.
- Oren, A. (2014) The Prokaryotes: Alphaproteobacteria and Betaproteobacteria. Rosenberg, E., DeLong, E.F., Lory, S., Stackebrandt, E. and Thompson, F. (eds), pp. 975-998, Springer Berlin Heidelberg, Berlin, Heidelberg.
- Oren, A. and Xu, X.-W. (2014) The Prokaryotes: Alphaproteobacteria and Betaproteobacteria. Rosenberg, E., DeLong, E.F., Lory, S., Stackebrandt, E. and Thompson, F. (eds), pp. 247-281, Springer Berlin Heidelberg, Berlin, Heidelberg.
- Paterson, D.L. (2012) Goldman's Cecil Medicine (Twenty Fourth Edition). Goldman, L. and Schafer, A.I. (eds), pp. 1874-1877, W.B. Saunders, Philadelphia.

- Puyol, D., Barry, E.M., Hulsen, T. and Batstone, D.J. 2017. A mechanistic model for anaerobic phototrophs in domestic wastewater applications: Photo-anaerobic model (PANM). *Water Res* 116, 241-253.
- Reis, M., Albuquerque, M., Villano, M. and Majone, M. (2011) *Comprehensive Biotechnology*. Moo-Young, M. (ed), pp. 669-683, Elsevier, Amsterdam.
- Rittman, B.E. and McCarty, P.L. (2012) *Environmental biotechnology: principles and applications*, McGraw Hill Education.
- Rosenberg, E. (2014) *The Prokaryotes*. Rosenberg, E. (ed), pp. 825-827, Springer, Berlin.
- Sattari, S.Z., Bouwman, A.F., Giller, K.E. and van Ittersum, M.K. 2012. Residual soil phosphorus as the missing piece in the global phosphorus crisis puzzle. *Proc Natl Acad Sci U S A* 109(16), 6348-6353.
- Soo, R.M., Skennerton, C.T., Sekiguchi, Y., Imelfort, M., Paech, S.J., Dennis, P.G., Steen, J.A., Parks, D.H., Tyson, G.W. and Hugenholtz, P. 2014. An expanded genomic representation of the phylum cyanobacteria. *Genome Biol Evol* 6(5), 1031-1045.
- Stomp, M., Huisman, J., Stal, L.J. and Matthijs, H.C. 2007. Colorful niches of phototrophic microorganisms shaped by vibrations of the water molecule. *ISME J* 1(4), 271-282.
- Trchounian, A. 2015. Mechanisms for hydrogen production by different bacteria during mixed-acid and photo-fermentation and perspectives of hydrogen production biotechnology. *Crit Rev Biotechnol* 35(1), 103-113.
- Uyar, B., Eroglu, I., Yücel, M. and Gündüz, U. 2009. Photofermentative hydrogen production from volatile fatty acids present in dark fermentation effluents. *Int J Hydrogen Energy* 34(10), 4517-4523.
- Venkidasamy, K. and Megharaj, M. 2016. Identification of electrode respiring, hydrocarbonoclastic bacterial strain *Stenotrophomonas maltophilia* MK2 highlights the untapped potential for environmental bioremediation. *Front Microbiol* 7(1965).

- Voet, D., Voet, J.G. and Pratt, C.W. (2006) Fundamentals of biochemistry: life at the molecular level, Wiley, New Jersey.
- Wang, X., Oehmen, A., Freitas, E.B., Carvalho, G. and Reis, M.A. 2017. The link of feast-phase dissolved oxygen (DO) with substrate competition and microbial selection in PHA production. *Water Res* 112, 269-278.
- Xue, L.L., Chen, H.H. and Jiang, J.G. 2017. Implications of glycerol metabolism for lipid production. *Prog Lipid Res* 68, 12-25.
- Yurkov, V. and Hughes, E. (2017) Modern topics in the phototrophic prokaryotes, pp. 193-214, Springer, Berlin.
- Zar, J.H. (2007) Biostatistical Analysis (5th Edition), Pearson, New York.
- Zhou, Q., Zhang, P. and Zhang, G. 2015. Biomass and pigments production in photosynthetic bacteria wastewater treatment: effects of light sources. *Bioresour Technol* 179, 505-509.

APPENDIX A: LAMP CHARACTERIZATION

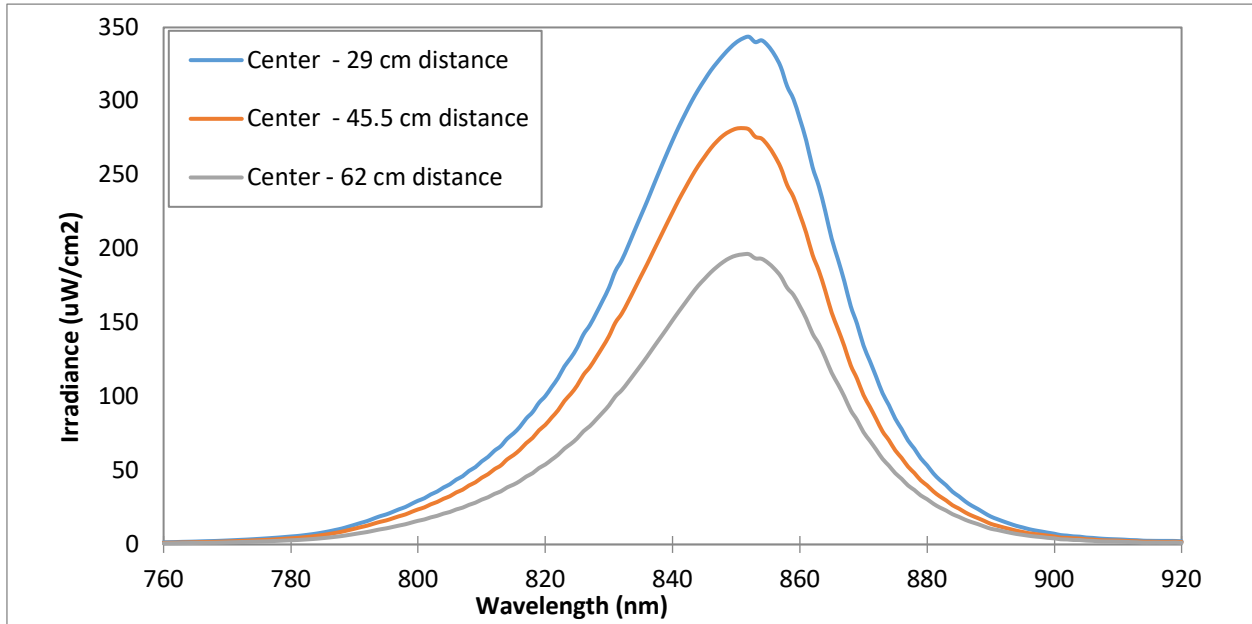


Figure A-1: 850 nm irradiance profile at variable distances. Measurements were taken from the center of the lamp at distances of 29 cm, 45.5 cm and 62 cm.

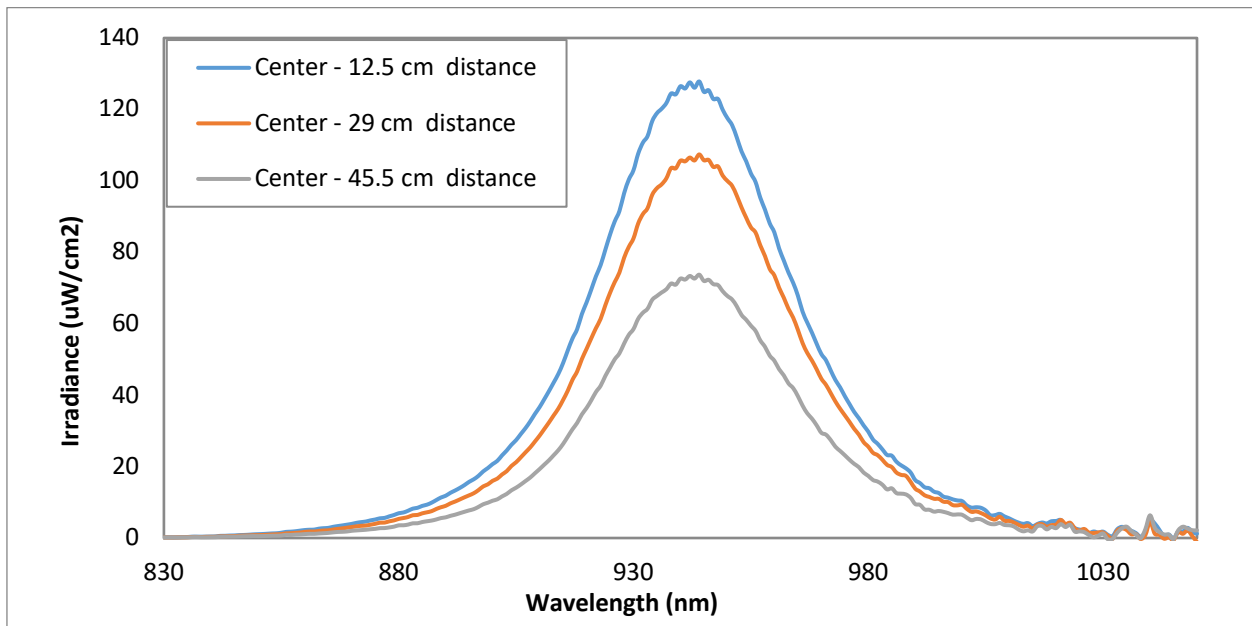


Figure A-2: 940 nm irradiance profile at variable distances. Measurements were taken from the center of the lamp at distances of 12.5 cm, 29 cm and 45.5 cm.

APPENDIX B: ENRICHMENT REACTOR IMAGES

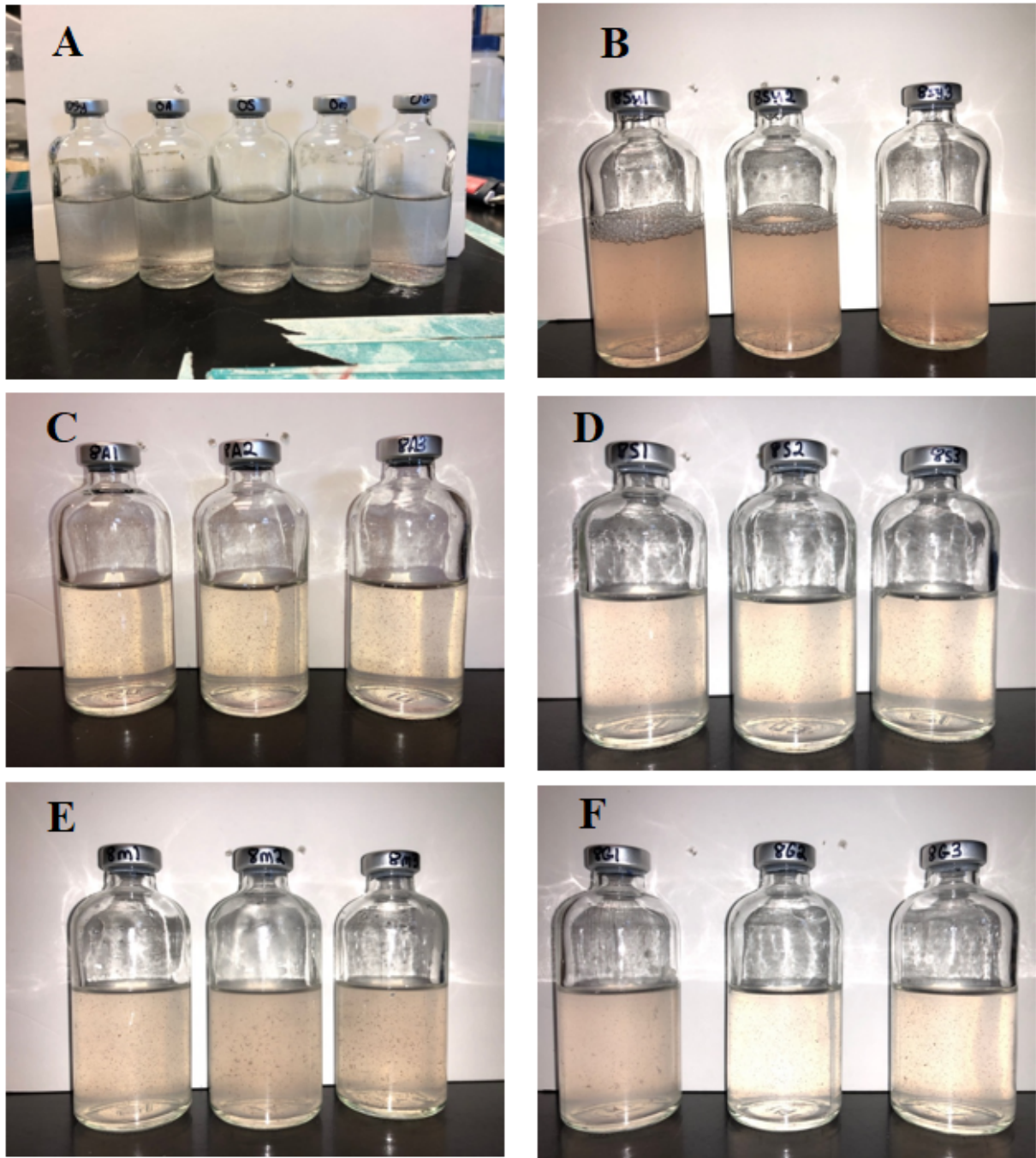


Figure B-1: Images of the reactors after the initial batch incubation. (A): Controls from left to right, Syntho, Acetate, Starch, Milk and Glycerol. (B): 850 nm Syntho reactors. (C): 850 nm Acetate reactors. (D): 850 nm Starch reactors. (E): 850 nm Milk reactors. (F): 850 nm Glycerol reactors.

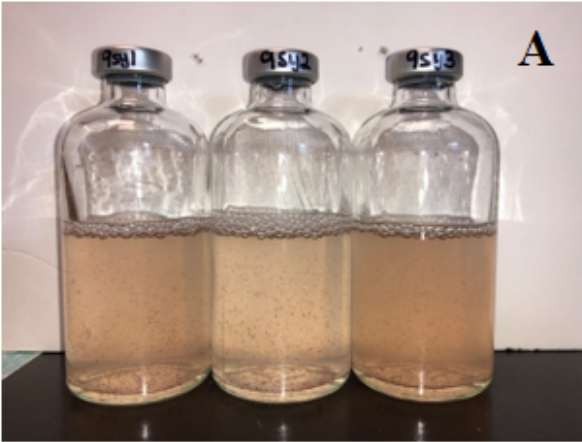


Figure B-2: Images of the reactors after the initial batch incubation. (A): 940 nm Syntho reactors. (B): 940 nm Acetate reactors. (C): 940 nm Starch reactors. (D): 940 nm Milk reactors. (E): 940 nm Glycerol reactors.

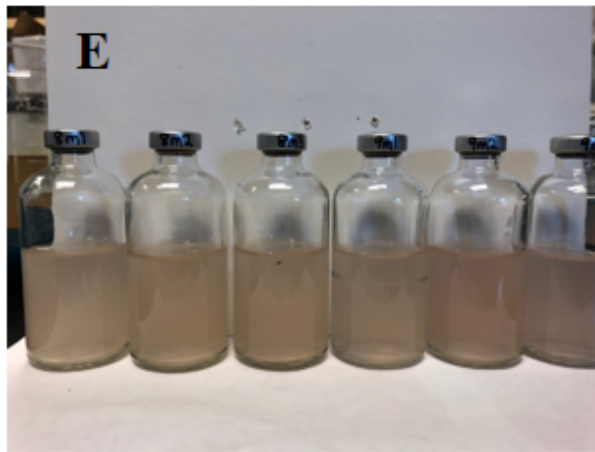
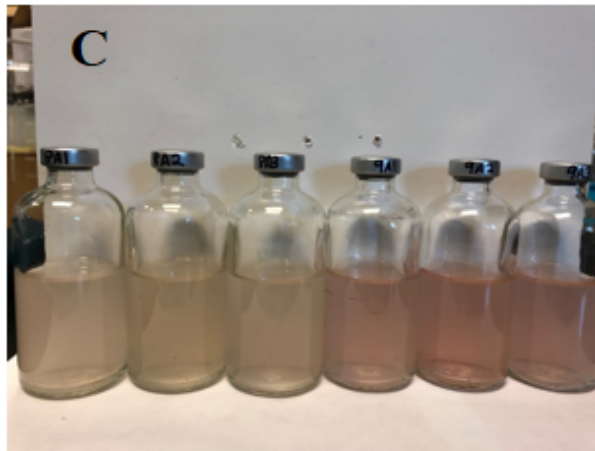
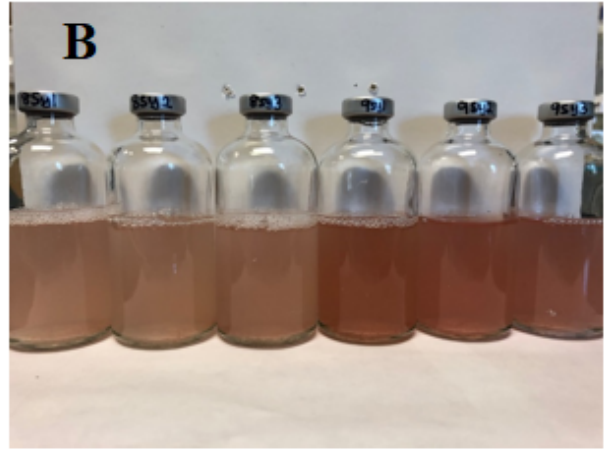
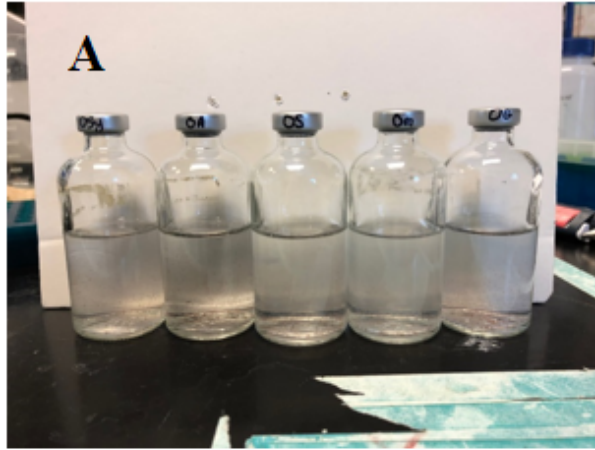


Figure B-3: Images of the reactors after the sequencing batch operation. (A): Controls from left to right, Syntho, Acetate, Starch, Milk and Glycerol. (B): Syntho reactors. (C): Acetate reactors. (D): Starch reactors. (E): Milk reactors. (F): Glycerol reactors.

APPENDIX C: QIIME 2 COMMANDS

1

. DATA IMPORT

```
qiime tools import \  
  --type  
'SampleData[PairedEndSequencesWithQuality]' \  
  --input-path manifest.txt \  
  --output-path paired-end-demux.qza \  
  --source-format  
PairedEndFastqManifestPhred33
```

2. QUALITY VISUALIZATION

```
qiime demux summarize \  
  --i-data paired-end-demux.qza \  
  --o-visualization paired-end-demux.qzv
```

3. QUALITY FILTER

```
qiime dada2 denoise-paired \  
  --i-demultiplexed-seqs paired-end-  
demux.qza \  
  --p-trim-left-f 22 \  
  --p-trim-left-r 22 \  
  --p-trunc-len-f 180 \  
  --p-trunc-len-r 228 \  
  --o-representative-sequences rep-seqs.qza \  
  --o-table table.qza \  
  --o-denoising-stats stats-dada2.qza
```

4. OUT SUMMARY

```
qiime feature-table summarize \  
  --i-table table.qza \  
  --o-visualization table.qzv \  
  --m-sample-metadata-file sample-  
metadata-inf-ml.txt  
qiime feature-table tabulate-seqs \  
  --i-data rep-seqs.qza \  
  --o-visualization rep-seqs.qzv
```

5 DIVERSITY ANALYSIS

```
qiime alignment mafft \  
  --i-sequences rep-seqs.qza \  
  --o-alignment aligned-rep-seqs.qza  
qiime alignment mask \  
  --i-alignment aligned-rep-seqs.qza \  
  --o-masked-alignment masked-aligned-rep-  
seqs.qza  
qiime phylogeny fasttree \  
  --i-alignment masked-aligned-rep-seqs.qza  
 \  
  --o-tree unrooted-tree.qza  
qiime phylogeny midpoint-root \  
  --i-tree unrooted-tree.qza \  
  --o-rooted-tree rooted-tree.qza
```

6. ALPHA AND BETA DIVERSITY ANALYSIS

```
qiime diversity core-metrics-phylogenetic \  

```

```
--i-phylogeny rooted-tree.qza \  
--i-table table.qza \  
--p-sampling-depth 80000 \  
--m-metadata-file sample-metadata-inf-  
ml.txt \  
--output-dir core-metrics-results
```

```
qiime diversity alpha-rarefaction \  
--i-table table.qza \  
--i-phylogeny rooted-tree.qza \  
--p-max-depth 125000 \  
--m-metadata-file sample-metadata-inf-  
ml.txt \  
--o-visualization alpha-rarefaction2.qzv
```

7. Alpha rarefaction plotting

APPENDIX D: PHYLOGENETIC CLASSIFICATION OF PURPLE BACTERIA

Table D-1: Phylogenetic classification of the purple bacteria within the *Proteobacteria* phylum.

Class	Order	Family	Genus	Species and strain
<i>Alphaproteobacteria</i>				
	<i>Caulobacterales</i>			
	<i>Caulobacteraceae</i>			
			<i>Brevundimonas</i>	<i>subvibrioides</i> (DSM 4735T)
	<i>Rhizobiales</i>			
	<i>Aurantimonadaceae</i>			
			<i>Fulvimarina</i>	<i>pelagi</i> (DSM 15513T)
	<i>Beijerinckiaceae</i>			
			<i>Methylocella</i>	<i>silvestris</i> (DSM 15510T)
	<i>Bradyrhizobiaceae</i>			
			<i>Bradyrhizobium</i>	<i>oligotrophicum</i> (DSM 12412T) <i>sp. (BTai1)</i>
			<i>Rhodoblastus</i>	<i>acidophilus</i> (DSM 137T)
			<i>Rhodopseudomonas</i>	<i>faecalis</i> (JCM 11668T) <i>palustris</i> (ATCC 17001T) <i>palustris</i> (ATCC 17003) <i>palustris</i> (ATCC 17005) <i>palustris</i> (DSM 126) <i>pseudopalustris</i> (DSM 123T) <i>renobacensis</i> (DSM 12706T)
	<i>Hyphomicrobiaceae</i>			
			<i>Blastochloris</i>	<i>sulfovirens</i> (DSM 729T) <i>viridis</i> (DSM 133T)
			<i>Prosthecomicrobium</i>	<i>hirschii</i> (ATCC 27832T)
			<i>Rhodomicrobium</i>	<i>udaipurensis</i> (JA643T) <i>vannielii</i> (DSM 162T)
			<i>Rhodoplanes</i>	<i>elegans</i> (DSM 11907T)
	<i>Methylobacteriaceae</i>			
			<i>Methylobacterium</i>	<i>aquaticum</i> (DSM 16371T) <i>oryzae</i> (DSM 18207T) <i>platani</i> (JCM 14648T) <i>populi</i> (NCIMB 13946T) <i>radiotolerans</i> (DSM 1819T)

		<i>tarhaniae</i> (DSM 25844T)
		<i>variabile</i> (DSM 16961T)
	Phyllobacteriaceae	
	Rhodobiaceae	
	Hoeflea	<i>phototrophica</i> (DSM 17068T)
	Afifella	<i>marina</i> (IM 163)
		<i>marina</i> (DSM 2698T)
		<i>marina</i> (IM 167)
		<i>pfennigii</i> (DSM 17143T)
	Roseospirillum	<i>parvum</i> (DSM 12498T)
Rhodobacterales		
	Rhodobacteraceae	
	Cereibacter	<i>changelensis</i> (DSM 18774T)
	Dinoroseobacter	<i>shibae</i> (DSM 16493T)
	Halovulum	<i>dunhuangense</i> (YYQ-30T)
	Jannaschia	<i>aquimarina</i> (DSM 28248T)
	Labrenzia	<i>alexandrii</i> (DSM 17067T)
	Loktanella	<i>vestfoldensis</i> (DSM 16212T)
	Nereida	<i>ignava</i> (DSM 16309T)
	Planktomarina	<i>temperata</i> (DSM 22400T)
	Rhodobaca	<i>bogoriensis</i> (DSM 18756T)
	Rhodobacter	<i>azotoformans</i> (IFO 16436T)
		<i>blasticus</i> (DSM 2131T)
		<i>megalophilus</i> (DSM 18937T)
		<i>sphaeroides</i> (DSM 158T)
		<i>veldkampii</i> (DSM 11550T)
		<i>weaveri</i> (TJ-12)
		<i>adriaticum</i> (DSM 2781T)
		<i>euryhalinum</i> (DSM 4868T)
		<i>kholense</i> (JA 297T)
		<i>marinum</i> (JA 128T)
		<i>sulfidophilum</i> (DSM 2351)
		<i>sulfidophilum</i> (DSM 1374T)
		<i>visakhapatnamense</i> (DSM 17937T)
	Roseibacterium	<i>elongatum</i> (DSM 19469T)
		<i>antarcticus</i> (DSM 11466T)
	Roseivivax	<i>atlanticus</i> (LMG 27156T)
		<i>halodurans</i> (DSM 15395T)
		<i>halotolerans</i> (DSM 15490T)
		<i>isopora</i> (DSM 22223T)

	<i>Roseobacter</i>	<i>denitrificans</i> (DSM 7001T) <i>litoralis</i> (DSM 6996T)
	<i>Roseovarius</i>	<i>indicus</i> (LMG 24622T) <i>mucosus</i> (DSM 17069T) <i>tolerans</i> (DSM 11457T)
	<i>Salipiger</i>	<i>mucosus</i> (DSM 16094T)
	<i>Sulfitobacter</i>	<i>guttiformis</i> (DSM 11458T) <i>noctilucicola</i> (DSM 101015T)
	<i>Thalassobacter</i>	<i>stenotrophicus</i> (CECT5294T)
Rhodospirillales		
Acetobacteraceae		
	<i>Acidiphilium</i>	<i>acidophilum</i> (ATCC 27807T) <i>angustum</i> (ATCC 35903T) <i>multivorum</i> (DSM 11245T) <i>rubrifiaciens</i> (DSM 16009T)
	<i>Paracraurococcus</i>	<i>ruber</i> (DSM 15832T)
	<i>Roseococcus</i>	<i>thiosulfatophilus</i> (DSM 8511T)
	<i>Rubritepida</i>	<i>flocculans</i> (DSM 14296T)
Rhodospirillaceae		
	<i>Caenispirillum</i>	<i>salinarum</i> (JCM 17360T)
	<i>Niveispirillum</i>	<i>cyanobacteriorum</i> (LMG 28334T)
	<i>Oceanibaculum</i>	<i>indicum</i> (LMG 24626T)
	<i>Pararhodospirillum</i>	<i>photometricum</i> (DSM 122T)
	<i>Phaeospirillum</i>	<i>fulvum</i> (MGU-K5) <i>molischianum</i> (DSM 120T)
	<i>Rhodocista</i>	<i>centenaria</i> (ATCC 51521) <i>trueperi</i> (ATCC 700224T)
	<i>Rhodospirillum</i>	<i>rubrum</i> (F11) <i>rubrum</i> (DSM 1068) <i>rubrum</i> (DSM 467T) <i>rubrum</i> (DSM 107)
	<i>Rhodovibrio</i>	<i>salinarum</i> (DSM 9154T) <i>sodomensis</i> (DSM 9895T)
	<i>Roseospira</i>	<i>mediosalina</i> (BN180T)
	<i>Skermanella</i>	<i>aerolata</i> (DSM 18479T) <i>stibiirensistens</i> (SB22T)
Rhodothalassiales		

<i>Rhodothalassiaceae</i>	<i>Rhodothalassium</i>	<i>salexigens</i> (DSM 2132T)
<i>Sphingomonadales</i>		
<i>Erythrobacteraceae</i>	<i>Erythrobacter</i>	<i>litoralis</i> (DSM 8509T) <i>longus</i> (DSM 6997T) <i>marinus</i> (HWDM-33T)
	<i>Erythromicrobium</i>	<i>ramosum</i> (DSM 8510T)
	<i>Porphyrobacter</i>	<i>dokdonensis</i> (SM 17193T) <i>neustonensis</i> (DSM 9434T) <i>sanguineus</i> (DSM 11032T)
<i>Sphingomonadaceae</i>	<i>Blastomonas</i>	<i>natatoria</i> (DSM 3183T)
	<i>Novosphingobium</i>	<i>fuchskuhlense</i> (DSM 25065T) <i>subterraneum</i> (DSM 12447T)
	<i>Sphingomonas</i>	<i>lacus</i> (CECT 8383T) <i>sanxanigenens</i> (DSM 19645T) <i>ursincola</i> (DSM 9006T)
<hr/> <i>Betaproteobacteria</i>		
<i>Burkholderiales</i>		
<i>Burkholderiaceae</i>	<i>Polynucleobacter</i>	<i>duraquae</i> (DSM 21495T)
<i>Comamonadaceae</i>	<i>Limnohabitans</i>	<i>planktonicus</i> (DSM 21594T)
	<i>Rhodoferax</i>	
<i>uncl. Burkholderiales</i>	<i>Ideonella</i>	<i>sakaiensis</i> (NBRC 110686T)
	<i>Roseateles</i>	<i>depolymerans</i> (DSM 11813T) <i>terrae</i> (CCUG 52222T) <i>benzoatilyticus</i> (ATCC BAA-35T) <i>gelatinosus</i> (IL144) <i>gelatinosus</i> (DSM 1709T) <i>gelatinosus</i> (IM 456) <i>gelatinosus</i> (IM 151) <i>gelatinosus</i> (DSM 149)
<i>Rhodocyclales</i>		
<i>Rhodocyclaceae</i>	<i>Methyloversatilis</i>	<i>universalis</i> (DSM 25237T)
	<i>Rhodocyclus</i>	<i>tenuis</i> (Imhoff 230) <i>tenuis</i> (DSM 109T)

Gammaproteobacteria

Cellvibrionales

Haliaceae

<i>Chromatocurvus</i>	<i>halotolerans</i> (DSM 23344T)
<i>Congregibacter</i>	<i>litoralis</i> (DSM 17192T)
<i>Luminiphilus</i>	<i>syltensis</i> (DSM 22749T)
<i>Pseudohalialia</i>	<i>rubra</i> (DSM 19751T)

Chromatiales

Chromatiaceae

<i>Allochromatium</i>	<i>vinosum</i> (DSM 180T) <i>vinosum</i> (MT86) <i>warmingii</i> (DSM 173T)
<i>Chromatium</i>	<i>okenii</i> (DSM 169T) <i>weissei</i> (DSM 5161)
<i>Halochromatium</i>	<i>glycolicum</i> (DSM 11080T) <i>roseum</i> (DSM 18859T) <i>salexigens</i> (DSM 4395T) <i>modestohalophilus</i> (DSM 25653T)
<i>Lamprobacter</i>	
<i>Marichromatium</i>	<i>bheemlicum</i> (DSM 18632T) <i>gracile</i> (DSM 203T) <i>purpuratum</i> (DSM 1591T)
<i>Rhabdochromatium</i>	<i>marinum</i> (DSM 5261T)
<i>Thermochromatium</i>	<i>tepidum</i> (DSM 3771T)
<i>Thiocapsa</i>	<i>bogorovi</i> " (BBS) <i>imhoffii</i> (DSM 21303T) <i>marina</i> (DSM 5653T) <i>pendens</i> (DSM 236T) <i>rosea</i> (DSM 235T) <i>roseopersicina</i> (DSM 217T)
<i>Thiococcus</i>	<i>pfennigii</i> (DSM 226) <i>pfennigii</i> (DSM 227) <i>pfennigii</i> (Pfennig 8320) <i>pfennigii</i> (DSM 228)
<i>Thiocystis</i>	<i>gelatinosa</i> (DSM 215T) <i>minor</i> (DSM 178T) <i>violacea</i> (DSM 207T) <i>violacea</i> (DSM 208) <i>violascens</i> (DSM 198T)
<i>Thioflavicoccus</i>	<i>mobilis</i> (ATCC 700959T)
<i>Thiohalocapsa</i>	<i>halophila</i> (DSM 6210T)

	<i>marina</i> (DSM 19078T)
<i>Thiolamprovum</i>	<i>pedioforme</i> (DSM 3802T)
<i>Thiorhodococcus</i>	<i>drewsii</i> (DSM 15006T)
	<i>kakinadensis</i> (DSM 18858T)
	<i>mannitoliphagus</i> (DSM 18266T)
	<i>minor</i> (DSM 11518T)
<i>Thiorhodovibrio</i>	<i>winogradskyi</i> (DSM 6702T)
	<i>sp.</i> (970)
<i>Thiohalocapsa</i>	<i>sp.</i> (ML1)
<i>Ectothiorhodospiraceae</i>	
<i>Ectothiorhodosinus</i>	<i>mongolicus</i> (DSM 15479T)
<i>Ectothiorhodospira</i>	<i>haloalkaliphila</i> (ATCC 51935T)
	<i>imhoffii</i> (JA 319)
	<i>magna</i> (DSM 22250T)
	<i>marina</i> (DSM 241T)
	<i>marismortui</i> (DSM 4180T)
	<i>mobilis</i> (DSM 237T)
	<i>shaposhnikovii</i> (DSM 243T)
	<i>vacuolata</i> (DSM 2111T)
	<i>variabilis</i> (DSM 21381T)
<i>Halorhodospira</i>	<i>abdelmalekii</i> (DSM 2110T)
	<i>halochloris</i> (DSM 1059T)
	<i>halophila</i> (DSM 244T)
	<i>halophila</i> (IM9622)
	<i>halophila</i> (IM 9626)
	<i>halophila</i> (Imhoff 9630)
	<i>neutriphila</i> (DSM 15116T)
<i>Thiorhodospira</i>	<i>sibirica</i> (ATCC 700588T)
<i>Ectothiorhodospira</i>	<i>sp.</i> (PHS-1)
	<i>sp.</i> (BSL-9)

Table is constructed using data from (Imhoff et al., 2017)